European Community On Flow, Turbulence and Combustion

6th ERCOFTAC SIG 33 workshop

Laminar-Turbulent Transition Mechanisms, Prediction and Control

June 17-20, 2007
Hirschegg, Kleinwalsertal, Austria

Program

and

Book of Abstracts

Programme for the SIG-33 workshop "Laminar-Turbulent Transition Mechanisms, Prediction and Control", June 17 - 20, 2007

Speaker	Authors	Title
Sunday, June 17		
18:30 - 19:30	**Dinner**	
19:45 - 21:00	**Session: 1**	**Chariman: J.-P. Archambaud**
PELTZER	Inken Peltzer, Wolfgang Nitsche	Experimental Investigation on a Two-dimensional Laminar Wing Glove
SEITZ	Arne Seitz	In-Flight Investigation of Tollmien-Schlichting Waves
WEISMüLLER	Michael Weismüller, Cameron Tropea	Boundary-Layer Receptivity of Laminar Airfoils to Atmospheric Turbulence
Monday, June 18		
7:45-8:30	**Breakfast**	
8:30 - 10:10	**Session: 2**	**Chariman: U. Rist**
ÅKERVIK	Espen Åkervik, Uwe Ehrenstein, Francois Gallaire, Dan S. Henningson	Two-dimensional Global Eigenmodes for the Flat Plate Boundary-layer Flow
CHEDEVERGNE	F. Chedevergne, G. Casalis	Biglobal Linear Stability Analysis and DNS Investigations of the Flow Induced by Wall Injection
RODRIGUEZ	Daniel Rodriguez, Vassilis Theofilis	Global Instability of Laminar Separation Bubbles
BRAUN	Stefan Braun	Transition in Laminar Separation Bubbles: Theoretical Treatment of a Benchmark Problem
10:40- 12:20	**Session: 3**	**Chariman: H. Fasel**
CASALIS	Estelle Piot, Gregoire Casalis, Ulrich Rist	Pre-streaky Flow Instability: DNS and LST
DE LANGE	J. Mans, Rick De Lange, Luca Brandt	Transition Through Streak/Streak Interactions
BRANDT	Philipp Schlatter, Rick DeLange, Luca Brandt	Numerical Study of the Stabilisation of Tollmien-Schlichting Waves by Finite Amplitude Streaks
BAGHERI	Shervin Bagheri, Dan Henningson	Performance of Reduced-Order Models of Fluid Systems
12:30 - 13:30	**Lunch**	
13:30 - 14:45	**Session: 4**	**Chariman: D. Henningson**
MONOKROUSOS	Antonios Monokrousos, Luca Brandt, Philipp Schlatter, Dan S.	Feedback Control and Estimation Applied to Boundary Layers Subject to Free Stream Turbulence
ALBRECHT	Thomas Albrecht, Hans Metzkes, Gerd Mutschke, Roger Grundmann, Gunter Gerbeth	Tollmien-Schlichting Wave Cancellation Using an Oscillating Lorentz Force
GRUNDMANN	Sven Grundmann, Jochen Kriegseis, Cameron Tropea	Experimental and Numerical Investigation of the Transition Delay Using Plasma Actuators
15:05 - 16:20	**Session: 5**	**Chariman: M. Kloker**
HANIFI	Martin G. Byström, Ardeshir Hanifi, Dan S. Henningson	Optimal Disturbances in Falkner-Skan-Cooke Boundary Layers
PRALITS	Jan Pralits, Paolo Luchini	Optimal Spatial Growth of Swept-Wing Instabilities Through Multiple-Scale Analysis
PUJALS	Gregory Pujals, Carlo Cossu, Sebastien Depardon	Optimal Perturbations of Zero Pressure Gradient Turbulent Boundary Layer
16:40- 18:20	**Session: 6**	**Chariman: S. Hein**
PIOT	Estelle Piot, Grégoire Casalis	Numerical Investigation of The Crossflow Instabilities Induced by a Periodic Roughness Array on a Swept Cylinder: Receptivity and Stability Study
BONFIGLI	Giuseppe Bonfigli, Markus J. Kloker	Interpretation of the Secondary Instability of Crossflow Vortices by Analogy with the Kelvin-Helmholtz Instability
FRIEDERICH	Tillmann Friederich, Giuseppe Bonfigli, Markus J. Kloker	Active Control of the Cross Flow Secondary Instability in a 3-D Boundary Layer by Blowing/Suction at the Wall
ARCHAMBAUD	Jean-Pierre Archambaud, Daniel Arnal, J. Fontaine, J.-L. Godard, J. Krier, F. Ternoy	Transition Control Experiments in the Supersonic S2MA Wind Tunnel (SUPERTRAC Project)
18:30 - 19:30	**Dinner**	

Tuesday, June 19

8:00 - 9:00	**Breakfast**	
9:00 - 10:15	Session: 7	Chariman: G. Casalis
FASEL	Hermann F. Fasel, Alexander Gross, Wolfgang Balzer	Numerical Investigation of Active Separation Control for Low-Pressure Turbine Blades
MISCHENKO	Andrey V. Boiko, Andrey V. Ivanov, Yuri S. Kachanov, Dmitri	Experimental and Numerical Study of Unsteady Goertler Vortices
SCHNEIDER	Tobias M. Schneider, Bruno Eckhardt	Dynamics at the Edge of Chaos in Pipe Flow
10:30 - 18:00	**Mountain Trip**	
18:30 - 19:30	**Dinner**	

Wednesday, June 20

8:00 - 9:00	**Breakfast**	
9:00 - 10:15	Session: 8	Chariman: L. Brandt
BAYSAL	Kudret Baysal, Ulrich Rist	Detection, Extraction and Tracking of Coherent Structures in Boundary Layers
MUELLER	Sebastian B. Mueller, Leonhard Kleiser	Transition to Turbulence in a Mach 0.8 Swirling Mixing Layer
BABUCKE	Andreas Babucke, Markus J. Kloker, Ulrich Rist	Direct Numerical Simulation of a Serrated Nozzle End for Jet-Noise Reduction
10:25 - 11:40	Session: 9	Chariman: A. Hanifi
LINN	Jens Linn, Markus J. Kloker	Effusion Cooling in Mach-6 Boundary-Layer Flow Investigated by DNS
STEMMER	Christian Stemmer	Hypersonic Transition Investigations in a Flat-Plate Boundary Layer at M=20
HEIN	Stefan Hein	Numerical Analysis of Entropy-Layer Instability in Hypersonic Blunt Cone Flows
12:00 - 13:00	**Lunch**	
13:30	Departure	

Experimental investigation on a two-dimensional laminar wing glove

Inken Peltzer   Wolfgang Nitsche

Abstract: *6th* ERCOFTAC SIG *33 workshop - Laminar-Turbulent Transition Mechanisms, Prediction and Control - Kleinwalsertal, Austria, June 17-20, 2007*

address: Dr.-Ing. Inken Peltzer
Prof. Dr.-Ing. Wolfgang Nitsche
Marchstr. 12, Sekr. F2
10587 Berlin, Germany
Institut of Aeronautics and Astronautics, Technical University Berlin
phone: +49 30 314 23094
fax: +49 30 314 22955
e-mail: Inken.Peltzer@tu-berlin.de

The investigation presented in this workshop is focused on the laminar-turbulent boundary layer transition on a two-dimensional airfoil, in particular at measuring the development and amplification of the Tollmien-Schlichting (TS) instabilities leading to transition. The process of generating the TS waves depends strongly on the environmental flow conditions. Therefore, it is necessary to investigate the transition under atmospheric conditions in flight experiments as well as wind tunnel tests. Various measuring techniques for in-flight and wind tunnel experiments were applied to measure the temporal and spatial propagation of natural TS waves. Additionally experiments with controlled generated disturbances with an array of spanwise distributed point sources were performed. Of substantial interest was the development from their early linear up to the weakly nonlinear stage of laminar turbulent transition.

A laminar wing glove was used for the measurements, which was developed for the Grob G103 TWIN II two-seater sailplane at the Institute for Aeronautics and Astronautics, Technical University of Berlin (fig.1). The measuring glove has a 2D center part of $1.0\,m$ span and a chord length of $1.22\,m$. It has an exchangeable wing segment, which can be equipped with different surface sensors or actuators. The sensor setup is also shown in fig.1. A spanwise array of 16 surface hot-wire sensors was located at a chord length of $33\,\%$. The surface hot-wire is a flush-mounted hot-wire welded across a narrow slot (width $< .1\,mm$) in the wing surface and was operated by a constant-temperature anemometer. This sensor was especially used for measuring the instabilities even in the early linear stage of amplification. Furthermore, an piezo foil sensor array of 74 sensors was used in the later stages downstream (at $40\,\%$ to $50\,\%$ chord length). Small loudspeakers
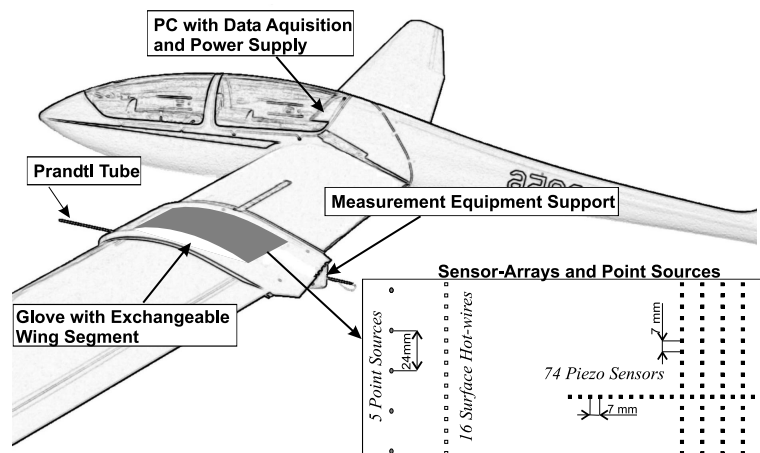

Figure 1: Sailplane with the glove including the sensor arrays

1
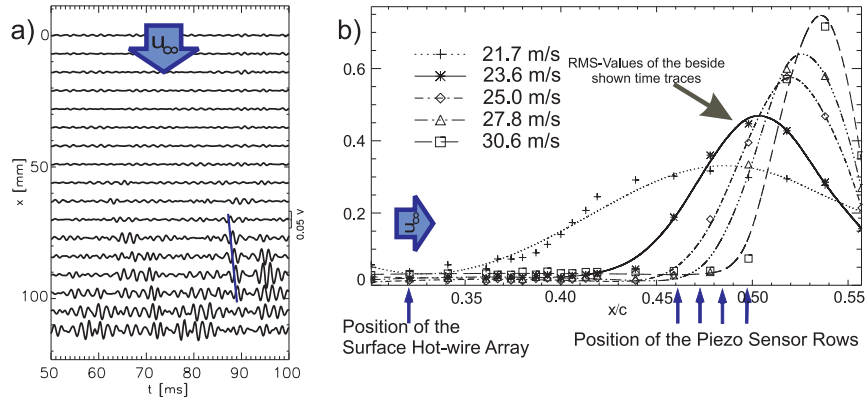
Figure 2: a) Time traces of the piezo sensors downstream, $u_\infty = 23.6 m/s$, b) RMS-Values of these sensors for different velocities
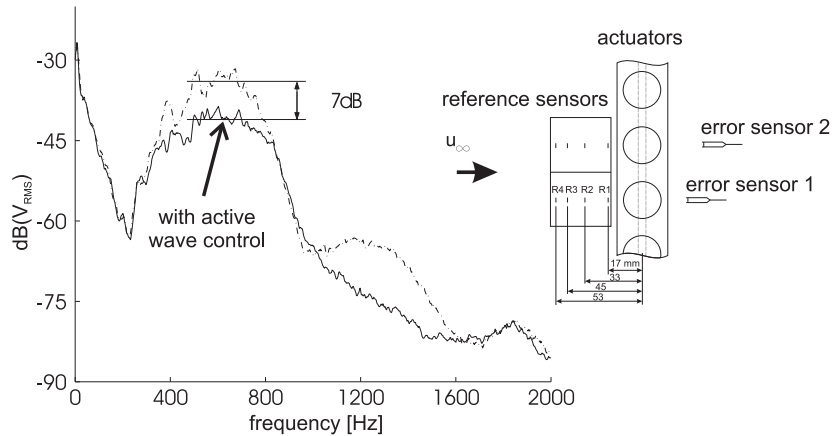

Figure 3: Preliminary result of a wind tunnel measurement with the glove with active wave control (AWC), frequency spectrum of error sensor 2 with and without AWC

were arranged in a spanwise manner (at 20% chord length) underneath the glove surface, and were optionally operated to introduce controlled disturbances into the boundary layer. The flight experiments were carried out at flight velocities from $22.2\,m/s$ to $25\,m/s$ (Reynolds numbers from $1.9 \cdot 10^6$ to $2.5 \cdot 10^6$).

The results in figure 2a) show clearly Tollmien-Schlichting (TS) instabilities in a very early stage of transition with tiny amplitudes, their amplification, the convective transport of wave packets and the transition to turbulent structures in the turbulent boundary layer. Figure 2b) shows the RMS-Values of the downstream arranged piezo sensors for different velocities. Since the maximum of the signal amplitudes indicates the transition, the RMS-curves show the location of transition on the glove. Also, the spanwise distribution of the TS instabilities were investigated extensively [1]. In addition an active sensor actuator system for cancellation of TS-waves on this laminar wing glove will be shown (fig. 3), which was developed based on these measurements and on investigation of Sturzebecher [2], where TS instabilities were damped on a generic windtunnel model.

References

[1] PELTZER, I. ; NITSCHE, W.: In-Flight and Wind Tunnel Measurements of Natural and of Controlled Instabilties on a Laminar Flow Airfoil. In: R. GOVINDARAJAN (Hrsg.): *Sixth IUTAM Symposium on Laminar-Turbulent Transition (Fluid Mechanics and its Applications 78)*. Netherlands : Springer Verlag, 2006, S. 261–266

[2] STURZEBECHER, D. ; NITSCHE, W.: Active Control of Tollmien–Schlichting Instabilities by Multi–Channel Sensor Actuator Systems. In: S. WAGNER, U. RIST, H.J. HEINEMANN, R. HILBIG (Hrsg.): *New Results in Numerical and Experimental Fluid Mechanics III (NNFM 77)*, Springer Verlag, 2002, S. 375–382

In-flight Investigation of Tollmien-Schlichting Waves

Arne Seitz

DLR, Institute of Aerodynamics and Flow Technology
Lilienthalplatz 7, 38108 Braunschweig, Germany; e-mail: arne.seitz@dlr.de

Tollmien-Schlichting waves are well known as primary instabilities in transition of boundary-layers from laminar to turbulent flow. But since almost all experimental investigations on this type of instability were made in wind-tunnels, mainly under conditions of controlled disturbance excitation, very little is known about the technical relevant case of naturally occurring Tollmien-Schlichting waves in free-flight. In order to learn more about this transition scenario, flight tests were performed with the test bed LFU-205 of DLR (fig. 1). The test equipment comprised:

- A 69-element hot-film array (fig. 2), surface mounted on a specially designed laminar glove on the right hand wing of the aircraft.
- A row of 48 pressure orifices to measure the c_P distribution in the region of the laminar glove.
- A pitot-static and a total temperature probe to measure the free stream properties.
- An infrared thermo vision system to detect the onset of turbulence on the laminar glove.

For the present work, the hot-films were utilized to measure skin friction fluctuations provoked by Tollmien-Schlichting waves propagating in the laminar boundary-layer. A calibration procedure was developed, which made it possible to quantify the amplitudes of the fluctuating output of the anemometry system in the dimension of a wall shear stress. From the signals, disturbance frequencies as well as spanwise wavenumbers were determined by a Fourier analysis in time and space. It was found, that a broadband spectrum of Tollmien-Schlichting instabilities, typical for wave packets, were involved. A visual inspection of the time histories, an example is given in fig. 3, shows that these wave packets occur stochastically and that they vary in intensity and spanwise extend.

A comparison between measured and calculated disturbance amplification of those Tollmien-Schlichting waves that form up the packets showed good agreement. Therefore, by means of linear stability analysis, it was feasible also to analyse the experimental data with the objective to specify average initial amplitudes of the waves at their point of neutral stability.
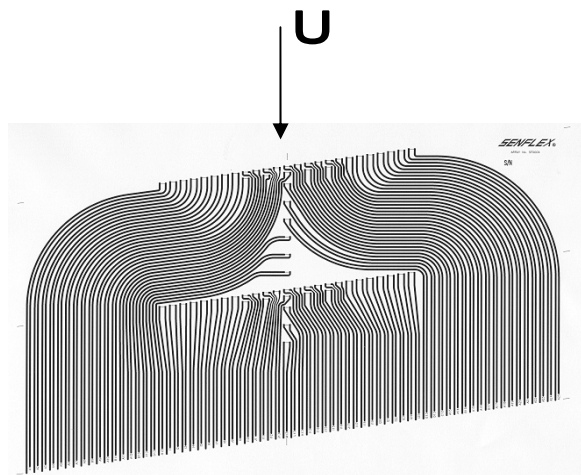

Figure 1: Flying testbed LFU-205 of DLR
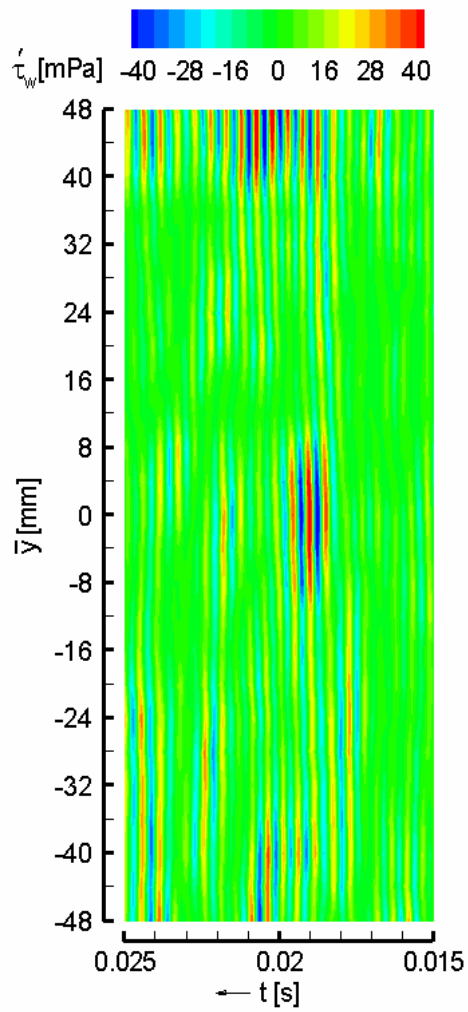

Figure 2: 69-element hot-film array

Figure 3: Time history of wall shear stress fluctuations of spanwise row of 25 sensors at a chord position of X/C = .37

Boundary-Layer receptivity of laminar airfoils to atmospheric turbulence

Michael Weismüller, Cameron Tropea

Fachgebiet Strömungslehre und Aerodynamik, TU Darmstadt

Introduction

A loss of glide performance is experienced by some modern sail-planes upon entering turbulent air in thermals. It is supposed that this loss in glide performance comes from an increase in drag caused by premature transition of the wing's boundary layer from laminar to turbulent. Whereas the phenomenon of external disturbances (e.g. free-stream turbulence, sound) travelling into the boundary layer, called receptivity, has been extensively investigated on a flat plate at zero angle of attack, much less work has been done on bodies with mean aerodynamic load. Also these investigations were carried out in well-controlled wind tunnel conditions which cannot be compared with atmospheric turbulence. In this project the characteristics of atmospheric turbulence (e.g. length-scales, vorticity) for the lower atmosphere and the influence on a wing's boundary layer will be investigated by in flight measurements.

Theoretical Background

Different mechanisms of transition are known. If weak disturbances enter the boundary-layer, the initial growth of disturbances is described by linear stability theory. This growth is weak and can be modulated by pressure gradients (e.g. flow around airfoil), surface mass transfer (e.g. suction), temperature gradients, etc. With increasing disturbance amplitude the mechanisms of transition change. With higher turbulence levels the fundamental transition type occurs, low turbulence levels lead to a subharmonic type.

The free-stream vorticity is another important factor influencing the transition type. Vorticity causes a premature transition of the fundamental type. When the linear grow of disturbances is bypassed the flow quickly becomes turbulent. This phenomenon has been documented in cases of surface roughness and high free stream turbulence.

Atmospheric Turbulence

Atmospheric turbulence can be classified by characteristic length- or time scales. Macro-scale turbulence influences flight operations only indirectly as a result of the weather phenomena, whereas convective- or micro-scale turbulence has direct influence.

The effects of convective-scale turbulence, also known as gust, have been researched extensively over the past century. The subject can be regarded as solved. According to Kolmogorov's theory, turbulent energy dissipates into heat only in micro-scales. Larger scale turbulence is converted into smaller scale turbulence while the total energy remains constant until the dissipation range is reached.

Only few in-flight measurements of turbulence levels in the lower atmosphere have been carried out. They give strong evidence that Kolmogorov's theory is applicable to atmospheric turbulence but in the majority of cases, these measurements didn't reveal the structure of

micro-scale turbulence. Therefore a high sampling rate of the measurement equipment combined with a low airspeed is required.

In-flight measurements show a change of turbulence level over the day. Also there is a significant difference between wind tunnel and in flight frequency spectra of the turbulence. No measurements of the vorticity vector of atmospheric turbulence are known.

Project goal

Within this project the influence of atmospheric turbulence on the boundary layer of a laminar airfoil will be investigated. This will be done in two steps. First, the characteristics of atmospheric turbulence will be investigated, later the influence on the transition process will be determined.

Approach

To investigate the atmospheric turbulence a hot film probe operated in constant temperature mode is mounted on the G109b, the test airplane of the Institute of Fluid Mechanics and Aerodynamics (SLA) at TU-Darmstadt. Due to the high sampling rate of the measurement equipment and the relatively slow airspeed a high spatial resolution in the dissipative scale can be achieved. A four-wire probe (right picture) is used in order to measure two velocity components and one component of the vorticity vector simultaneously. Turbulence spectra for different weather conditions, altitudes and times of day will be measured and compared to the turbulence spectra of SLA's low speed wind tunnel.
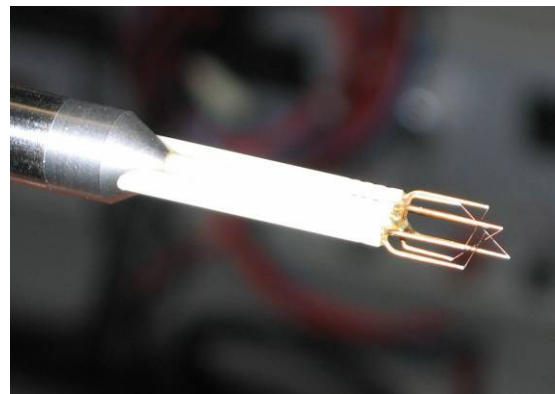
Boundary layer effects will be investigated with hot film sensor arrays or microphones and pressure tabs, alternatively, on a laminar wing glove on the G109's wing. The rectangular wing glove with an airfoil section comparable to modern glider laminar airfoils has a part with 2D flow. With this setup the influence of the turbulence level on the transition will be investigated. To gain a better insight into the receptivity process the experimental data will be compared to numerical simulations.

Results

The resolution of first test measurements did not cover the dissipative range but indicate that the energy cascade theory is applicable on atmospheric turbulence. More results from further in-flight measurements will be available by the time of the workshop.

Two-dimensional global eigenmodes for the flat plate boundary-layer flow

E. Åkervik[*], U. Ehrenstein[†], François Gallaire[‡]and D. S. Henningson [*]

March 26, 2007

Abstract: The stability of a two-dimensional flat plate boundary-layer flow is studied by means of global eigenmodes of the linearized Navier–Stokes operator. The flow disturbance variables are expanded in the basis of eigenmodes and the growth potential is revealed by the computation of optimal initial condition and optimal forcing. We have found that the flow should be excited by upstream located structures leaning against the shear in order to get the maximum energy response downstream.

A steady state base flow is obtained by marching the Navier–Stokes in time using DNS. The resulting velocity field is interpolated on a Chebyshev-Chebyshev grid and the global eigenmodes are computed by linearizing about this base flow. The resulting eigenvalue problem is far too large to be solved by standard QR/QZ algorithms, but iterative techniques such as the Krylov/Arnoldi has proven to efficiently capture a large part of the spectrum (Ehrenstein & Gallaire, 2005). Once computed, the eigenmodes serve as a reduced basis both in order to describe the dynamics and to build a reduced order model for control.

The optimal initial condition and the optimal forcing can be computed by means of singular value decomposition (SVD) of the evolution matrix and the resolvent, respectively. By expanding the flow in the basis of eigenmodes these tasks becomes computational tractable. Both the transient growth and optimal forcing analysis show that the optimal excitation of the flow is achieved through Orr type of structures (see Butler & Farrell, 1992) located upstream. The subsequent evolution of the flow disturbances consist of structures rising up, followed by the onset of TS waves as depicted in figure 1.

The expansion of the flow dynamics in two-dimensional temporal stability modes is hence shown to provide an alternative way, with respect to the conventional locally parallel flow assumption, of studying the instability of the flat-plate boundary layer.

In order to control the flow disturbances, we introduce one sensor and one actuator. The sensor measures the wall shear stress and the actuator, which is a volume forcing on the wall normal velocity component, should be placed in the vicinity of branch I so as to trigger the most efficient response from the flow. In the present work we use the linear quadratic

---

[*]Linné FLOW Centre, KTH Mechanics , SE-100 44 Stockholm, Sweden.

[†]IRPHÉ, Université de Provence, F-13384 Marseille Cedex 13, France

[‡]Laboratoire J.A. Dieudonné, Parc Valrose, F-06108 Nice Cedex 02, France
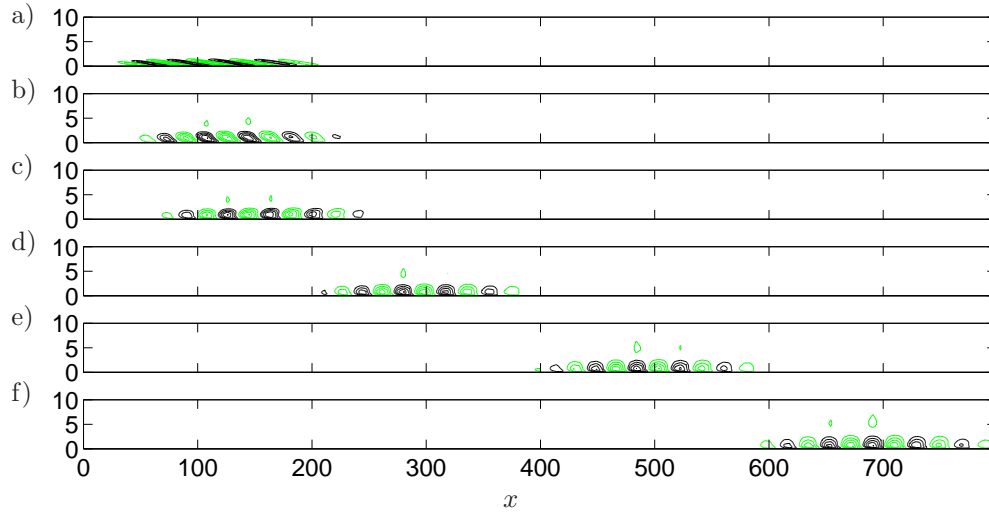
a)

b)

c)

d)

e)

f)

Figure 1: Time evolution for streamwise velocity with the combined Orr and TS mechanism. Note that the amplitude is growing from frame to frame. a) $t = 0$, b) $t = 240$, c) $t = 480$, d) $t = 720$, e) $t = 960$ and f) $t = 1200$.

gaussian (LQG) control synthesis, where the two subproblems of full information control and estimation are solved separately in an optimal manner. Combining the two leads to an optimal measurement feedback control, where the estimated flow is used for control feedback. The design of the controller is intimately related to model reduction and the usual procedure is that of projecting the equations onto a smaller subspace. Given their ability to reproduce the flow dynamics, the global eigenmodes provides a suitable basis for such a projection (cf. Åkervik *et al.*, 2007). Preliminary results are shown, focusing on the input output behaviour, i.e. the dynamics relating the actuator to the sensor, comparing the reduced system to full DNS.

References

EHRENSTEIN, U. & GALLAIRE, F. 2005 On two-dimensional temporal modes in spatially evolving open flows: the flat-plate boundary layer. *J. Fluid Mech.* **536**, 209.

BUTLER, K. M. & FARRELL, B. F. 1992 Three-dimensional optimal perturbations in viscous shear flow. *Phys. Fluids A* **4**, 1637–1650.

ÅKERVIK, E., HŒPFFNER, J., EHRENSTEIN, U. & HENNINGSON, D. S. 2007 Optimal growth, model reduction and control in a separated boundary-layer flow using global eigenmodes. *J. Fluid Mech.* To appear.

Biglobal Linear Stability Analysis and DNS investigation of the flow induced by wall injection

F. Chedevergne & G. Casalis

ONERA-DMAE, 2. av. Ed. Belin 31055 Toulouse FRANCE

francois.chedevergne@onera.fr, gregoire.casalis@onera.fr

In the framework of the thrust oscillations studies arising in solid rocket motors, the stability of the flow induced by wall injection has been carried out for several years. First a linear stability analysis has been used taking into account that we consider an open and non-parallel flow. The results exhibit a discrete set of temporally stable modes. However, these modes are exponentially growing in the streamwise direction of the flow. Thus, a competition between the spatial amplification and the temporal damping determines the possible merging of these modes. In addition to the linear stability theory (LST), DNS computations are perfomed. Several goals are targeted, in particular the comparison with the LST and the link with acoustic cavity modes.

1   Biglobal Linear Stability Theory

1.1   Modelisation

The first step is to model the flow inside the solid rocket motors. We consider in the present paper the single phase flow induced by uniform wall injection. The geometry is a simple semi-infinite cylinder of radius R where gas is injected through the lateral wall at a constant value V_{inj}. Using these two parameters the lengths and the velocities are made dimensionless. This is a strongly
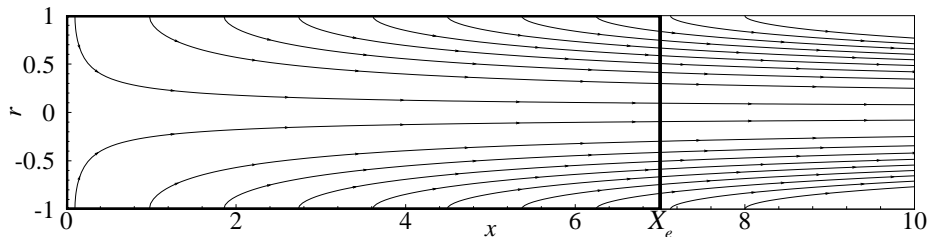

Figure 1: Streamlines of the basic flow and computational domain $[0, X_e] \times [0, 1]$

non-parallel flow, especially in a region close to the injection wall. Some streamlines are plotted in figure 1.

A Reynold number is defined using R and V_{inj} : $Re = \dfrac{V_{inj} R}{\nu}$, where ν is the kinematic viscosity.

The second step consists in performing a linear stability is using the present model flow as basic flow. A perturbation method is used such that any physical quantity Q is written as a superposition of a mean value $\bar{Q}$ and a fluctuating part q. As the mean value, *i.e.* the basic flow, only depends on x and r, the fluctuation is searched as :

$$q = \hat{q}(x, r) \exp[i(n\theta - \omega t)] \tag{1}$$

In this expression, n is an integer representing the azimuthal wave number, ω is a complex number, its real part stands for the circular frequency and its imaginary part for the temporal growth rate. In the present work, only the axisymmetric modes are considered, *e.g.* $n = 0$, thus a streamfunction $\hat{\phi}$ can be defined for the perturbation. The linearized Navier-Stokes equations written for the streamfunction $\hat{\phi}$ lead to a partial differential equation (E) in (x, r) of order 4. This equation is solved for $(x, r) \in [0, X_e] \times [0, 1]$, see figure 1 ; an exit abscissa X_e must be defined in order to perform the calculation. Boundary conditions are imposed for the streamfunction, the critical point is to determine an appropriate outflow condition at $x = X_e$. The chosen condition is a linear extrapolation of the streamfunction as done usually for other open flows, see [9]. After discretization in the computational domain, (E) is written as a generalized eigenvalue problem $\underline{\underline{A}} \, \underline{\Phi} = \omega \, \underline{\underline{B}} \, \underline{\Phi}$. Then, an Arnoldi algorithm [3] is used to compute the eigenvalues ω and the associated eigenfunctions $\underline{\Phi}$ whose coefficients are the discretized values of $\hat{\phi}$.

1.2 Linear Stability Theory (LST) Results

One result of the calculation is the set of complex eigenvalues ω which defines the spectrum of the stability problem. Two examples for $Re = 1975$ are given in figure. 2 corresponding to two values of X_e. Different major comments can be made on these results. First the spectra are
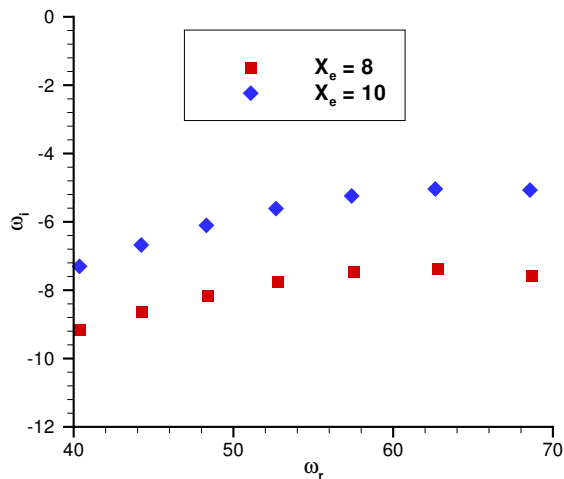

Figure 2: Sets of eigenvalues in the complex (ω_r, ω_i) plane for $Re = 1975$. Two values of X_e are presented : $X_e = 8$ in red squares and $X_e = 10$ in blue diamonds.

discrete. There is only a discrete set of circular frequencies that can develop in the flow. Another

charateristic is that the spectra are weakly affected by the modification of the exit abscissa X_e in terms of frequencies. In other words the circular frequencies ω_r remain almost identical when X_e is changed. However, the temporal growth rates ω_i are modified. Figure 2 shows that the larger X_e is , the higher ω_i is. The last comment concerns the temporal growth rates ω_i which are always negative. This means that the modes will be exponentially damped in time. However, the associated eigenfunctions are exponentially growing in the streamwise direction. Figure 3 presents the spatial evolution of the real part of the eigenfunction $u_x(x,r) = \frac{1}{r}\frac{\partial \hat{\phi}}{\partial r}$ associated with the eigenvalue $\omega = 40.409 - 9.164i$ in the case $X_e = 8$. It clearly shows a strong amplification
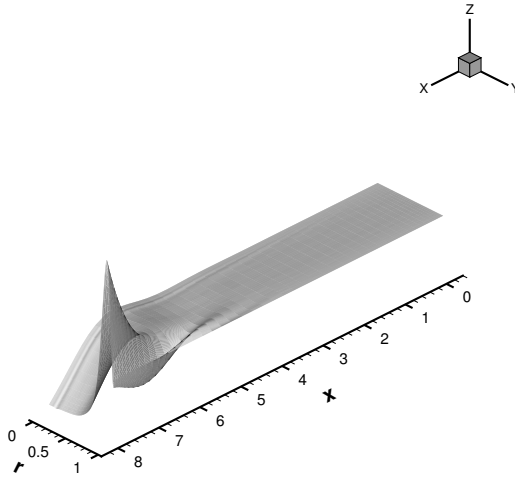

Figure 3: Spatial evolution of $Re(\hat{u}_x(x,r))$ for the eigenmode $\omega = 40.409 - 9.164i$.

(exponential-like amplification) in the streamwise direction. Thus for a given eigenvalue, there are two opposite effects : the perturbation decreases when time is running and it is exponentially growing in the longitudinal direction x. Thanks to these biglobal linear stability results succesfull comparisons have been made with experiments, see *e.g.* [2] and [4]. The obtained agreement indicates that coupling mechanisms should exist. In fact the stable eigenmodes must be excited to merge in the flow. It appears thus that DNS computations could bring some new information on such interactions. However, firstly it must be analysed if DNS calculations confirm the results of the LST.

2 Direct Numerical Simulation

2.1 Procedure

DNS computations are performed with the use of an ONERA code called CEDRE. The spatial discretization is based on a finite volume approach. A code description can be found in [6] and more specific information concerning the code validation for space applications are given in [7]. For the present study, laminar Navier-Stokes computations are performed. In order to be realistic,

3

the characteristic length and velocity are chosen to match experimental ones [5]. It means that R is equal to $R = 0.03$ m and that the injection velocity is about unity : $V_{inj} \approx 1$ m/s, leading to a Reynolds number $Re \approx 2000$.

First, for steady computations an implicit time scheme is used with a fixed value of the CFL number : $CFL = 10$. The idea is to compute the basic flow which will be used for the linear stability calculations. One difficulty is linked to the boundary layer which develops at $x = 0$. But it only acts in the vicinity of the front wall, where the fluctuation is nearly zero, see figure 3. For more details see [8]

The computation provides a steady flow which is then used as basic flow for the stability calculation. Once the stability results are completed, unsteady computations can be started.

For unsteady computations an explicit time scheme is used with a time step $\Delta t = 5.10^{-9}$ s. The resulting CFL_{max} number is 0.3. As mentioned above, the first goal of the DNS calculations is to validate the results exhibited by the linear stability theory. The adopted stragtegy is to start the unsteady computation (from a new time origin $t = 0$ s) by superimposing a given eigenfunction, coming from the stability calculation, to the previously computed basic flow. For example the eigenfunction $Re(\hat{u}_x^{(0)})$ of figure 3 ($^{(0)}$ correspond to $t = 0$ s), calculated on the stability grid is projected on the computational grid and superimposed to the basic flow with a given amplitude A_0. A_0 is such that the maximum value of $Re(\hat{u}_x^{(0)})$, reached at $x = X_e$, is $0.01 \times 8\pi$. Thus, the maximum of $Re(\hat{u}_x^{(0)})$ corresponds to 1% of the maximum longitudinal velocity amplitude of the basic flow $\bar{U}_x$ in the case $X_e = 8R$. In addition to the real part of the longitudinal velocity component $Re(\hat{u}_x^{(0)})$, the associated real part of the radial velocity component $Re(\hat{u}_r^{(0)})$ is also superimposed to the basic flow with the appropriate amplitude given by the LST results [1]. Once the superimposition is done, the computation is started. At $t = 0.02$ s, that is to say after 4.000.000 iterations, the computation is stopped.

2.2 Comparisons with the LST

Two differents cases will be presented in this section. They correspond to two different values of X_e : $X_e = 8R$ and $X_e = 10R$. Signals coming from different numerical sensors inside the computed flow are analyzed. As the values of X_e are different and as A_0 are identical in both cases, at a given location (x, r) the signal amplitude of case $X_e = 10$ is lower than for case $X_e = 8$ because of the strong spatial amplification of the eigenfunction. For example, figures 4(a) and 4(b) show the comparison between the evolutions of the unsteady parts of the signals and the theoretical ones for the radial velocity component $x = 8R$. In fact, any velocity component u of the LST mode is predicted to evolve as :

$$u = A_0 \left[Re(\hat{u}^{(0)}) \cos \left(\frac{V_{inj}}{R} \omega_r t \right) + Im(\hat{u}^{(0)}) \sin \left(\frac{V_{inj}}{R} \omega_r t \right) \right] e^{\frac{V_{inj}}{R} \omega_i t} \tag{2}$$

where $\hat{u}^{(0)}$ is the complex eigenfunction of the mode which real part is introduced at $t = 0$. For $X_e = 10R$, $10u_r$ is plotted on figure 4(b) to compensate the low amplitude obtained in this case. Both figures 4(a) and 4(b) show a perfect agreement between the computed evolutions and the theoretical ones. The radial velocity components exhibit decreasing oscillatory behaviors with

---

[1]Other strategies can be used. For example S. Apte and V. Yang in [10] and [11] impose a white noise or an acoustic excitation to performe LES calculations which exhibit instabilities.
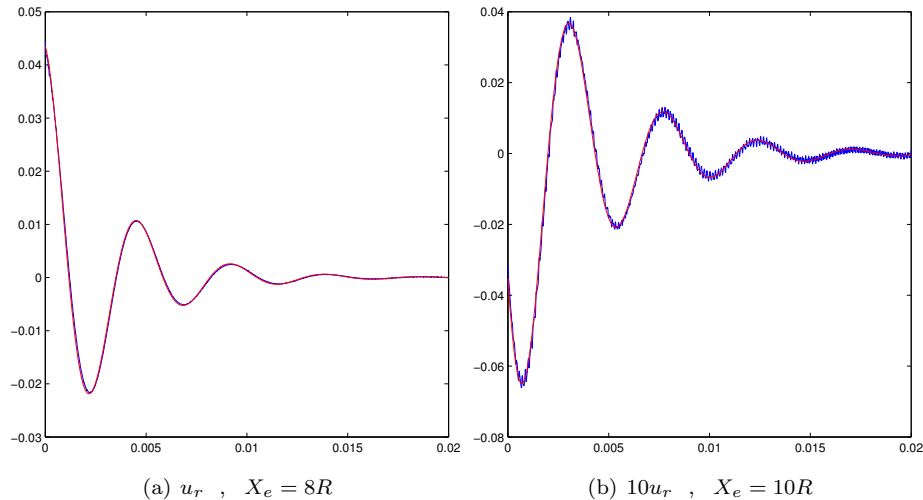
(a) u_r , $X_e = 8R$ (b) $10u_r$, $X_e = 10R$

Figure 4: Computed unsteady radial velocity component u_r (blue) compared to the theoretical evolutions (red) 2. The superimposed eigenmodes are $\omega = 40.409 - 9.164i$ (case $X_e = 8R = 0.24$ m) and $\omega = 40.367 - 7.302i$ (case $X_e = 10R = 0.3$ m). The sensors are located at $x = 8R$ and near the injection wall $(x, r) = (8, 0.866)R = (0.24, 0.02598)$ m for case $X_e = 8R$ and $(x, r) = (8, 0.891)R = (0.24, 0.02670)$ m for case $X_e = 10R$.

frequencies and temporal growth rates identical to those predicted by the LST. Thus, the DNS calculations confirm the results of the LST, in particular the dependence of ω_i with respect to X_e.

2.3 Acoustic cavity modes generation

However, the agreement between computed signals and theory is far from being perfect for the longitudinal velocity component signals where differences appear after a short time, see for example 5(a). The excellent agreements obtained on the radial velocity components in both cases $X_e = 8R$ and $X_e = 10R$ suggest that the observed differences on the longitudinal velocity components are due to development of other fluctuations. The only possible candidates in such a configuration are the acoustic cavity modes. Analytical solutions developed by Majdalani and Flandro [12] give the rotationnal correction due to the presence of the gas ejection on the plane waves. This correction is also known as the acoustic boundary layer. Thanks to these analytical solutions, the unsteady signals can be decomposed on the acoustic modes basis. More precisely, using the least square technique, for a given sensor, the computed pressure signal is projected on the basis of the hundred first acoustic cavity modes [2]. Then the decomposition (amplitudes and phases) is used to compared the velocity components anywhere in the domain. As the time evolution is unknown for the acoustic modes, a hand-made function is calculated to match the signal for one sensor and is reported for all others. It has to be pointed out that this function is

---

[2]The pressure signal is used for several reasons. The first one is that the pressure fluctuation coming from the stability mode is almost negligible. The second is that there is no rotationnal correction on the pressure. The acoustic boundary layer only exists on the velocity components.

the same [3] in both cases $X_e = 8R$ and $X_e = 10R$.

As an example, the signals of sensor $(x, r) = (8, 0.866)R = (0.24, 0.02598)$ m of case $X_e = 8R$ are analysed. Figures 5(a) and 5(b) present the comparisons between the computed signals and the theory. For figure 5(a) which compares the longitudinal velocity component evolutions u_x,
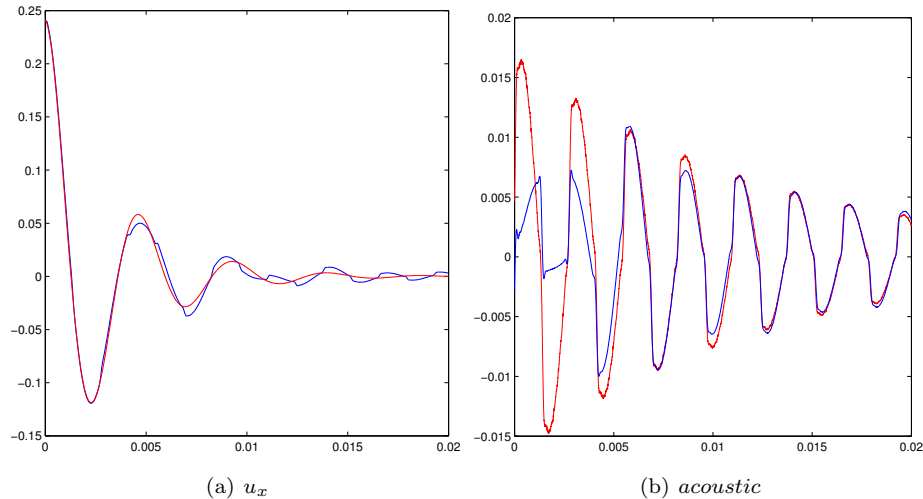

(a) u_x (b) *acoustic*

Figure 5: These results are obtained for case $X_e = 8R$ for the LST mode $\omega = 40.409 - 9.164i$ at $(x, r) = (8, 0.866)R = (0.24, 0.02598)$ m. On the left, a comparison between the unsteady longitudinal velocity component signal (blue) and the theoretical evolutions (red) 2 is plotted. On the right, the difference between the unsteady longitudinal velocity component signal and its theoretical evolution (blue) is compared to a combinaison of 100 acoustic cavity modes (red).

some differences are observed after $t = 0.004$ s. This difference corresponds to the development of acoustic cavity modes. Figure 5(b) provides the comparison between this difference and the combination of 100 hundred cavity modes. The combination reproduces the computed evolution of the acoustic cavity modes. A very good agreement is obtained anywhere in the (x, r) plane or for different X_e values on both pressure and longitudinal velocity component u_x (the radial velocity of the acoustic boundary layer is negligible in our configuration which helps the comparison with the LST modes) [4].

3 Conclusion

First of all, the eigenmodes given by the biglobal linear stability analysis are exact solutions of the linearized Navier-Stokes equations. In particular, the influence of X_e is well predicted. It does not have anything to do with extrapolation condition used at the exit for the stability calculations.

A second interesting point is that the eigenmodes can lead to the existence of acoustic modes.

---

[3]In the two exhibited results there is no non-linear effects for the fluctuations and so the damping of the acoustic modes is only due to viscous effects and/or numerical dissipation. This explains why both results exhibit the same amplitude evolution for the acoustic modes.

[4]Moreover, given that the amplitudes are small, which allows linear behaviors, the acoustic of the pipe has a harmonic distribution. The amplitude of each acoustic cavity mode is $1/n^2$, where n stands for the mode number.

In fact any perturbation inside the pipe would give this result. However, when a LST mode corresponding to a higher value of ω_r which leads to a frequency close those of the first acoustic cavity mode, a coupling is obtained. In this case, the linear behaviors described in this paper are no longer observed. There are energy transfer between the LST modes and the acoustic ones.

To have a better understanding of the experiments, the next step is to see if acoustic modes could lead to the merging of eigenmodes. This is a challenging problem, the eigenmodes being stable modes. This work is under progress.

References

[1] G. I. Taylor. *Fluid flow in regions bounded by porous surfaces.* Proc. of the Royal Soc. Series A, London, vol.234, p.456-475, 1956.

[2] F. Chedevergne and G. Casalis. *Biglobal Linear Stability Analysis of the Flow Induced by Wall Injection.* Physics of Fluids, vol.18, January 2006.

[3] C. Canuto, M.Y. Hussaini, A. Quarteroni, T.A. Zang. *Spectral Methods in Fluid Dynamics.* Springer-Verlag, 1988.

[4] F. Chedevergne and G. Casalis. *Detailed Analysis of the Thrust Oscillations in Reduced Scale Solid rocket Motors.* 42nd AIAA/ASME/SAE/ASEE Joint Propulsion Conference & Exhibit, July 2006.

[5] G. Avalon and D. Lambert. *Campagne d'essais VALDO, période d'essai 2000- 2001.* Technical report RT 2/05424 DEFA ONERA, October 2001.

[6] P. Chevalier and B. Courbet and D. Dutoya and P. Klotz and E. Ruiz and J. Troyes and P. Villedieu. *CEDRE : development and validation of a multiphysic computational software.* 1st European Conference for Aerospace Sciences (EUCASS), Moscow, Russia 2005.

[7] F. Vuillot and D. Scherrer and M. Habiballah. *CFD code validation for space propulsion applications.* 5th International Symposium on Liquid Space Propulsion, Chattanooga, Tennessee 2003.

[8] F. Chedevergne and G. Casalis. *Front Wall Boundary Layer Influence on the Stability of the Flow induced by Wall Injection.* 7th ONERA-DLR Aerospace Symposium, October 2006.

[9] V. Theofilis. *Advances in global linear instability analysis of nonparallel and three-dimensional flows.* Progress in Aerospace Sciences, 2003.

[10] S. Apte and V .Yang. *Unsteady Flow Evolution in Porous Chamber with Surface Mass Injection, Part 1 : Free Oscillation.* AIAA Journal, August 2001.

[11] S. Apte and V .Yang. *Unsteady Flow Evolution in Porous Chamber with Surface Mass Injection, Part 2 : Acoustic Excitation.* AIAA Journal, August 2001.

[12] J. Majdalani and G.A. Flandro. *The oscillatory pipe flow with arbitrary wall injection.* Proceedings of the Royal Society, Series A, vol.458, p.1621-1651,May 2002.

GLOBAL INSTABILITY AND CONTROL OF LAMINAR SEPARATION BUBBLES

D. RODRIGUEZ AND V. THEOFILIS

School of Aeronautics, Universidad Politécnica de Madrid, Pza. Cardenal Cisneros 3, E-28040 Madrid, Spain

vassilis@aero.upm.es

Abstract

Our present concern is with identification and systematic classification of the parameters defining the race between two-dimensional shedding and three-dimensional global instability of two-dimensional laminar separation bubbles in incompressible flow. Attention is paid to separation bubbles generated in a flat plate boundary layer subject to Howarth's (1938) adverse-pressure gradient in the Reynolds number range $Re \in [10000, 50000]$, within which BiGlobal instability in this flow was first discovered by Theofilis (1999) and Theofilis *et al.* (2000). It has since been abundantly demonstrated that BiGlobal instability of separated flows is a prevalent phenomenon in realistic applications, both in steady, e.g. the NACA0012 airfoil (Theofilis and Sherwin 2001; Theofilis *et al.* 2002) as well as in steady and time-periodic separated flows, e.g. the T-106/300 low pressure turbine (LPT) blade (Abdessemed *et al.* 2004, 2006).

Presently, four lines of work are pursued. First, a two-dimensional direct numerical simulation methodology, along the lines discussed by Briley (1971), has been used for the recovery of laminar separated basic states on a flat-plate boundary layer subject to an adverse pressure gradient. A key parameter controlling whether separation remains steady is the streamwise extent, $x \in [x_1, x_2]$, of the streamwise deceleration, whereby x_1 indicates the point of adverse-pressure gradient imposition; keeping x_1 fixed, x_2 is found to diminish as the Reynolds number increases. However, three-dimensional global instability is already present at all Reynolds number values examined, such that basic states obtained may analyzed with respect to their stability, both from the local and the global point of view; first results on the basic states analyzed have been reported elsewhere (Theofilis 2007).

Second, BiGlobal instability analyses are performed, with the aim to recover both convectively and absolutely unstable three-dimensional disturbances. An example of the former is shown in figure 1; shown are the real parts of the amplitude functions of the disturbance velocity component normal to the wall, and that of the disturbance pressure. Such results, identifiable in the global eigenspectrum at all Reynolds numbers examined, correspond to (globally) *stable* disturbances which, in the context of a local or non-local (respectively based on a Rayleigh/Orr-Sommerfeld or Parabolized Stability Equations) analysis would be associated with spatially *amplifying* instabilities. The explanation, of course, lies in the convective nature of the local/non-local instabilities, which is consistent with their recovery as stable BiGlobal eigenmodes.

Third, the question of laminar separated flow control is being pursued by solution of the adjoint BiGlobal eigenvalue problem. By contrast to the classic flat-plate problem (Hill 1995), the present analysis monitors fully nonparallel basic states, with the aim to recover regions in space where flow sensitivities may be exploited for flow control. Validation studies have been completed in the pressure-driven rectangular duct flow, in the classic lid-driven cavity case, as well as in the aforementioned LPT flow.

Last, but not least, both the direct and the adjoint eigenvalue problems are solved using a newly-developed parallel eigenvalue problem solver. The solver is based on tensor-product spectral collocation in Cartesian domains, optimized dense linear algebra libraries and massive parallelization. First results on the adjoint BiGlobal eigenvalue problem pertinent to laminar separation bubble on the flat plate, as well as details on the numerical algorithms supporting the work, will be presented at the conference.

Figure 1: Amplitude functions of the real part of the wall-normal disturbance velocity, $\hat{v}(x, y)$ and disturbance pressure, $\hat{p}$, of a three-dimensional *stable* travelling global mode *generated* by the steady laminar two-dimensional bubble (dashed-line) at $Re = 3 \times 10^4$.
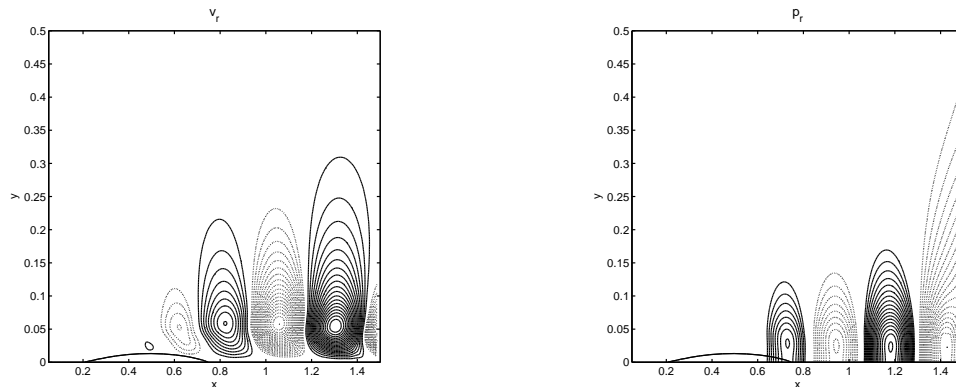
Acknowledgments

References

1 ABDESSEMED, N., SHERWIN, S. J., AND THEOFILIS, V.: On Unstable 2D Basic States in Low Pressure Turbine Flows at Moderate Reynolds Numbers, AIAA Paper 2004-2541 in 34th Fluid Dynamics Conference and Exhibit, AIAA, Portland, Oregon, 2004.

2 ABDESSEMED, N., SHERWIN, S. J., AND THEOFILIS, V.: Linear Stability of the flow past a low pressure turbine blade, AIAA Paper 2004-3530 in 36th Fluid Dynamics Conference and Exhibit, AIAA, San Francisco, California, 2006.

3 BRILEY, W. R.: A numerical study of laminar separation bubbles using the Navier-Stokes equations, *J. Fluid Mech.*, **47**, (1971), pp. 713–736.

4 HILL, D. C.,: Adjoint systems and their role in the receptivity problem for boundary layers, *J. Fluid Mech.*, **292**, (1995), pp. 183–204.

5 HOWARTH, L.,: On the solution of the laminar boundary-layer equation, *Proc. R. Soc. Lond. A*, **164**, (1938), pp. 547.

6 THEOFILIS, V.: On instability properties of incompressible laminar separation bubbles on a flat plate prior to shedding. *AIAA Paper 2007-0540*. 45th AIAA Aerospace Sciences Meeting, Reno, NV, Jan. 8-11, 2007.

7 THEOFILIS, V.: Global linear instability in laminar separated boundary layer flow. *Proc. of the IUTAM Laminar-Turbulent Symposium V*, edited by H. Fasel and W. Saric, Sedona, AZ, USA, (2000), pp. 663 – 668.

8 THEOFILIS, V., HEIN, S., AND DALLMANN, U.: On the origins of unsteadiness and three-dimensionality in a laminar separation bubble. *Phil. Trans. Roy. Soc. London (A)*, **358**, (2000), pp. 3229–324.

9 THEOFILIS, V. AND SHERWIN, S. J.: Global instabilities in trailing-edge laminar separated flow on a NACA-0012 aerofoil. Paper No. ISABE-2001-1094 in International Symposium on Air-breathing Engines XV, Bangalore India, September 3-7, 2001, ISABE, San Francisco, California, 2001.

10 THEOFILIS, V., BARKLEY, D., AND SHERWIN, S. J.: Spectral/hp element technology for flow instability and control, *Aero. J.*, **106**, (2002) pp. 619–625.

Transition in laminar separation bubbles: theoretical treatment of a benchmark problem

Stefan Braun

Institute of Fluid Mechanics and Heat Transfer, Vienna University of Technology, Austria

stefan.braun@tuwien.ac.at

Channel type flows with special boundary conditions (e.g. suction slot or wall deformation, Fig. 1) are - due to their relatively simple geometry - often used to study the phenomenon of localised boundary layer separation and the associated transition process from laminar to turbulent flow. High Reynolds number asymptotic analysis shows that the essence of this flow problem can be reduced to a similarity law which also describes the behaviour of separation bubbles at the suction side of slender airfoils or smooth backward facing steps. An important conclusion is the existence of a critical value of the parameter α controlling separation, up to which steady flow conditions may exist (depending on the acting disturbance level). Above this limit the theory predicts self-sustained oscillations (periodic bubble 'bursting' events and the associated vortex shedding) even in the absence of any disturbances. Furthermore, the effects of flow control devices (in the form of e.g. suction/blowing disturbance stripes, Fig. 1) can be incooperated into the analysis and optimised with respect to the delay or forced initiation of transition. A more detailed investigation of near critical flows indicates - under well defined conditions - the emergence of characteristic structures (Λ-vortices) which precede transition.

The aim of the presentation is to illustrate the power of perturbation methods and to point out open questions in view of benefits which might be gained from alternative approaches (e.g. direct numerical simulation).
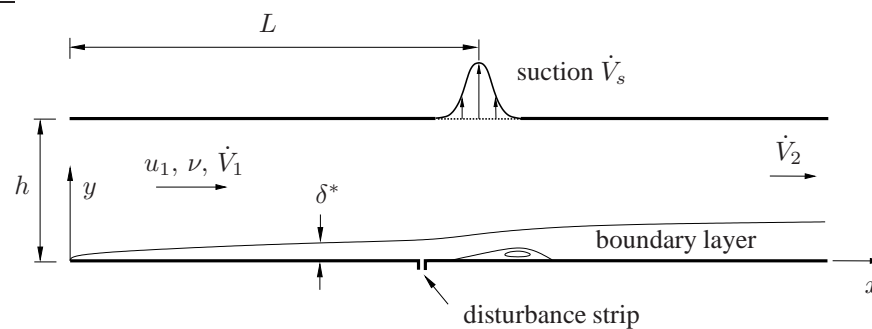

Figure 1: *Channel flow benchmark problem* (schematic, time averaged); characteristic Reynolds number $Re = u_1 L/\nu \gg 1$, typical boundary layer displacement thickness $\delta^* \ll h$, volume flux per unit length $\dot{V}_1 = u_1 h$, $\dot{V}_2 = \dot{V}_1 - \dot{V}_s$, relative suction rate (control parameter) $\alpha = \dot{V}_s/\dot{V}_1 \ll 1$

Pre-streaky flow instability : DNS and LST

E. Piot[1], G. Casalis[1], U. Rist[2]

[1] ONERA DMAE – 2, avenue Edouard Belin, 31055 Toulouse Cedex, France

[2] IAG, Universität Stuttgart, Pfaffenwaldring 21, D-70550, Stuttgart, Germany

The present work deals with the intrinsic instability of the laminar boundary layer downstream a periodic array of micro-roughness elements placed on a line parallel to the leading edge of a flat plate. Whereas a two-dimensional roughness always has a destabilizing effect, such regularly placed three-dimensional roughness elements induce downstream streaks which may have a stabilizing effect thanks to recent detailed experiments and theoretical studies[1]. These streaks take the form of a perturbation in $\cos \beta z$ superimposed to the 2D Blasius flow, where z is the spanwise coordinate and $2\pi/\beta$ the distance between two consecutive roughness elements.

However, such streaks of sine type only arise at some distance downstream the roughness. The goal of the present study is to focus on the flow localized immediately downstream the roughness elements, where the induced perturbation does not behave as a sine function, even if it is periodic with respect to z. The laminar flow in that region is called hereafter a "pre-streaky flow" whose linear stability is analyzed thanks to two numerical tools : DNS (Direct Numerical Simulations) performed by U. Rist and coworkers and LST (Linear Stability Theory) performed by E. Piot and G. Casalis.

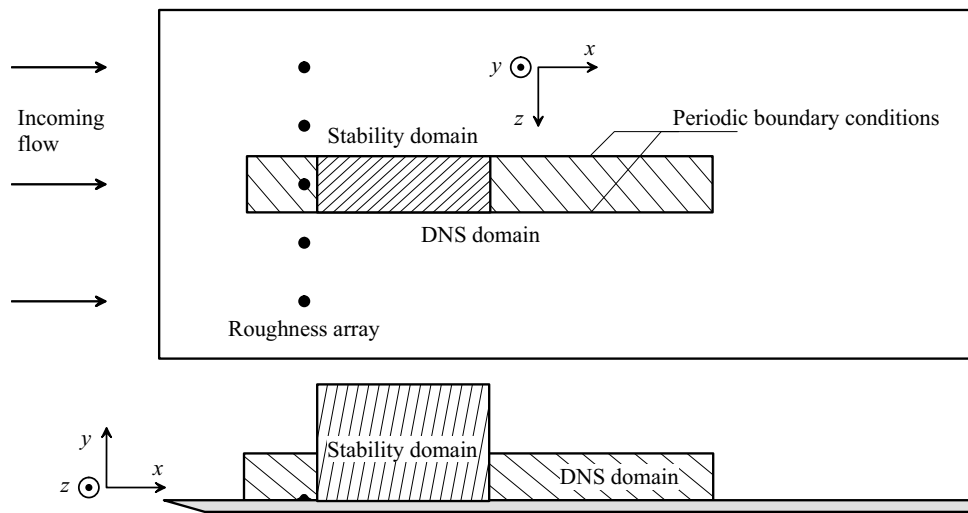The general configuration, as well as the used coordinate system are illustrated in figure 1. The

FIG. 1 – Sketch of the configuration and the numerical domains for DNS and LST.

height h of the considered roughness is $\delta_1/2$ with δ_1 the Blasius displacement thickness at the x-position of the roughness, the corresponding Reynolds number is $R_h = 121$. Using steady boundary conditions for the incoming flow, the DNS provides a steady flow (after some transients). An example is plotted in figure 2. The perturbation induced by the roughness is very localized in two hairpin-type vortices and is not spread out along the full spanwise region. On the other hand this pre-streaky flow appears to be slightly dependent on x.

---

[1] see e.g. the paper of J.H.M. Fransson, L. Brandt, A. Talamelli, C. Cossu, "Experimental and theoretical investigation of the nonmodal growth of steady streaks in a flat plate boundary layer" in Physics of Fluids, vol. 16, 2004
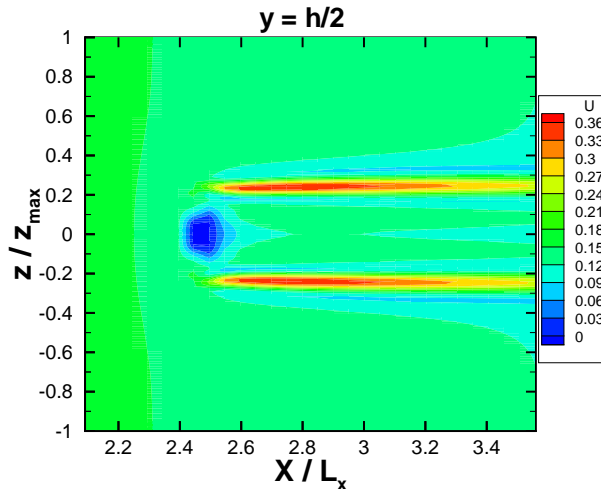
y = h/2

Fig. 2 – Iso-streamwise velocity component U. The z-axis is stretched by a factor 2.38.

A linear stability of the base flow described just above is then performed using the usual quasi-parallel approximation : at a given x abscissa, the base flow velocity field is considered as independent in x, it is simply updated when changing the abscissa. The necessary so-called biglobal approach[2] leads to the following modal mathematical form for the fluctuation :

$$q(x, y, z, t) = \hat{q}(y, z) \exp i(\alpha x - \omega t)$$

for any fluctuating quantity q. In the present approach, α is a complex number, as in the so-called usual spatial theory, its real part represents a wave number and its imaginary part the opposite of the streamwise growth rate. Conversely, ω is a real number associated to the frequency of the considered perturbation. The linearized Navier-Stokes equations lead to a generalized eigenvalue problem written as a partial differential equations system in y and z for the three fluctuating velocity components and the fluctuating pressure. The boundary conditions in y are similar to those used for the classical Orr-Sommerfeld problem, whereas boundary conditions in z only force chosen parity condition. For a given value of the circular frequency ω, different complex eigenvalues α are found, corresponding to different modes called $\beta_0, \beta_1, \ldots, \beta_n, \ldots$ in the following. This notation comes from the fact that these modes may be considered as modified 2D TS wave (for β_0) and modified oblique TS waves $(\beta_1, \ldots)$, the modification being induced by the periodic roughness rank. More explanations will be given in the oral presentation.

Performing the stability analysis at different x values leads to the x-evolution of the spatial growth rates for the different modes which can be compared to the corresponding values obtained for the base flow without roughness (2D Blasius flow). It is observed that the pre-streaky flow is less unstable in comparison with the 2D Blasius flow, especially for the β_0 mode. This result generalizes thus the aforementioned stabilizing effect of the streaky flow.

In addition to this first result, DNS have also being performed with a forced 2D TS wave superposed to the steady Blasius flow for the upstream boundary condition. The obtained DNS results can be compared to the present instability modes calculated with the biglobal approach. The analysis shows that the perturbation calculated by the DNS is not a modal one, however it can be analyzed thanks to the biglobal modes, this will be explained in the oral presentation.

---

[2] see e.g. the paper "Advances in global linear instability analysis of nonparallel and three-dimensional flows" published by V. Theofillis in Aerospace Sciences, vol. 39 in 2003.

Transition through streak/streak interactions

J. Mans[1], H. C. de Lange[1], and Luca Brandt[2]

[1]TUE Mechanical Engineering, 5600 MB Eindhoven, The Netherlands

[2]KTH Mechanics, SE-100 44 Stockholm, Sweden

Recent numerical simulations [1] and flow experiments [4] have proven the importance of unsteadiness and interaction among streaks. Streaks appear randomly and elongate in the streamwise direction while growing; it is observed that their leading and trailing edge travel at different velocities (and also that some streak can move faster than others). These facts (random generation and stretching) lead to streak interactions. A necessary condition for this to happen is a sufficiently high streak-creation rate. Therefore, these 'collisions' are mainly observed for sufficiently high levels of free-stream turbulence.

The aim of this work is to investigate the nature of these interactions/collisions and analyse the corresponding breakdown patterns. In this paper we compare numerical model results for the interaction between streaks with experimental results of bypass transition structures. It will be shown that the structures which result for the model collisions are also present in the interactions of streaks as they are experimentally observed. This leads to recognizing symmetric and asymmetric collisions as an important mechanism for bypass transition at moderate to high main-stream turbulence levels.

Tools. The experimental set-up consists of an optical accessible measuring section (made of glass) in which a flat plate is mounted. The measuring section is 2.7 m long, 0.57 m wide and 0.45 m high. The main stream velocity is set at a value of about 0.12 m/s and free-stream turbulence is generated by a static grid, which results in a turbulence intensity of about 6% with an integral length scale of about 25 mm. The details of the set-up can be found in [4].

The simulation code employed for the present computations was developed at KTH Mechanics[3] and uses spectral methods to solve the three-dimensional, time dependent, incompressible Navier–Stokes equations. The flow is initialized by prescribing a developing Blasius profile ($u_{blas}(x,y)$). In addition two sequential streaky disturbances of finite length are generated at the inflow of the computational domain by forcing them in the fringe region only during a prescribed time interval.

Symmetric and Asymmetric breakdown. First, we look at the model results for a phase shift of $\Delta\phi=\pi$ and $\Delta\phi=\pi/2$ (see figure 1). It can be seen that for $\Delta\phi=\pi$, the secondary streak-pattern collides head-on with the low-momentum fluid that remains after the primary low-speed streak. After some time this leads to a wave-packet traveling on the tail of the low-speed streak, which results in islands of low-speed fluid in a symmetrically broken high-speed streak. For a phase-shift of $\Delta\phi=\pi/2$, the results shows the effect of asymmetric interaction. The initial interaction area is now positioned at the $z > 0$-part of the low-speed streak. Instead of the symmetric split, the secondary high-speed streak now fully bends towards the closest primary high-speed streak. The wall-

normal vorticity that is generated at the bends of this connection, results in a sinuous pattern in the low-speed streak.

Next, we turn to the experimental results of bypass transition. In these experiments three transition signatures have been recognised [4]: sinuous, varicose and single branch. The latter two have been ascribed to a collision scenario, while the origin of the former (the sinuous) has not yet been identified experimentally. A possible cause might be Streak-Transient growth as described in [?]. In figure 2 two PIV-results are depicted which show the typical flow-field of the collision related breakdown. The top-figure shows the signature of a symmetric collision: low-speed islands embraced by symmetrically oscillation high-speed streaks. This leads to the generation of patches of low-speed fluid with a spanwise size and streamwise repetition rate very similar to the model structures for a phase-shift $\Delta\phi=\pi$. The same goes for the bottom figure 2. In this case the collision is asymmetric which leads to the single branches of low- and high-speed fluid entraining the streaks. Again, the size, structure and repetition rate of the fluctuations strongly resembles the model structures now at the phase-shift $\Delta\phi=\pi/2$.

References

[1]   Brandt L, Schlatter P, Henningson DS, Transition in boundary layers subject to free-stream turbulence, *J. Fluid Mech.*, 517:167-198, 2004.

[2]   Hoepffner JPJ, Brandt L, Henningson DS, Transient growth on boundary layer streaks, *J. Fluid Mech.*, 537:91-100, 2005.

[3]   Lundbladh A, Berlin S, Skote M, Hildings C, Choi J, Kim J, Henningson DS, An efficient spectral method for simulation of incompressible flow over a flat plate, *Techn. Report* 1999; KTH/MEK/TR-99/11-SE, KTH, Department of Mechanics, Stockholm.

[4]   Mans J, Streak development and breakdown during bypass-transition, *PhD-thesis* 2007; Technische Universiteit Eindhoven.
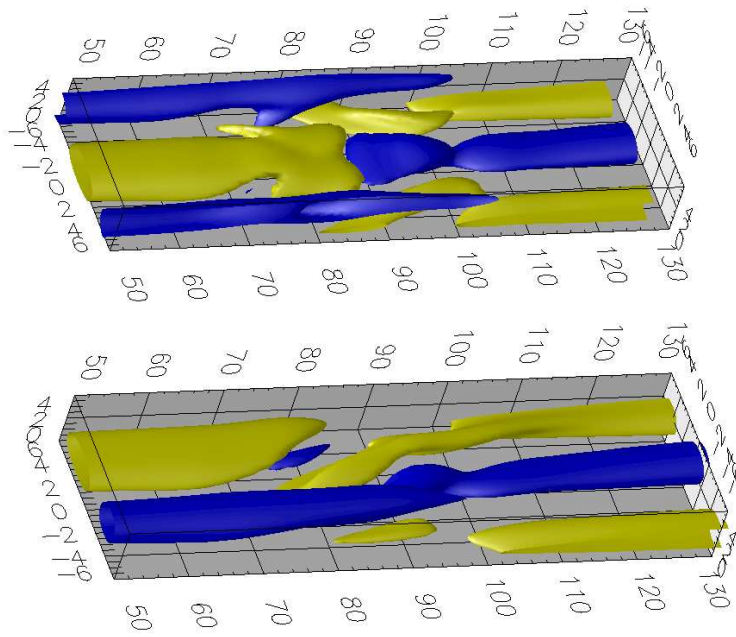
Figure 1: The structures of the streaks for $\Delta\phi = \pi$ (top) and $\Delta\phi = \pi/2$ (bottom), depicted are the low- ($u-u_{blas}$=-0.1:blue) and high- ($u-u_{blas}$=0.1:yellow) speed streak.
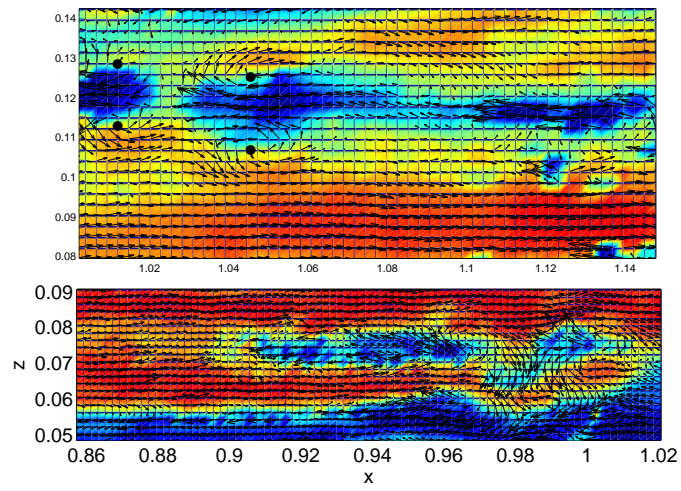

Figure 2: The PIV-results of varicose (top) and single branch (bottom) breakdown

3

Numerical study of the stabilisation of Tollmien-Schlichting waves by finite amplitude streaks

P. Schlatter[1], H.C. de Lange[2], and L. Brandt[1]

[1] KTH Mechanics, 100 44 Stockholm, Sweden

[2] TUE Mechanical Engineering, 5600MB Eindhoven, The Netherlands

1   Introduction

The reduction and control of the viscous drag force exerted on thin bodies moving in a fluid is of great technical interest. Several active and passive methods to achieve a delay of laminar-turbulent transition have been developed in the past. The study by Cossu and Brandt [1] showed the stabilisation of the Tollmien-Schlichting (TS) waves by steady streaks of finite amplitude in the Blasius boundary layer. In the presence of streaks, the unstable TS-waves evolve from two-dimensional waves to spanwise modulated waves, referred to as streaky TS-waves. They have similar phase speed as their two-dimensional counterpart and are less unstable. The experiments in Ref. [2] confirmed the theoretical predictions and demonstrated that such a stabilising effect can indeed lead to transition delay [3]. In this study, we perform a numerical study of such a stabilisation in a realistic framework in order to investigate the effect of streaks of varying amplitude, spacing, and the corresponding sensitivity of the transition delay. In particular, the evolution of perturbations at low streak amplitudes is considered.

2   Simulation Approach

The presented simulation results are obtained using a spectral method to solve the three-dimensional, time-dependent, incompressible Navier-Stokes equations [5]. The periodic boundary conditions in streamwise direction are combined with a spatially developing boundary layer by the implementation of a "fringe region". In this region, the flow is forced to the prescribed inflow velocity field, which in this case consists of a Blasius boundary layer profile (zero-pressure gradient) with added optimal streaks (see below). The inflow is at Reynolds number $Re_{\delta_0^*} = U_\infty \delta_0^* / \nu = 300$, where ν is the fluid viscosity, U_∞ the free-stream velocity and δ_0^* the displacement thickness at the inlet. The simulation box has dimensions $L_x \times L_y \times L_z$ equal to $2000 \times 60 \times 180$ in the streamwise, wall-normal and spanwise directions, made non-dimensional based on δ_0^*. Results are obtained with a resolution $N_x \times N_y \times N_z$ of $512 \times 121 \times 128$ grid points. With this resolution the use of large-eddy simulation (LES) is necessary to obtain accurate results. For this purpose the ADM-RT model is employed, which was found to be well suited for spectral simulations of transitional flows [6].

TS-Wave Generation. The TS-waves are forced at $Re_x = 60000$ by a harmonic volume force acting in the wall-normal direction at a non-dimensional frequency $F = 120$, corresponding to $\omega_0 = 0.036$. The rms-TS amplitude at branch I is approximately 0.76%. Small-amplitude steady, spanwise random noise is also introduced. This will trigger K-type transition shortly after branch II if no control is applied. Figure 1 displays the wall-normal velocity profile slightly after branch I in comparison with linear stability theory (LST), and the growth rate of the wall-normal maximum of the streamwise velocity fluctuation compared to results from solving the parabolic stability equations (PSE). Good agreement is obtained for both the velocity profile and the growth rate.

Streak Generation. The complete velocity vector field obtained with the linear code developed in Ref. [4] is used to force the desired streaky perturbation at the inflow of the computational domain. These streaks are introduced in the fringe region by adding them to the inflow Blasius profile. The streaks considered are optimally growing perturbations, i.e. solution of the linearised boundary-layer equations, and are characterised by the spanwise wavenumber $\beta_0 = 2\pi 10/L_z$ and the streamwise location of their maximum amplitude ($Re_x \approx 250000$). The latter values are chosen to approximatively match the streaks in the experiments [2]. Four values of the initial streak amplitude have been considered so far; they give rise to steady modulations of the boundary-layer flow at the inlet of maximum amplitude $A_{st} = \frac{1}{2}\max_y(u_{max} - u_{min})/U_\infty$ of 10%, 5%, 2.7% and 2%, respectively.

3   Results

Several LES using the above setup have been performed. Simulation results obtained by averaging in time and in the spanwise direction are displayed in figure 2 to quantify the transition delay obtained

1

in the presence of the steady streaks. The uncontrolled reference case is given by the two-dimensional forcing at $F = 120$ (exciting two-dimensional TS-waves) and a steady forcing random in the spanwise direction (leading to K-type breakdown). When increasing the streak amplitude, transition location moves monotonically downstream. The skin-friction coefficient c_f remains at the laminar value for the two cases with streaks of largest amplitude, an increase of c_f by a few percent being only observable where they reach their peak amplitude. The explanation for the observed stabilisation is provided in figure 2b) where the shape factor H_{12} associated to the base flows under consideration is reported. The presence of the streaks progressively reduces the value of H_{12} in the initial laminar region thus stabilising the flow.

Analysis of the spectral content of the velocity fields has been performed by Fourier transforming a number of full velocity fields in time and in the spanwise direction, where modes are denoted by (ω, β)-pairs in the following. The results are presented in figure 3 for two streak amplitudes, $A_{st} = 10\%$ and 2.7%. The case of streak amplitude of 2.7% (figure 3a)) highlights a new physical phenomenon observed at those low streak amplitudes: Initially, the $(0, \beta_0)$ streaky mode is dominating, reducing the growth of the streaky TS-waves $(\omega_0, 0 \ldots 2\beta_0)$. (Comparison with the uncontrolled case is not shown here due to lack of space.) Further downstream, $Re_x > 4 \cdot 10^{-5}$, however, a significant growth of oblique modes (ω_0, β_0) is seen. This induces, by nonlinear interactions, a strong amplification of the steady $(0, 2\beta_0)$ mode, i.e. a doubling of the initial streaks is observed (see also the visualisation in figure 4). Towards the end of the domain, also a growth of the mode $(\omega_0, \beta_0/3)$ can be observed, possibly leading to breakdown after the outflow boundary. For the largest streak amplitude considered in figure 3b), the fundamental streak can be seen as the only dominant mode. Both the two-dimensional and oblique TS-waves are quickly damped, and the first harmonic of the streak $(0, 2\beta_0)$ remains as the second largest mode.

Instantaneous flow visualisations are shown in figure 3 for three streak amplitudes, $A_{st} = 0\%$, 2.7% and 10%. Aligned Λ-structures, typical of the K-type scenario, can be seen in the uncontrolled case. For low spanwise modulations, the splitting of the initial streak mentioned above is clearly visible in the rear third of the domain. Amplification of oblique modes is observed at the end of the computational domain, suggesting transition of the new streaky base flow $(0, 2\beta_0)$ just downstream of the outflow. For the largest streak amplitude, the growth of the TS-waves is quenched in agreement with the experimental findings, and a clean streaky flow with slowly decaying streak amplitude is seen.

4 Conclusions and Outlook

The experimental results presented in Ref. [3] have been successfully reproduced in our numerical simulations using LES. We are indeed able to show the stabilising effect of finite amplitude steady streaks on the TS-waves and the following transition delay in a realistic numerical setup. The effect of varying the streak amplitude is analysed, and a new phenomena is outlined at low streak amplitudes where more complicated nonlinear interactions are obviously possible. In view of the full paper, we intend to examine the response of the boundary layer to fully three-dimensional excitations, an important study which was not carried out in the experiments. Further, we will consider time-periodic forcing of increasing amplitude in order to gain more understanding on the breakdown of the streaky TS-waves. Additionally, the influence of a varying streak spacing onto the stabilising effect shall also be considered.

References

[1] C. Cossu and L. Brandt. Stabilization of Tollmien-Schlichting waves by finite amplitude optimal streaks in the Blasius boundary layer. *Phys. Fluids*, 14(8):L57–L60, 2002.

[2] J. H. M. Fransson, L. Brandt, A. Talamelli, and C. Cossu. Experimental study of the stabilization of Tollmien-Schlichting waves by finite amplitude streaks. *Phys. Fluids*, 17(054110):1–15, 2005.

[3] J. H. M. Fransson, A. Talamelli, L. Brandt, and C. Cossu. Delaying transition to turbulence by a passive mechanism. *Phys. Rev. Lett.*, 96(064501):1–4, 2006.

[4] O. Levin and D. S. Henningson. Exponential vs algebraic growth and transition prediction in boundary-layer flow. *Flow Turbulence Combust.*, 70:183–210, 2003.

[5] A. Lundbladh, S. Berlin, M. Skote, C. Hildings, J. Choi, J. Kim, and D. S. Henningson. An efficient spectral method for simulation of incompressible flow over a flat plate. Technical Report TRITA-MEK 1999:11, KTH Stockholm, Sweden, 1999.

[6] P. Schlatter, S. Stolz, and L. Kleiser. LES of transitional flows using the approximate deconvolution model. *Int. J. Heat Fluid Flow*, 25(3):549–558, 2004.
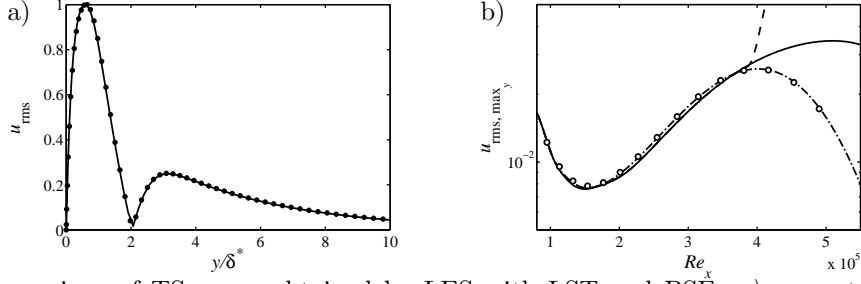
Figure 1: Comparison of TS-waves obtained by LES with LST and PSE. a) u_{rms} at $Re_x = 216000$, ——LES, • LST. b) Wall-normal maximum of u_{rms} for ----uncontrolled case with random 3D disturbances, ——2D nonlinearly-saturated TS-wave, —·—linear low-amplitude TS-wave (rescaled), ○ PSE.
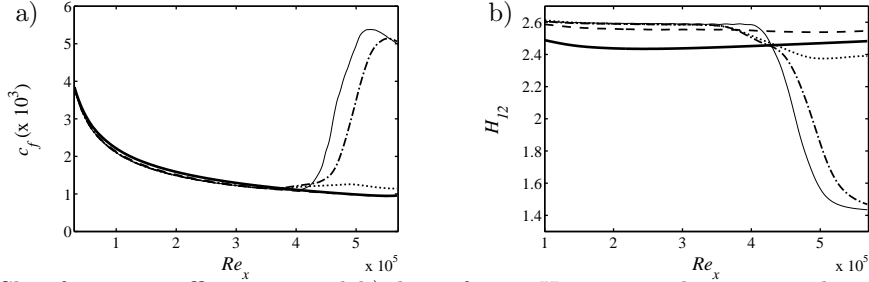

Figure 2: a) Skin friction coefficient c_f and b) shape factor H_{12} averaged in time and spanwise direction. ——$A_{\mathrm{St}} = 10\%$, ----$A_{\mathrm{St}} = 5\%$, ······· $A_{\mathrm{St}} = 2.7\%$, —·—$A_{\mathrm{St}} = 2\%$, ——$A_{\mathrm{St}} = 0\%$ (uncontrolled).
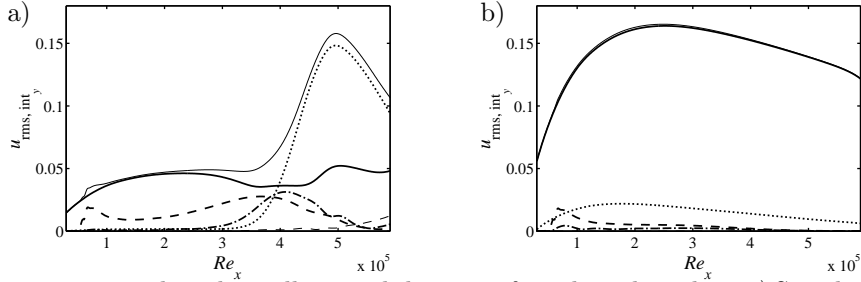
Figure 3: Energy integrated in the wall-normal direction for selected modes. a) Streak amplitude 2.7%. b) Streak amplitude 10%. ——Steady streak $(0, \beta_0)$, ----TS-wave $(\omega_0, 0)$, ······· first harmonic of streak $(0, 2\beta_0)$, —·—first harmonic of streaky TS-wave (ω_0, β_0), ----oblique mode $(\omega_0, \beta_0/3)$, ——sum of all displayed modes.
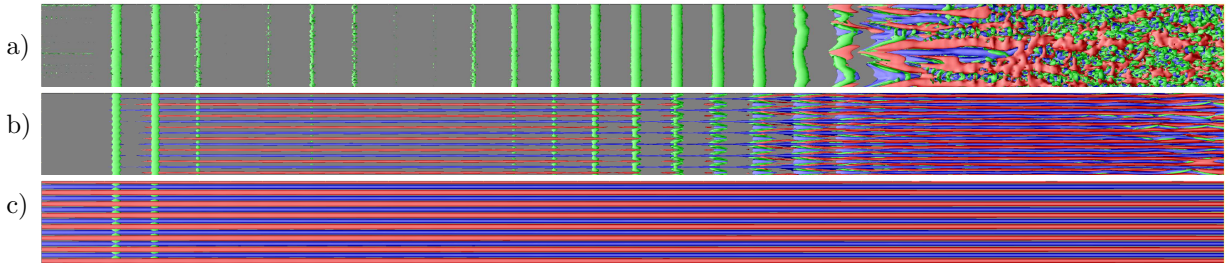

Figure 4: Top view of the three-dimensional flow structures for a) the uncontrolled case $A_{\mathrm{st}} = 0\%$, b) $A_{\mathrm{st}} = 2.7\%$, and c) $A_{\mathrm{st}} = 10\%$. Green isocontours represent the λ_2 vortex-identification criterion, red and blue isocontours are positive and negative disturbance velocity, respectively. Flow from left to right.

Performance of reduced-order models of fluid systems

Shervin Bagheri & Dan Henningson

Linné Flow Centre, KTH Mechanics

SE-100 44 Stockholm, Sweden

The discretization of the Navier-Stokes equations leads to a large-scale model with at least a couple of million of unknowns. Therefore, it is not suitable for a specific application, such as stability analysis, optimization or for control design. However, for each application, there exist certain features of the flow dynamics that are much more important than others. Often, these features can be preserved in a reduced-order model. One common way of obtaining a reduced-order model is based on projecting the field onto a very small subspace which only contains the essential dynamics of interest. Three sets of vectors than span different subspaces and thus are appropriate for different tasks are Global, POD and Balanced modes (Figure 1).

We show, using a model equation for non-normal and non-parallel fluid systems, the linear Ginzburg-Landau equation, the performance and limitations of reduced-order models for different applications. For example, to construct an efficient reduced-order controller, which is successful in suppressing disturbances, it is necessary that the actuator and sensor can be expressed with a few modes only. Consequently,
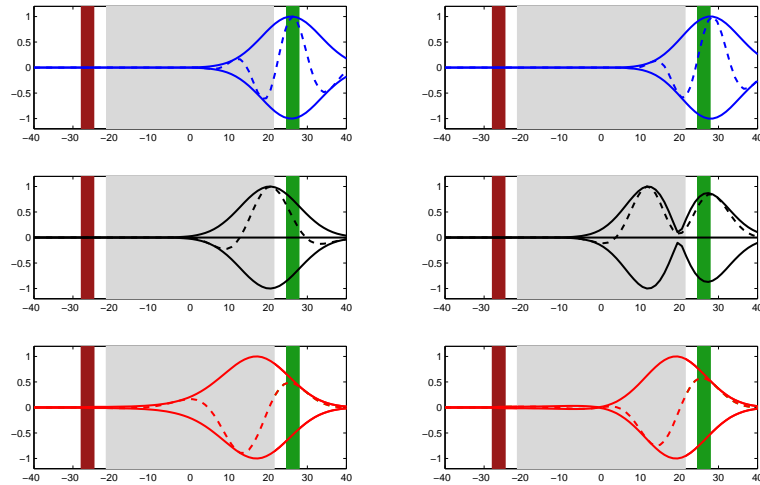

Figure 1: The first and second Global (top plots), POD (middle plots) and Balanced modes (bottom plots). The shaded region marks the spatial domain of the flow where disturbances grow exponentially. The green and red bars mark 99% of the spatial support of the actuator and sensor respectively.
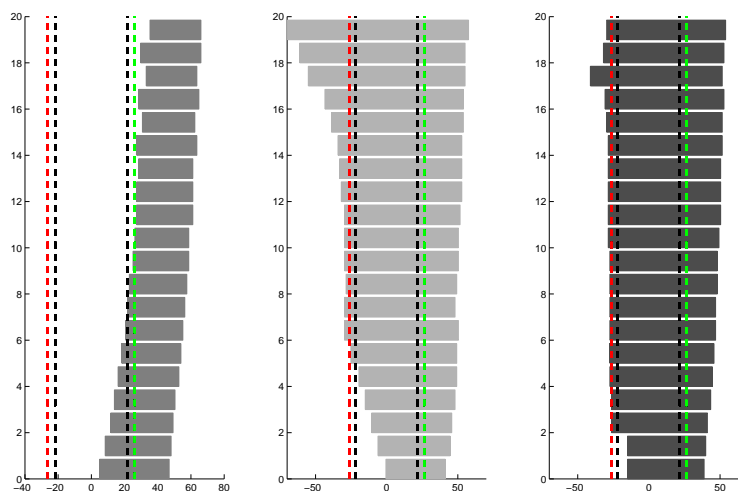
Figure 2: The spatial support (defined as region where the amplitude of a mode is larger than 99% of it maximum amplitude) of the 20 first Global (left), POD (middle) and Balanced (right) modes. The convective unstable domain is marked with dashed black lines, the actuator and sensor location are marked with dashed green and red lines, respectively.

the location of the actuator and sensor should be within the subspace spanned by the given modes. Similarly, when computing the optimal transient growth of disturbances in non-normal flows, it is necessary that the subspace spanned by the given modes contain the convective unstable domain of the flow, as illustrated in Figure 1 and 2. Finally, for large-scale problems, iterative techniques such as the Arnoldi algorithm are required to compute different modes. We will show some preliminary results of modes obtained by such techniques from high-dimensional problems arising from the discretization of Navier Stokes equations.

Feedback control and estimation applied to boundary layers subject to free-stream turbulence

A. Monokrousos, L. Brandt, P. Schlatter, and D. S. Henningson

Linné Flow Centre, KTH Mechanics, SE-100 44 Stockholm, Sweden

Control of wall-bounded transitional and turbulent flows is examined in the present investigation owing to the high potential benefits in technical applications. Any reduction of the frictional drag, for example, implies relevant savings of the operational cost of commercial aircrafts and cargo ships. Recently, much effort has been put in the combination of computational fluid dynamics and control theory. While early attempts of flow control were based on physical intuition or on a trial-and-error basis, more systematic approaches are now followed.

A linear model-based feedback control approach, that minimises an objective function which measures the perturbation energy, can be formulated where the Orr-Sommerfeld and Squire equations model the flow dynamics. The latter equations describe the linear development of perturbations evolving in a parallel base flow. The requirement implicit in this formulation is the need of complete state information. However, the control problem can be combined with a state estimator to relax this requirement. The so-called Kalman and extended Kalman filter have been implemented in order to reconstruct the flow in an optimal manner by only considering measurements of the pressure and the streamwise and spanwise shear stresses on the wall.

Previous studies have shown the importance of physically relevant stochastic models for the estimation problem which turns out to be crucial for fast convergence [3]. Such stochastic noise needs to describe accurately enough the unmodelled dynamics, like uncertainties and nonlinearities. Based on these models the estimator is shown to work for both infinitesimal as well as finite amplitude perturbations in direct numerical simulations.

Here, the combined control and estimation problem, also referred to as a compensator, is applied to spatially developing boundary layers as in [2], where the compensator is shown to reduce the perturbation energy of both modal and non-modal disturbances. The linear control, in the form of wall blowing and suction, is applied to transitional flow in boundary layers exposed to high levels of free-stream turbulence [1], a flow characterised by strong nonlinear interactions. In the presence of free-stream turbulence intensities of 1% or more transition occurs rapidly, bypassing the classical scenario triggered by the viscous, thus slower, exponential amplification of unstable Tollmien-Schlichting waves. The former scenario, denoted bypass transition, is characterised by the appearance inside the boundary layer of streamwise elongated streaky structures of alternating high and low streamwise velocity. As these streaks grow downstream, they undergo wavy motions which precede the breakdown into regions of intense randomised flow, turbulent spots. The spots grow in size and merge until the flow is fully turbulent. This scenario was chosen since it closely resembles, though on a larger scale, the near-wall dynamics of a turbulent flow and it is therefore an ideal test configuration. Being our work purely numerical at this stage, in a control experiment two velocity fields are marched simultaneously forward in time. One represents the actual flow where measurements are taken and the other the estimator in which the flow is reconstructed through the forcing based on the measurements. The latter simulation can be very expensive for highly nonlinear flows. In order to reduce the computational cost of the estimation, the use of Large-Eddy Simulation (LES) was introduced as a means for model reduction. In LES only the large energy-containing eddies are simulated, while the effect of the small scales is modelled (sub-grid scale stresses). The use of LES can reduce the cost of the computation of the estimated flow to about 1%. The use of LES has been first validated in a series of simulations where full-information control is applied (see figure 1). At the present stage, we have been able to tune the estimation and control parameters in order to achieve a satisfactory performance both in term of the estimation error and the actual reduction of disturbance growth in the real flow field.

The presented simulation results are obtained using a spectral method to solve the three-dimensional, time-dependent, incompressible Navier-Stokes equations. The periodic boundary conditions in stream-wise direction are combined with a spatially developing boundary layer by the implementation of a "fringe region". In this region, the flow is forced to the prescribed inflow velocity field, which in this case consists of a Blasius boundary layer profile (zero-pressure gradient) with additional free-stream turbulence. The ADM-RT model, which was found to be well suited for spectral simulations of transitional flows [4], is employed as sub-grid scale model in the LES.

The inflow is located at Reynolds number $Re_{\delta_0^*} = U_\infty \delta_0^*/\nu = 300$, where ν is the fluid viscosity, U_∞ the free-stream velocity and δ_0^* the displacement thickness at the inlet. The level of free-stream turbulence considered in a first set of simulations was set to $Tu = 4.7\%$, which leads to turbulent breakdown at $Re_x \approx 250000$ (uncontrolled). However the non-linearity of the disturbances within that flow is very strong. Since our control method is based on linear theory, we decided to complement our study with an additional case with $Tu = 3\%$. There, transition is expected to occur at $Re_x \approx 10^6$. For both turbulence intensities the simulation boxes used have dimensions long enough to accommodate the relevant flow evolution related to disturbance growth and transition. The LES resolution was chosen in agreement with previous studies in transitional incompressible flow [4].

Control is applied by blowing and suction through a slit at the wall. For the case with $Tu = 4.7\%$ the control is located in the range $Re_x \in [5 \times 10^4, 1.5 \times 10^5]$. The target laminar profile is the parallel Blasius profile extracted at $Re_x = 6.7 \times 10^4$. Such a location, close to the beginning of the control region, has been chosen since preliminary studies showed it to give a better performance. However for the case with $Tu = 3\%$ a measurement strip must be included upstream of the control region. Thus the control region is moved downstream and is located in the range
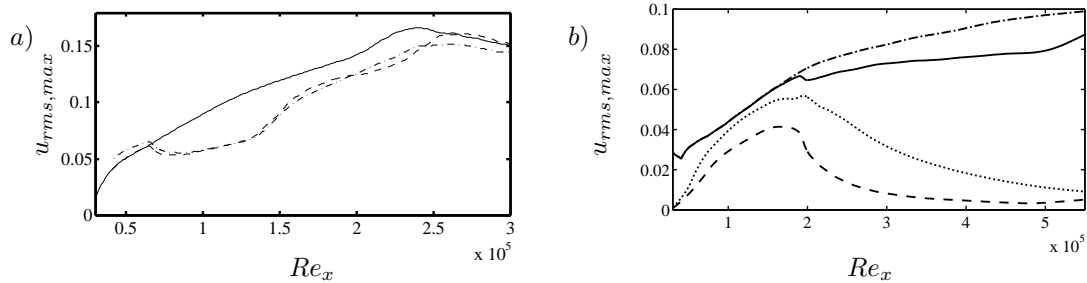
Figure 1: Wall-normal maximum of the streamwise velocity fluctuations. *a)* Full information control with $Tu = 4.7\%$. ——— no control, controlled with ----LES and —·—DNS. *b)* Compensator with $Tu = 3\%$. —·—Statistics from the uncontrolled run, ——— of the compensated run, ----control applied to the estimated flow, ··· uncontrolled flow of the estimator.
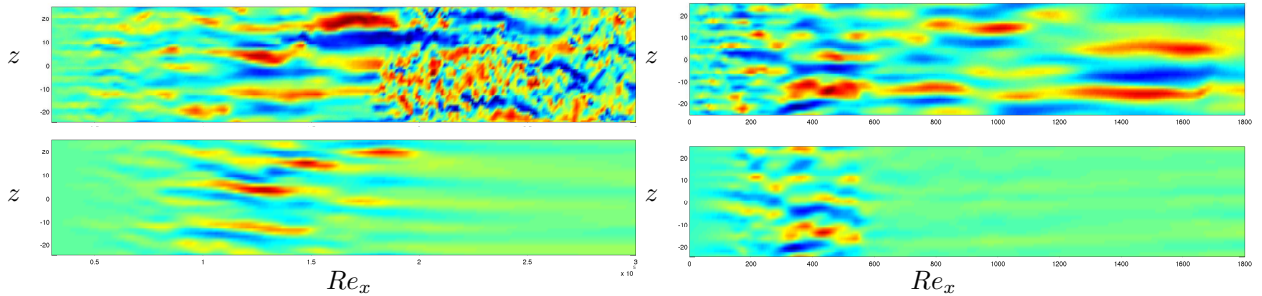

Figure 2: Streamwise velocity perturbation in a plane parallel to the wall at $y/\delta_0^* = 2$ for *(left)* $Tu = 4.7\%$ and *(right)* $Tu = 3\%$. The top row depicts the actual flow where the measurements are taken (uncontrolled for $Tu = 4.7\%$ and compensated for the $Tu = 3\%$ case), whereas the bottom row shows the estimated velocity field. Red indicates positive perturbation velocity and blue negative.

$Re_x \in [1.6 \times 10^5, 2.7 \times 10^5]$ while the measurements region in the range $Re_x \in [4.5 \times 10^4, 1.5 \times 10^5]$.

Figure 1 displays a comparison between the two turbulence intensities as well as LES and DNS results. The wall-normal maximum of the streamwise velocity fluctuations can be considered as a good measurement of the streak amplitude within the boundary layer and thus indicate the performance of a control technique. In figure 1a) the comparison between DNS and LES confirms the accuracy and reliability of the LES method with respect to the DNS. It can be seen that the control is able to delay transition by quenching the streak growth in the region where it is active. A study of the control/compensator efficiency in comparison with the uncontrolled case using LES is depicted in figure 1b). It can be seen that control acting on the estimated field is able to completely damp the wall streaks. Additionally, the control applied to the real flow (compensated run) leads to a reduction of the streak growth after the control region.

The performance of the estimator and compensator is shown by figure 2 for an instantaneous snap shot. The velocity field from the real flow, where the wall measurements are taken, is depicted in the top part, whereas the estimated velocity is displayed in the bottom figure. Similar conclusion as already given for the above figure 1 are confirmed. The shape and strength of the streaks within the measurement region is reproduced fairly well by the estimator. Additionally, control acting on the estimator seems to be very efficient. Whereas in the real flow the control is able to damp the streaks only within and closely after the control region, the streaks seem to reappear towards the end of the computational domain due to continuous forcing by free-stream modes.

Presently further improvement of the estimator is performed. Stability issues still plague the estimated flow limiting the strength of the estimator forcing. This issues are investigated and addressed and once they are resolved a significant improvement of the estimator performance is expected leading to an effective compensation.

The authors wish to thank E. Åkervik, J. Hœpffner, and M. Chevalier for many fruitful discussions.

References

[1] L. Brandt, P. Schlatter, and D. S. Henningson. Transition in boundary layers subject to free-stream turbulence. *J. Fluid Mech.*, 517:167–198, 2004.

[2] M. Chevalier, J. Hoepffner, E. Åkervik, and D. S. Henningson. Linear feedback control and estimation applied to instabilities in spatially developing boundary layers. *J. Fluid Mech.*, 2006. Submitted.

[3] J. Hoepffner, M. Chevalier, T. R. Bewley, and D. S. Henningson. State estimation in wall-bounded flow systems. Part 1. Perturbed laminar flows. *J. Fluid Mech.*, 534:263–294, 2005.

[4] P. Schlatter, S. Stolz, and L. Kleiser. LES of transitional flows using the approximate deconvolution model. *Int. J. Heat Fluid Flow*, 25(3):549–558, 2004.

Tollmien-Schlichting wave cancellation using an oscillating Lorentz force

Thomas Albrecht[1], Hans Metzkes[1], Gerd Mutschke[2], Roger Grundmann[1], Gunter Gerbeth[2]

[1]Institute for Aerospace Engineering,
Technische Universität Dresden, 01062 Dresden, Germany

[2]MHD Department, Institute of Safety Research,
Forschungszentrum Dresden, P.O. Box 51 01 19, 01314 Dresden, Germany

1   Introduction

Following the principle first published by Milling[1], a Tollmien-Schlichting (TS) wave can be cancelled by superposing a counter-phased wave, hence delaying laminar-turbulent transition. Attracted by the rather low control power demands (compared to mean velocity profile modification), many numerical and experimental works appeared since then, e.g. [2, 3]. If the fluid under consideration is low conductive, such as seawater with an electrical conductivity $\sigma \approx 5\,\mathrm{S/m}$, a Lorentz force acting directly within the fluid is able to control the flow. Driven by an external electric field, almost arbitrary time signals may be generated. Unfortunately, the Lorentz force resulting from a Riga plate shown in Fig. 1(left) is inhomogeneous in spanwise direction. In the present study, we investigate the feasibility of this force for wave cancellation by Direct Numerical Simulation.

2   Lorentz force actuation

A Lorentz force $\boldsymbol{F} = \boldsymbol{j} \times \boldsymbol{B}$ arises from magnetic induction $\boldsymbol{B}$ and electric current density $\boldsymbol{j}$. The latter is described by Ohm's law in moving media $\boldsymbol{j} = \sigma(\boldsymbol{E} + \boldsymbol{u} \times \boldsymbol{B})$, where $\boldsymbol{E}$ and $\boldsymbol{u}$ denote the applied electric field and the velocity field, respectively. When assuming $\boldsymbol{B} \approx 1T$ and $u \approx 1m/s$, due to the low conductivity, the induced current density $\sigma(\boldsymbol{u} \times \boldsymbol{B})$ is insufficient to generate a reasonable Lorentz force. Hence, an external electric field has to be applied which dominates the equation. Given the actuator design of the Riga plate, and neglecting the induced current density, the electric and magnetic fields can be computed decoupled from the velocity field during pre-processing. Being inhomogeneous in spanwise direction with strong peaks appearing above the electrode's and magnet's edges, the resulting force has significant wall-normal and spanwise components near the actuator's ends, but is mostly streamwise oriented in the middle. Its decay in wall-normal direction is approximately exponential and scales with the actuator's stripe size a. The force oscillates sinusoidally in time using the TS wave frequency, while the streamwise extend is adjusted to one half of the TS wave length. For 2d calculations, we use a spanwise averaged force.

3   Results

Artificial disturbances are introduced near the inflow boundary by means of an body force oscillating at a dimensionless frequency $F^+ = 108$. The Reynolds number is 585, based on the inflow displacement thickness. Fig. 1(right) shows the location of the computational domain, including disturbance input and actuation, relative to the neutral stability curve.

Plotted in Fig. 2, the uncontrolled TS wave ($Z = 0$, dotted line) grows until it reaches branch II of the neutral stability curve at $x = 381$ (local Re = 1193), which is in agreement to linear stability theory (LST). Beyond this point, it decreases again. During many 2d calculations using a spanwise averaged force, we adjusted amplitude, penetration depth, and phase φ of the actuation to minimize the remaining TS wave amplitude. Results are shown by the dashed line: downstream of the actuation at $-9 \leq x \leq 9$, the amplitude gradually reduces by more than an order of magnitude. When applying the more realistic, inhomogeneous force (3d case, solid lines) at the same conditions a, Z, φ, the TS wave is no longer purely two-dimensional after actuation, but modulated in spanwise direction. To determine its amplitude and two-dimensionality, we extracted the $\hat{u}_{rms}$-value from the peak plane $z = 0$ (named peak amplitude in the following) and performed spanwise FFT's at these $\hat{u}_{rms}$ (x,y)-positions, respectively. For clarity, only the first three non-zero modes are shown. Similar to 2d, the mean wave amplitude (mode 0) reduces during actuation, but higher modes initially rise from zero to almost the same level as mode 0, thus indicating a highly three-dimensional TS wave, and actually *increasing* the peak amplitude temporarily. For $x > 30$, however, all modes decrease, and the higher modes quickly settle down around 10^{-7}. Finally, at $x \approx 180$, the TS wave can be considered two-dimensional again, further evolving as predicted by LST.

Given the low amplitude $\hat{u}_{rms} < 10^{-2}$ of the TS wave (streamwise mode 0), the flow is secondary stable, where spanwise modes decay. Hence the three-dimensionality of the cancelling wave degrades the actuator's performance only slightly, and the for both 2d and 3d case, the wave amplitude is reduced by more than 90%.

References

[1] R. W. Milling. Tollmien-Schlichting wave cancellation. *Phys. Fluids*, 24(5):979 − 981, 1981.

[2] H. W. Liepmann and D. M. Nosenchuck. Active control of laminar-turbulent transition. *J. Fluid Mech.*, 118:201–204, 1982.

[3] V. V. Kozlov and V. Y. Levchenko. Laminar-turbulent transition control by localized disturbances. In *Turbulence Managment and Relaminarisation*. Springer Verlag, 1987. IUTAM-Symposium, Bangalore, India, 1987.
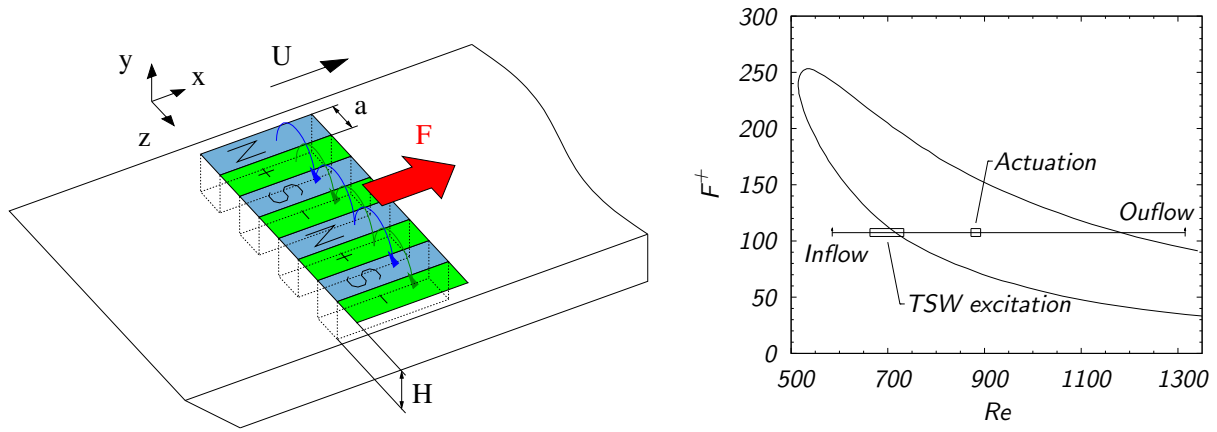
Figure 1: Actuator design (left) and position of computational domain relative to neutral stability curve (right).
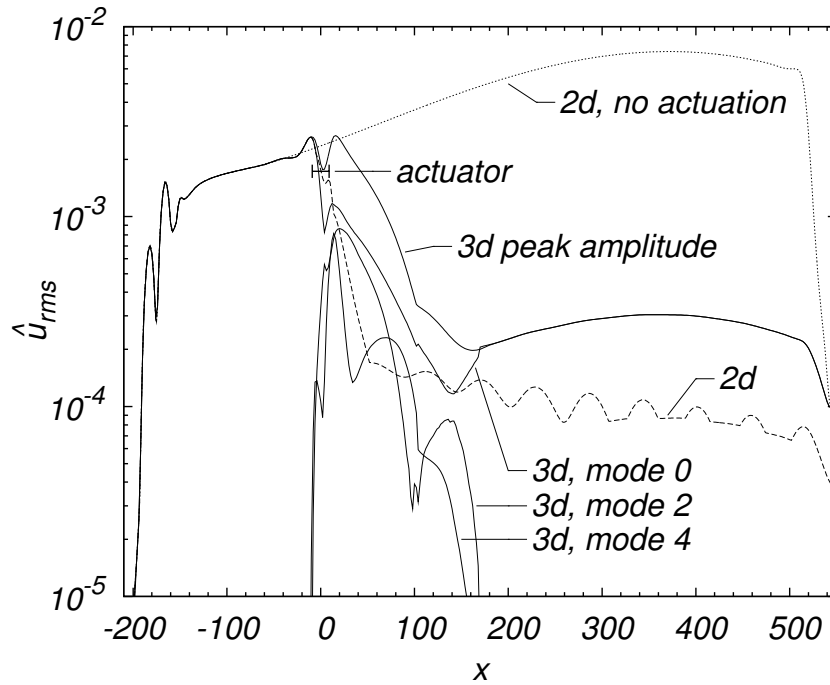

Figure 2: TS wave amplitudes vs. downstream coordinate x.

3

Experimental and Numerical Investigation of the Transition Delay Using Plasma Actuators
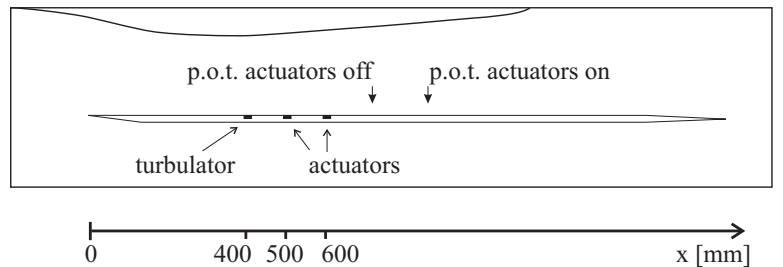
Sven Grundmann, Jochen Kriegseis, Cameron Tropea

Institute of Fluid Mechanics and Aerodynamics
Technical University of Darmstadt

In the present work plasma actuators were applied in a flat-plate boundary layer with an adverse pressure gradient to influence the transition of the boundary layer. One actuator $400\,mm$ downstream of the leading edge imparts perturbations into the boundary layer to promote transition. Two steady operating plasma actuators further downstream damp a mentionable amount of the perturbations which results in a delay of the transition.

Experimental Setup

The point of transition of a laminar boundary layer with zero pressure gradient at low speeds lies several meters downstream of the leading edge, which is longer than the plate used in our experimental setup. To realize transition at a shorter distance on the plate, an insert is placed on the roof of the wind tunnel, creating an adverse pressure gradient of $15\,Pa/m$. It is well-known that an adverse pressure gradient accelerates the natural transition process because the boundary-layer velocity profiles that develop allow a faster growth of Tollmien-Schlichting instabilities. A sketch of the experimental setup is shown in figure 1.

The first actuator, denoted turbulator, induces disturbances and is placed 400mm downstream of the leading edge, the position at which the adverse pressure gradient begins. And two plasma actuators follow at the positions $500\,mm$ and $600\,mm$. All experiments are conducted with a

Figure 1: Experimental and numerical setup

freestream velocity of $8\,m/s$ at the end of the test section. The turbulence intensity at the inlet of the test section is $T_i = 0.003$.
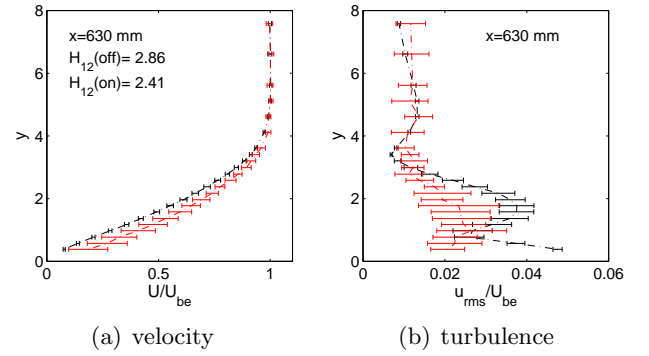
Electrical turbulator

In the first set of experiments a plasma actuator is used to induce perturbations into the boundary layer at $x = 400\,mm$. It is operated in pulsed mode with a modulation frequency of $55\,Hz$. The perturbations travel downstream and pass the two control actuators that damp their the amplitudes. Figure 2a shows the laminar boundary layer profiles behind the second control actuator. They show only slight difference but the profiles of the velocity fluctuations in figure 2b show that the turbulence level is reduced about a factor of two. Figure 2c shows the comparison of the velocity Profiles with and without control actuators operating. The uncontrolled boundary layer has already become turbulent while the controlled flow is still laminar. Figure 2d shows the developments of the shape factors of the controlled and the uncontrolled boundary layers. A delay of the transition of about $150\,mm$ is apparent.

(a) velocity　　(b) turbulence　　(c) velocity　　(d) Shape factor
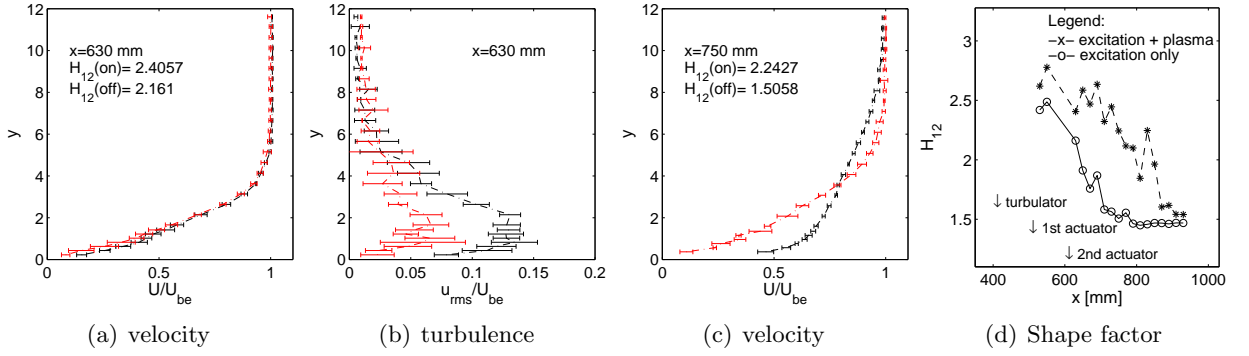
Figure 2: a,b,c velocity and turbulence profiles. Black lines: Control actuators off, red lines: Control actuators on. d: Shape factor with and without control actuators.

Mechanical turbulator

In a second set of experiments a mechanical turbulator is used to induce the perturbations. The turbulator in this case is a vibrating surface of $6\,mm$ length in streamwise direction. This has been done to proof that no electrical interferences between the electrical turbulator and the control actuators lead to a weaker performance of the electrical turbulator that could result in an apparent transition delay.

Figure 3a shows the velocity Profiles behind the second control actuator. A larger difference between the two profiles appears. It

(a) velocity　　(b) turbulence

Figure 3: Velocity and turbulence profiles. Black lines: Control actuators off, red lines: Control actuators on.

has been observed that the acceleration of the boundary layer by the control actuators decays faster with increasing turbulence in the boundary layer. The perturbations are much smaller than in the first experiments which leads to a stronger change of the velocity profile. The turbulence profiles in figure 3b show again a reduction of the perturbations. The perturbations generated by the vibrating surface have a clear sinusoidal distribution. Therefore the uncontrolled turbulence profile has a shape that allows the conclusion that very clean Tollmien-Schlichting-Waves travel in the boundary layer.


(a) time series　　(b) frequency spectrum
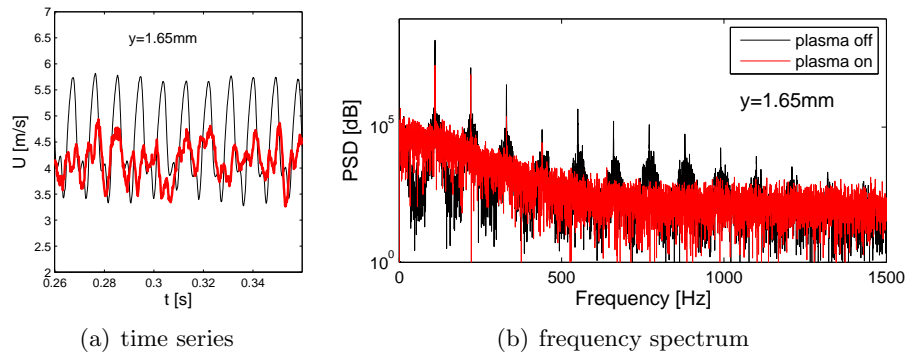
Figure 4: Time series and frequency spectrum of the velocity at a height of $y = 1.65\,mm$

Figures 4a and 4b show the time series and the power spectrum density of a measurement in a

2

height of $y = 1.65\,mm$ at the same position $x = 630\,mm$. The uncontrolled signal shows the TS-Waves while the controlled flow has a significantly smaller amplitude. The frequency spectrum shows that the amplification of the harmonics of the excitation frequency $(110\,Hz)$ is suppressed by the control actuators.

Numerical Results

A recently started numerical project shall accompany the experimental investigations. It is planned to improve an existing numerical model of the plasma actuator. Investigations performed with LES and DNS will help to understand the exact mechanism of the damping of perturbations. The numerical work continues previously published numerical investigations, which have predicted the delay of transition using plasma actuators. First investigations are performed with FLUENT using the beta version of the k-k_l-ω Model, which promises more accuracy in predicting transition using RANS. The results are presented in the following figures:

(a) x=530mm   (b) x=630mm   (c) x=870mm   (d) x=910mm
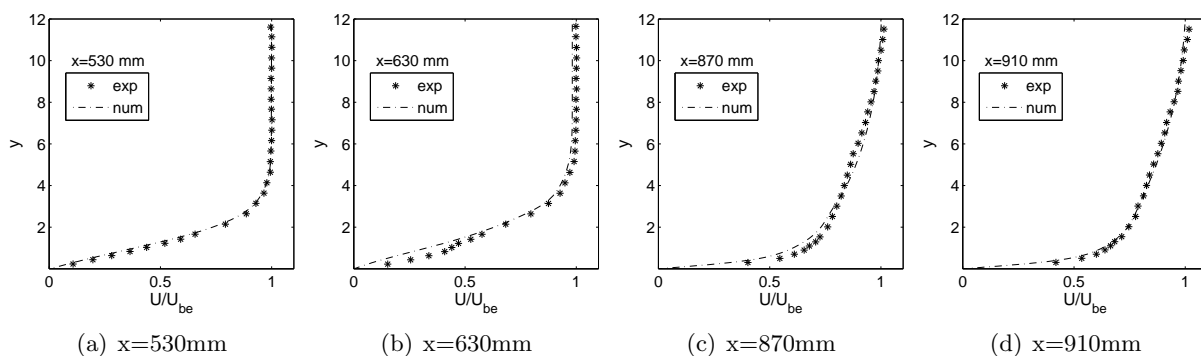
Figure 5: Comparison of the base flow on the test section without turbulator and control actuators

Figures 5a to 5d show the comparison of the base flow of the test section without turbulator and control actuators. The comparison between the velocity profiles from experiment and simulation show very good agreement, even with an adverse pressure gradient in the simulation domain. Current simulations are running to validate the actuator model that includes a source term for the kl equation additional to the source terms for the momentum equations.

Summary

The damping of disturbances using plasma actuators resulting in a delay of the transition from a laminar to a turbulent boundary layer has been shown experimentally. Two different ways of introducing perturbations into the boundary layer have been investigated. The successful generation of Tollmien-Schlichting-Waves and the damping of their amplitudes could be shown. First numerical results show very good agreement with the experimental results and promise to deliver valuable insights into the fluid mechanics of the plasma actuators.

Optimal Disturbances in Falkner-Skan-Cooke Boundary Layers

M. Byström[1], A. Hanifi[1,2], D.S. Henningson[1]

[1]*Linné Flow Centre, KTH, Dept. of Mechanics, SE-100 44 Stockholm, Sweden*
[2]*Swedish Defence Research Agency, FOI, SE-164 90 Stockholm, Sweden*

The algebraic growth of spanwise periodic, stationary disturbances with infinite wave length in the propagation direction is studied in the sub-critical Falkner-Skan-Cooke boundary layers. The optimal temporal linear growth in parallel swept boundary layers has earlier been studied by Corbett & Bottaro [2]. Our analysis are performed in a spatial framework where the non-parallel effects are included. A well-known, adjoint-based optimization procedure [1] is used to find the initial disturbances associated with the maximum energy growth. It is shown that these optimal disturbances take the form of tilted vortices in the cross-flow plane. The vortices give rise to tilted streaks of alternating high and low streamwise velocity (see Fig. 1).
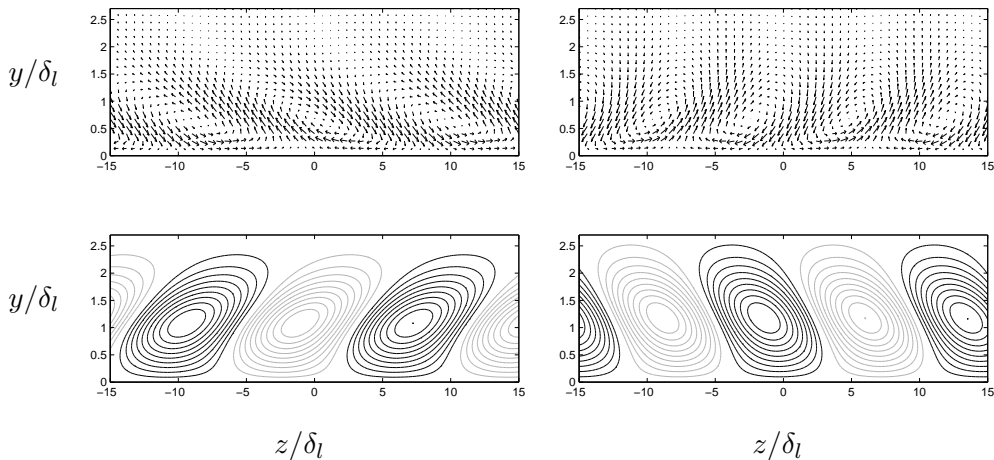

Figure 1: *Upper: Vector representation of initial optimal disturbances in the Falkner-Skan-Cooke boundary layers, projected onto the cross-flow plane. Lower: Downstream response to the optimal disturbances, contours of positive (black) and negative (grey) streamwise velocity in the cross-flow plane. Left: Favorable pressure gradient, $\beta_H = 0.1$. Right: Adverse pressure gradient, $\beta_H = -0.05$.*

Further, the streamwise interval was extended to include the supercritical part of the boundary layer. As the disturbances evolve downstream into this region, the algebraic growth growth pass over to exponential amplification. A comparison to calculations with parabolized stability equations
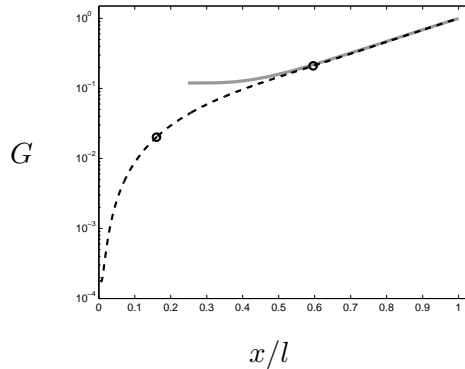
G

x/l

Figure 2: *Energy growth of the optimal disturbance (black dashed line), algebraic growth followed by exponential growth. Data from a PSE calculation of a cross-flow mode (grey line) with the same spanwise wavenumber, $\beta/\delta_l = 0.34$, is included for comparison.*

shows that the disturbances evolve into cross-flow modes in the supercritical flow. The disturbance shape does not undergo any dramatic changes as the disturbances evolve from the sub-critical to the super-critical flow. It is therefore concluded that similar physical mechanisms drive both the algebraic and the exponential instabilities.

References

[1] P. Andersson, M. Berggren, and D. Henningson, *Optimal disturbances and bypass transition in boundary layers*, Phys. of Fluids **11** (2001), 134.

[2] P. Corbett and A. Bottaro, *Optimal linear growth in swept boundary layers*, J. Fluid Mech. **435** (2001), 1–23.

Optimal spatial growth of swept-wing instabilities through multiple-scale analysis

JAN PRALITS AND PAOLO LUCHINI

Dipartimento di Ingegneria Meccanica , Università di Salerno, 84084 Fisciano (SA), Italia
jpralits@unisa.it, luchini@unisa.it

Transition from laminar to turbulent flow in boundary layers on swept wings is usually caused by perturbations with infinitesimal amplitude which grow as they propagate downstream. These perturbations are, insofar as convective instabilities, commonly analysed using spatial linear stability theory (LST) in order to obtain their respective growth rate and amplification. The growth rate is used to obtain from a multiple-scale approximation or parabolic stability equation, the integrated amplification over a spatial span and predict the point of transition. It is well know that in swept-wing flow the perturbations which first attain an amplification level which can cause transition are of inviscid type and usually denoted as crossflow vortices (CFV). These perturbations are due to the inflection point in the crossflow component of the mean flow which is caused by the influences of sweep and pressure gradient present in the flow. The CFV manifest themselves as stationary vortices aligned to within a few degrees of the local inviscid streamlines, on which travelling waves might be superimposed. The growth rate of the leading normal mode of the CFV, obtained using the Orr-Sommerfeld equation, in many cases manages well to compare with experiments. However, when the integrated amplification is sought, there are obvious doubts that a high frequency approximation, such as either multiple-scale analysis or parabolic stability equation is, can be applied to this type of perturbations which are inherently low or zero frequency. Nevertheless both modal and algebraic growth were studied by Corbett & Bottaro [1] in their investigation concerning optimal perturbations in swept-wing flows. They used the temporal framework with the mean flow approximated by Falkner-Skan-Cooke similarity solutions and showed that the most amplified disturbances take the form of vortices almost aligned with the external streamline, and later evolve into streaks. They also reported, for certain cases of adverse pressure gradient, that perturbations simultaneously undergo exponential and algebraic growth, and that the wavenumber region of maximum algebraic growth coincides with a region of maximum exponential growth.

The aim of the current work is twofold. First, to analyse the order of magnitude of the errors of a multiple-scale approximation as applied to crossflow instabilities and give a sounder theoretical basis to its use in transition prediction. Second, to apply an approach similar to Corbett & Bottaro[1] in a spatial framework and discuss the relative importance of algebraic and exponential contributions to the growth as far as transition prediction is concerned.

The results will be discussed with reference to a number of practical applications. These will include some of those cases which were denoted "pathological" in a past European project, with the aim to determine whether the algebraic component of amplification has a role in their behaviour.

References

[1] P. Corbett and A. Bottaro. Optimal linear growth in swept boundary layers. *J. Fluid Mech.*, 435:1–23, 2001.

Optimal perturbations of zero pressure gradient turbulent boundary layers

Gregory Pujals[1,2], Carlo Cossu[1] & Sebastien Depardon[2]

[1] *LadHyX, CNRS/École Polytechnique, F-91128 Palaiseau Cedex, France*
[2] *PSA Peugeot Citroën, Centre Technique de Velizy, 2 Route de Gisy, 78943 Vélizy-Villacoublay Cedex, France*

We compute the optimal perturbations of a zero pressure gradient turbulent boundary layer over a flat plate up to a Reynolds number, based on displacement thickness, of 20000. Two mean velocity profiles are used as basic flow: Musker's explicit closed-form expression, which is valid continuously from the wall up to the freestream (*AIAA J.* **17** 1979), and the experimental profiles of Österlund (*PhD Thesis*, KTH, 1999). The analysis of the Orr-Sommerfeld-Squire system with a non uniform turbulent eddy viscosity model reveals that, even if all the eigensolutions are damped, some perturbations may experience transient growth before decay. The optimal perturbations consist of spanwise periodic streamwise vortices which evolve into streamwise streaks. Two specific spanwise wavelengths of disturbances lead to local maximum energy amplification. One is found to scale with the boundary layer thickness. The other one scales with the typical width of near-wall streaks. These findings extend to the turbulent boundary layer profiles the results recently obtained for the turbulent plane Poiseuille flow by del Àlamo & Jiménez (*J. Fluid Mech.* **559** 2006).

Numerical investigation of the crossflow instabilities induced by a periodic roughness array on a swept cylinder : receptivity and stability study

E. Piot[*], G. Casalis[†]

A three-dimensional direct numerical simulation of the crossflow instabilities excited by surface roughness in a subsonic swept boundary layer is performed. A periodic roughness array is placed just upstream the first neutral point of a laminar boundary layer on a swept cylindrical leading-edge. A direct numerical simulation of the flow over this geometry is performed, and the obtained instabilities are studied and characterized with the help of the linear stability theory. The amplitude of the receptivity process is obtained with help of the biorthogonal decomposition method of Tumin [1], extended to a 2.5D base flow.

1   Geometry and numerical code

A cylinder whose radius is $R_c = 0.1$m, is swept at an angle $\varphi = 60°$ with respect to a uniform incoming flow with velocity magnitude $Q_\infty = 50$m/s. Two coordinates systems are shown in

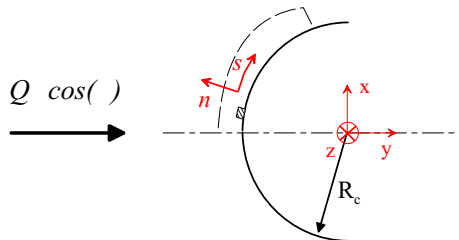

Figure 1: Swept cylinder geometry.

Figure 1. Velocity components in the global coordinates are denoted by u in the vertical (x) direction, v in the horizontal (y) direction, and w in the spanwise (z) direction. The incoming velocity is given by $[0, Q_\infty \cos(\varphi), Q_\infty \sin(\varphi)]$ in this coordinate system. Moreover, the cylinder is idealized as having infinite-span. In the body-fixed coordinate system, the arc-length along the surface of the cylinder is denoted by s, the distance normal to the surface by n, and z is again the spanwise direction. Velocity components in this coordinate system are denoted by v_s, v_n, and w for the s-, n-, and z- directions, respectively. To simulate the effects of a periodic roughness array, a single roughness element is meshed and periodic boundary conditions are imposed in the spanwise direction, while a standard no-slip condition is enforced at the wall surface. At the upper boundary, the non-reflective boundary condition developed by Thompson [2] is used to avoid numerical reflections, where the reference flow is the potential flow solution around a cylinder. On the $s = 0$ plane, a symmetry boundary condition is imposed, making it possible to compute only one half of the configuration. Finally, the outflow condition is treated thanks to the use of a sponge area (progressive stretching of the computational grid) which aims at damping the flow fluctuations before they reach the downstream boundary. If δ denotes the boundary layer thickness of flow along the attachment line, the roughness is a parallelepiped of nearly square cross section $(1.6\delta \times 1.625\delta)$ and its height is $h = 0.1\delta = 6.9\,10^{-5}$m. The roughness chordwise location is $s/R_c \approx 8°$. The

---

[*]PhD student, estelle.piot@onera.fr, ONERA DMAE.
[†]Research Engineer, gregoire.casalis@onera.fr, ONERA DMAE.

roughness element is resolved with $(5 \times 7 \times 9)$ points in the (s, n, z) directions, and 61 points are used within the boundary layer in the wall normal direction. A sensitivity study to the grid discretization in the n direction has shown that this mesh was fine enough to obtain converged results.

The Navier-Stokes equations are solved numerically using the multi-purpose ONERA solver sAbrinA. The numerical method relies on the use of high-order numerical schemes: the spatial scheme is a classical fourth-order accurate centered explicit finite difference discretization, while a compact explicit third-order accurate Runge-Kutta algorithm is used for time advancement. Since such a centered scheme is non-dissipative, it does not prevent the growth of spurious high-frequency numerical errors, and therefore requires a stabilization step. For that purpose, a tenth-order accurate symmetric linear filter is applied to the flow variables at each time step.

2 Results

Frist, the flow around the smooth cylinder is computed. This flow has been validated by comparison to the results of a boundary-layer code. The agreement is very good as soon as the DNS-computed wall pressure is used in the boundary layer code. This wall pressure differs from the potential flow one,which is due to the outflow treatment.

A direct numerical simulation is then performed for the case of a periodic roughness array placed on the cylinder surface. After some transients, the computed flow contains a steady part and an unsteady part, which is oscillating at a constant and single frequency $f = 3430$Hz. The temporal mean value of the flow is denoted by the symbol $< . >_0$, the instantaneous velocity in the chordwise direction thus reads as :

$$v_s(s, n, z, t) = < v_s >_0 (s, n, z) + v_s^{unst}(s, n, z) \cos(2\pi t/f + \phi_{v_s})$$

where ϕ_{v_s} stands for a phase. A similar decomposition is used for each velocity component. The steady flow can be decomposed into three components :
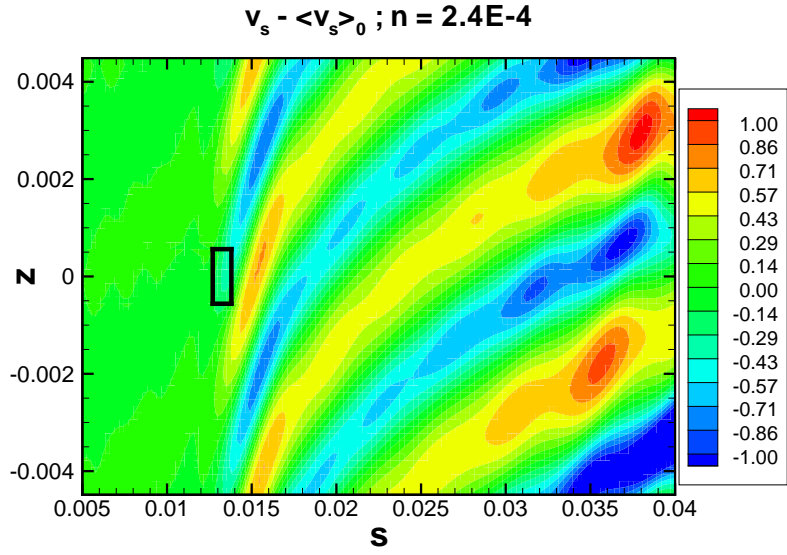
$$< v_s >_0 (s, n, z) = V_s^{cyl}(s, n, z) + v_s^r(s, n, z) + v_s^{iw}(s, n, z)$$

where V_s^{cyl} is the flow around the smooth cylinder, v_s^r is the deformation of the smooth swept cylinder flow induced by the roughness, and v_s^{iw} is a steady instability wave. A similar decomposition is performed for the wall-normal and spanwise velocity components.
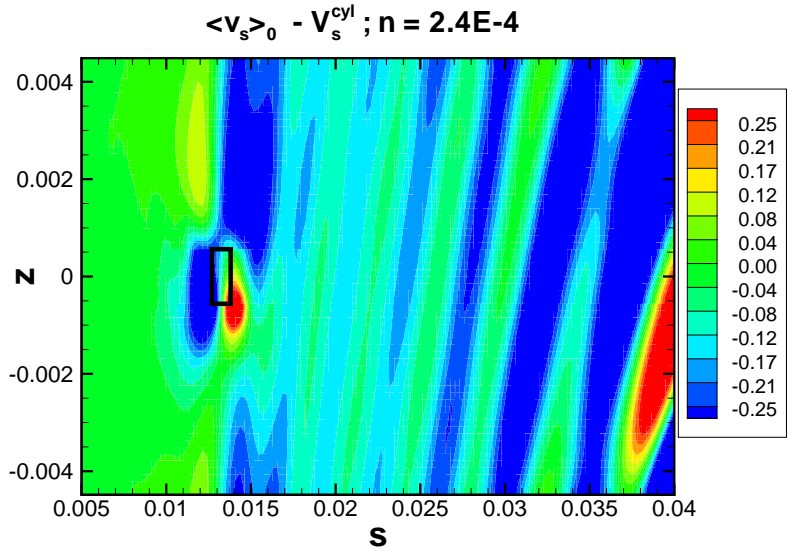
Figure 2 shows the evolution of $v_s - < v_s >_0$ and $< v_s >_0 - V_s^{cyl}$ at a fixed n location, slightly above the roughness top ($n \approx 3.5h$, with h the roughness height). A linear stability study of the flow without roughness, $(V_s^{cyl}, V_n^{cyl}, W^{cyl})$, has been performed for the frequency $f = 3430$Hz and a spanwise wavenumber 2β, where $\beta = 2\pi/\lambda_z$ with λ_z the spanwise extent of the computational domain. This analysis shows that this traveling crossflow wave is the most amplified, and that its spatial evolution compares very well to the DNS unsteady flow. On the contrary, the eigenfunctions predicted by an Orr-Sommerfeld analysis for the zero-frequency and for the wavenumber β differ significantly from the steady DNS flow. This is due to the presence of the roughness induced response v_s^r. To distinguish the steady crossflow wave from the latter, the steady flow is decomposed onto the steady eigenmode with help of the biorthogonal method. Moreover, as this method allows to evaluate precisely the amplitude of the eigenmodes in the DNS flow, it is possible to obtain the amplitude of the receptivity process, for both the unsteady and steady case.

References

[1] Tumin, A., "Multimode decomposition of spatially growing perturbations in a two-dimensional boundary layer," *Phys. Fluids*, Vol. 15, No. 9, 2003, pp. 2525–2540.

[2] Thompson, K.W., "Time dependent boundary conditions for hyperbolic systems," *J. Comput. Phys.*, Vol. 68, 1987, pp. 1–24.

$$\text{v}_s - <\text{v}_s>_0 \; ; \text{n} = 2.4\text{E-4}$$

(a) $v_s - <v_s>_0$

$$<\text{v}_s>_0 - \text{V}_s^{cyl} \; ; \text{n} = 2.4\text{E-4}$$

(b) $<v_s>_0 - V_s^{cyl}$

Figure 2: Unsteady and steady part of the v_s velocity at $n = 2.4\,10^{-4}$m ($\approx \delta/3$). The location of the roughness is represented by a rectangle, but the roughness is nearly square when an iso-stretching is applied to s and z. The lengths and the velocities are dimensional (in m and m/s).

Interpretation of the secondary instability of crossflow vortices by analogy with the Kelvin-Helmholtz instability
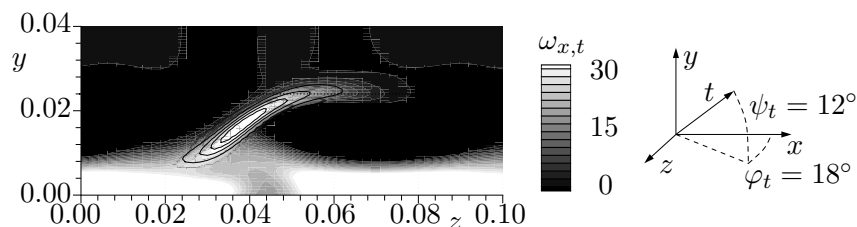
G. Bonfigli [1], M. Kloker [2]

[1] ETH Zürich, Institut für Fluiddynamik (IFD)

[2] Universität Stuttgart, Institut für Aerodynamik und Gasdynamik (IAG)

The identification and characterization of high-frequency secondary instabilities of crossflow (CF) vortices have been fully accomplished in the last few years experimentally [4], theoretically (secondary linear stability theory, SLST, see [2]), and by means of spatial DNS [3]. Whereas agreement between all approaches is satisfactory from a qualitative point of view, quantitative comparisons showed non-negligible deviations between amplification rates from DNS and SLST. The origin of the disagreement could be traced back to an unexpected sensitivity of the problem with respect to very small changes in the primary state [1].

We propose a detailed interpretation of the secondary instability in CF boundary layers by analogy with the Kelvin-Helmholtz (KH) instability of the plane mixing layer. Unstable vortical cores develop in the CF case in correspondence of marked shear layers of the primary state. However, differently from the KH scenario, their orientation is not prescribed a priori. It is rather determined by a kinematic condition equivalent to the requirement that the shape of unstable eigenfunctions remains unchanged, while the associated vorticity is convected by the underlying primary velocity field. Even if the unstable shear layers are mainly connected to gradients of the streamwise velocity component (u) in the plane normal to the primary vortex axis, also the wall-normal and crossflow velocity components (v and w, respectively) are relevant to determine the orientation of secondary vortex cores through the kinematic condition. As a result, changes in v and w may influence the amplification rates of secondary modes, since the strength of the primary shear layer effectively seen by secondary vortex cores depends on their orientation. Furthermore, both in the KH and in CF scenarios, amplification rates were found to be very sensitive with respect to moderate velocity components normal to the unstable shear layer.

As a further result, the KH analogy shows that secondary perturbations associated to different shear layers at the side of different primary vortices develop independently from each other. Consequently the assumption of spanwise periodicity made in most SLST codes is not a limitation, since the behaviour of secondary perturbations is not influenced by the presence of periodically repeated shear layers and secondary disturbances. Detuning is futile in the SLST. The figure displays isocontours for the normalized amplitudes of a type-I eigenmode (lines $\Delta = 0.2$) and for the primary vorticity component parallel to the direction t of the secondary-vortex axes (shade). The plane (y, z) is normal to the primary-vortex axis, the orientation of t is documented in the insert. The secondary mode clearly develops within a shear layer of the primary flow.

[1] G. Bonfigli and M. Kloker. *J. Fluid Mech.*, accepted for publication.

[2] W. Koch, F. P. Bertolotti, A. Stolte, and S. Hein. *J. Fluid Mech.*, 406:131–174, 2000.

[3] P. Wassermann and M. Kloker. *J. Fluid Mech.*, 456:49–84, 2002.

[4] E. B. White and W. S. Saric. *J. Fluid Mech.*, 525:275–308, 2005.

Active control of cross-flow secondary instability in a 3-d boundary layer by localized blowing/suction at the wall

T. Friederich[1], G. Bonfigli[2], M. Kloker[1]

[1] Universität Stuttgart, Institut für Aerodynamik und Gasdynamik (IAG)
[2] ETH Zürich, Institut für Fluiddynamik (IFD)

The identification and characterization of high-frequency secondary instabilities of crossflow (CF) vortices have been fully accomplished in the last few years experimentally [4], theoretically (secondary linear stability theory, SLST, see [2]), and by means of spatial DNS [3]. Whereas all approaches agree qualitatively, SLST has been found to significantly under-predict the maximum secondary growth. The disagreement could be traced back to an unexpected sensitivity of the problem with respect to very small changes in the velocity components lying in the crosscut of the primary state [1].

As a consequence, the growth rates of secondary instability mechanisms in the CF scenario are likely to be highly susceptible to moderate suction or blowing at the wall which provides a good possibility to delay transition to turbulence. By means of spatial DNS we investigate how the amplitude growth rates of (artificially excited) high-frequency secondary instabilities can be reduced drastically exploiting the aforementioned sensitivity. A first example is shown below: The mode with the highest growth rate (Fig.1) is a S-shaped *type-I* mode (Fig. 2a). Localized "hole-like" blowing with no net mass flow (a synthetic jet) has been applied between $0.675 \leq x \leq 0.725$. The blowing peak lies underneath the amplitude maximum of this most unstable mode at $z=0.077$ where also the minimum of the wall-normal gradient of the primary-state streamwise velocity is situated. By a proper choice of the blowing intensity (here $v_{max}/u_e=0.1$) the amplitude growth of the most unstable mode can be weakened considerably (Figs. 1, 2b). Note that the localized blowing causes only a weak deformation of the streamwise-velocity primary state in this case. Further investigations, also with non-synthetic jets and suction, are ongoing.
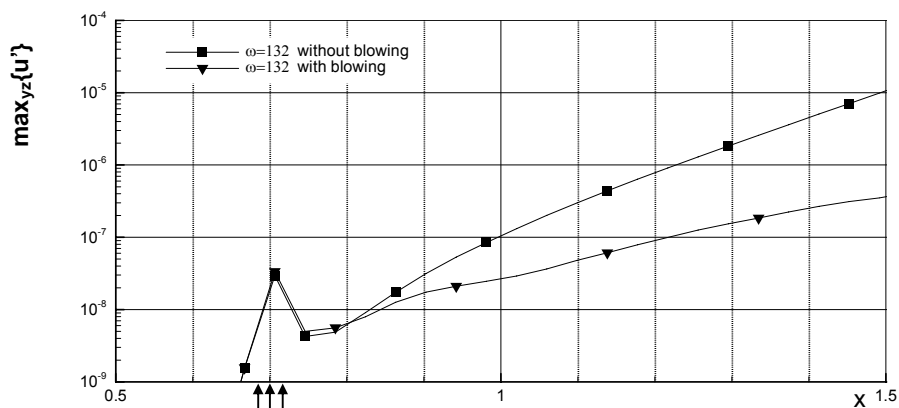

Fig. 1: Downstream development of u-disturbance amplitudes with/without blowing (arrows).
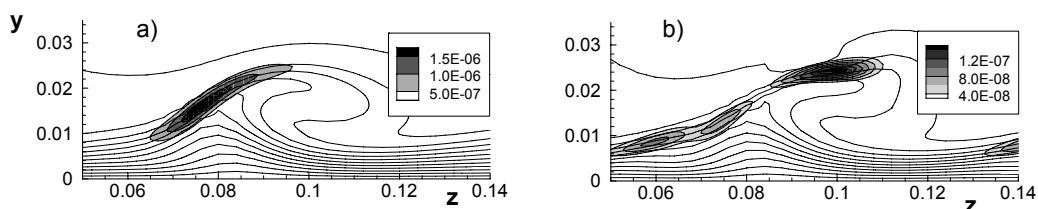

Fig. 2: u-disturbance amplitude distribution at x=1.3 of mode ω=132 (shaded) and u-velocity distribution (lines, Δ=0.1): a) without, b) with blowing.

[1] G. Bonfigli and M. Kloker. *J. Fluid Mech.*, 2007, in press.
[2] W. Koch, F. P. Bertolotti, A. Stolte, and S. Hein. *J. Fluid Mech.*, 406:131–174, 2000.
[3] P. Wassermann and M. Kloker. *J. Fluid Mech.*, 456:49–84, 2002.
[4] E. B. White and W. S. Saric. *J. Fluid Mech.*, 525:275–308, 2005.

Transition control experiments in the supersonic S2MA wind tunnel (SUPERTRAC project)

Archambaud J-P., Arnal D., Fontaine J., Godard J-L., Krier J., Ternoy F.

The present paper deals with the control of the laminar-turbulent transition on a swept wing in supersonic conditions. This study corresponds to a work package of the European Project SUPERTRAC (SUPERsonic TRAnsition Control) initialised in January 2005. The nine partners of SUPERTRAC have been involved in this task. The paper describes mainly the work concerning the model manufacturing, the experiments and some typical results.

This workpackage had two objectives: the first one was to control the transition due to crossflow (CF) instabilities present on a swept wing, by using Micron-Sized Roughness elements (MSR); the second one was to stop the turbulent contamination along the leading edge by means of appropriate Anti-Contamination Devices (ACD). These two actions must be carried out separately, but using the same wing geometry. The work included both numerical and experimental activities, with tests in the ONERA S2MA wind tunnel in Modane.

Model definition

The numerical phase of preparation of MSR and ACD studies has been already presented at the ICAS meeting [1], and so it will be briefly explained here. For MSR investigation, this preliminary phase determined a certain number of configurations to be tested (initial disturbance amplitude and wavelength). For ACD experiments, seven different shapes have been defined (five different bumps, two hollow shapes).

The selected profile for the test is symmetrical, thick (e/c=20%), and the chord is equal to 0.4m. Tests are realized at 0° angle of attack. In addition, the contamination Reynolds number $\overline{R}^*$ estimation has demonstrated that this profile was appropriate to MSR tests at moderate sweep angle (laminar flow on leading edge for $\varphi \leq 30°$) and to ACD tests at high sweep angle (turbulent flow on leading edge for $\varphi \geq 60°$).

Model manufacturing

The manufacturing of the model has been made at ONERA_Lille [2, 3]. The wing has a chord of 0.4m, a span of 1.5 m and a weight of 200 Kg. It is composed of a removable leading edge part and a main body. The control devices, MSR and ACD, are placed on the removable part. Two sections are equipped with pressure taps, one at mid-span, the second near the wing tip.

Each MSR row is composed of about 35 small cylinders made of paint (height 10 micron, diameter 0.2 and 0.15 mm), distributed with a spanwise spacing equal to the "killer" disturbance wavelength ($1 \leq \lambda \leq 2$mm).The rows are placed at the critical abscissa in parallel to the attachment line. Two groups of two rows each (same spacing, diameter 0.2 and 0.15 mm) have been put on each side of the model. Unfortunately, only one row with MSR diameter of 0.15 mm was acceptable. The flow in the wake of each group was observed by one infrared camera.

Each ACD is manufactured on a small removable portion of leading edge, the different ACD being interchangeable rapidly. The ACD is located at about three times the wall boundary layer thickness from the wind tunnel wall. Three hot films located respectively just upstream and downstream of the ACD and near the tip of the wing measure the shear stress fluctuations, informing about the nature of the boundary layer (laminar, transition, turbulent).

Experiments in the S2MA wind tunnel

The test campaign has been performed in the S2MA wind tunnel, in October 2006 [4]. The presentation will show some typical results.

MSR have been tested at wing sweep angle of 20°, 25° and 30°, at Mach number 1.5 and 2.0, for total pressure values between 0.5 and 1.25 bar. In the first analysis, MSR seem to move the transition

upstream but not at the roughness elements themselves. No positive effect is observed. This rather disappointing result could be explained by a two big height of the MSR. The figure 1 shows an example of infrared image observed behind a group of rows.

ACD have been tested at wing sweep angle of 65°, at Mach number 1.7 (subsonic leading edge) and 2.7 (supersonic leading edge), for total pressure values between 0.3 and 1.4 bar. The action of the different ACD was varying, depending on the shape. Results allowed to rather well understand the global mechanism of each shape. A certain shape has been particularly efficient, pushing away the critical value of $\overline{R}*$ from 250 to about 400 at Mach number 2.7, which is an interesting success in supersonic.

The detailed analysis of the results is in progress. It will be presented in further papers.

Conclusion
A lot of knowledge has been acquired at each stage of this study in supersonic: numerical prediction, manufacturing, testing. Concerning the MSR investigation, a technological step seems to be necessary in order to manufacture suitable very small roughness elements producing the numerically predicted disturbance amplitudes. For the ACD investigation, the potential gain has been clearly demonstrated for a suitable bracelet shape. On the basis of these results, a category of ACD should be improved from a shape and size point of view.

References
 [1]   Supersonic laminar flow control studies in the SUPERTRAC project, D. Arnal, C.G. Unckel, J. Krier, J-M. Sousa, S. Hein. Technical Report.
[2]   Report on model manufacturing, F. Ternoy.
[3]   Design of the S2MA model with mocron-sized roughness elements and anti-contamination devices, J-P. Archambaud, D. Arnal, J-L. Godard, F. Ternoy, M. Deschamps.
[4]   Summary of the S2MA wind tunnel tests. Preliminary analysis, J. Fontaine.
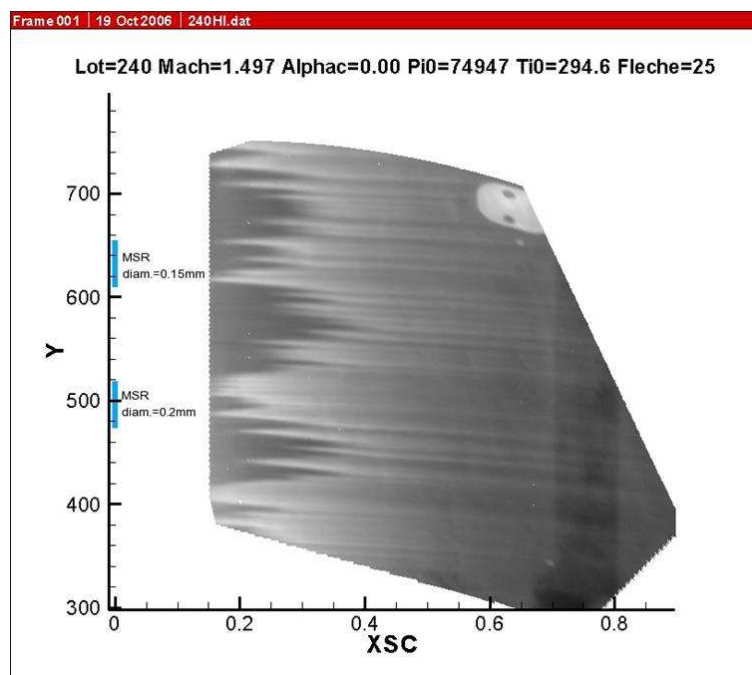
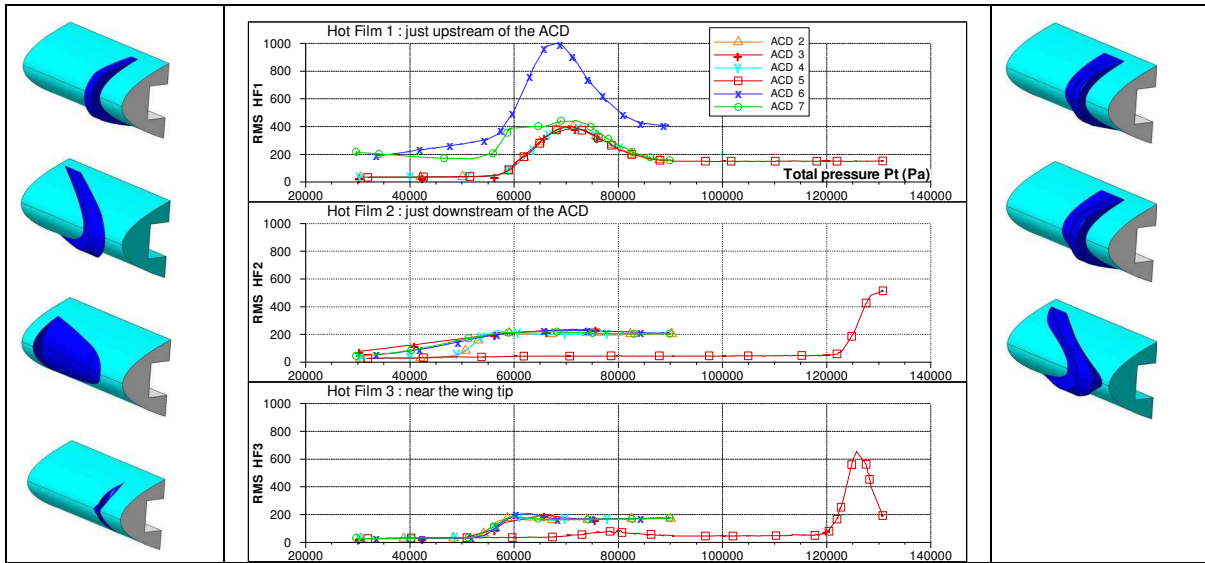*figure 1 : Example of infrared image (MSR tests)*

Figure 2 : ACD effect detected by the hot films

NUMERICAL INVESTIGATION OF ACTIVE SEPARATION CONTROL FOR LOW-PRESSURE TURBINE BLADES

H. F. Fasel, A. Gross, W. Balzer
Department of Aerospace and Mechanical Engineering
University of Arizona, Tucson

Low-Pressure Turbine (LPT) stages are important components of many modern jet engines. In the recent past, the increasing importance of unmanned aerial vehicles (UAVs) for military operations has spawned a need for smaller and smaller jet engines, in which LPT operating Reynolds numbers can drop to relatively low values. In these operating ranges, boundary layers remain laminar over a large streamwise extent of the turbine blades, even in the presence of elevated free stream turbulence. As a consequence, the laminar boundary layer flow separates from the blades, causing significant losses in turbine and overall engine performance. Since it was recognized that Active Flow Control (AFC) could counter such unfavourable conditions, Rivir and co-workers[1], in experimental investigations at the Air Force Research Laboratory (AFRL), systematically explored the potential of employing AFC for LPT blades. Separation-induced wake losses were reduced by up to 60% when Vortex Generator Jets (VGJs) were employed, i.e. when fluid was injected into the boundary layer through a spanwise array of small holes. Similar performance improvements were obtained with only a fraction of the mass flux when pulsed blowing with VGJs was employed.

The experiments at AFRL have shown that AFC can lead to significant performance improvements, even when implemented into an existing, conventional LPT blade design. Therefore, if the integration of AFC for LPT blades were considered from the very beginning of engine development, more aggressive designs could be contemplated which may ultimately lead to lighter and more fuel-efficient engines and result in vehicles with greater operating ranges or wider operating envelopes. In our investigation, numerical simulations are employed to aid in the understanding of the physical mechanisms that are relevant for controlling flow separation from LPT blades. We are performing both two- and three-dimensional simulations of a linear LPT cascade as well as of a flat-plate model geometry, utilizing various Navier-Stokes codes which have been developed in our research group.

With regard to the simulations of the full cascade geometry, we are performing 3-D Implicit Large Eddy Simulations (ILES), both with and without AFC by pulsed VGJs.. In addition to the simulations of the LPT cascade, we are performing fully-resolved Direct Numerical Simulations (DNS) of a flat-plate boundary layer which is subjected to LPT blade conditions. In these simulations, both steady as well as pulsed VGJs are injected into the boundary layer. For steady VGJs, we have found that the relative effectiveness of the various VGJ configurations appears to be highly dependent on parameters such as the hole diameter and the jet blowing ratio. For pulsed VGJs, on the other hand, the dominant physical mechanism seems to be related to the formation of large-scale spanwise-coherent structures, which develop as a consequence of the hydrodynamic instability of the flow with respect to 2-D disturbances. In other words, by pulsing within the range of naturally unstable frequencies, this instability can successfully be exploited.

1. Bons, J.P., Sondergaard, R., Rivir, R.B., Turbine Separation Control Using Pulsed Vortex Generator Jets, ASME Journal of Turbomachinery 123, 198-206, 2001.

Experimental and Numerical Study
of Unsteady Görtler Vortices

A. V. Boiko, A. V. Ivanov, Y. S. Kachanov and D. A. Mischenko

Institute of Theoretical and Applied Mechanics of SB RAS, 630090, Novosibirsk, Russia.

The Görtler instability is responsible for amplification of stream-wise counter-rotating vortices, whose growth is able to lead to a premature laminar-turbulent transition in boundary-layer flows on concave walls [1, 2]. The majority of previous experiments were devoted to the steady Görtler vortices, despite the unsteady ones are also observed in transitional flows quite often. Moreover, even for the steady Görtler vortices no good quantitative agreement between the experimental and theoretical linear-stability characteristics was obtained, especially for disturbance growth rates. The difficulties are connected with a rather poor accuracy of measurements at zero disturbance frequency, a possible influence of nonlinearity, and an admixture of non-modal (transient) growth mechanism (the near-field of disturbance sources).

The present work had aimed to overcome these difficulties by experimenting with controlled traveling rather than steady perturbations, by performing measurements at low disturbance amplitudes, and by careful estimating the disturbance-source near-field. Simultaneously, we carried out linear-stability calculations and performed a detailed direct comparison of the numerical and experimental data.

The hot-wire measurements were conducted in the low-turbulence wind tunnel T-324 of ITAM SB RAS in a 2D boundary layer developed over a concave wall with a radius of curvature 8.37 m. The free-stream velocity of the flow was 9.18 m/s. The Görtler numbers $G = (U_e \delta_1 / \nu)(\delta_1 / R)^{1/2}$ grew downstream inside the measurement region from 10 to 17. The linear-stability characteristics were both measured and calculated for Görtler vortices with the span-wise wavelengths λ_z of 8, 12 and 24 mm ($\Lambda = (U_e \lambda_z / \nu)(\lambda_z / R)^{1/2} = 775, 274$ and 149). The vortex with frequencies 0.5, 2, 5, 8, 11, 14, 17 and 20 Hz were excited with a disturbance source of blowing-suction type.

The numerical part of the investigation included solution of (i) parallel linear stability equations of Görtler vortices [1, 2] and (ii) parabolic linear stability equations [3] (both approaches generalized to the case of traveling perturbations).

It is found that outside the disturbance source near-field region, the excited perturbations represent either quasi-steady (at very low frequencies) or unsteady (at higher frequencies) first least stable Görtler mode. A very good quantitative agreement between all numerical and experimental stability characteristics is obtained for all studied frequencies and span-wise wave numbers, including the disturbance increments, the phase velocities, and the eigenfunctions. The solutions based on parabolic equations provided a somewhat better agreement with experiment than the parallel theory.

The calculations based on the parallel linear stability theory show that as the frequency of the Görtler vortex grows, the border of the instability region on G-Λ plane is modified initially only slightly. At higher frequencies it is modified significantly by shrinking and splitting into several localized contours so that in a certain range of Λ (close to the most amplified modes) the growth of Görtler number is able to stabilize the flow with respect to unsteady first Görtler modes. These results are also found to be in consistence with the experimental observations.

REFERENCES

1. **Floryan J.M.** On the Görtler instability of boundary layers // *Prog. Aerosp. Sci.* – 1991. – Vol. 28. – P. 235—271.
2. **Saric W. S.** Görtler vortices // *Ann. Rev. Fluid Mech.* – 1994. – Vol. 26. – P. 379—409.
3. **Hall P.** The linear development of Görtler vortices in growing boundary layers // *J. Fluid Mech.*, 1983. – Vol. 130. – P. 41—58.

Dynamics at the Edge of Chaos in Pipe Flow

Tobias M. Schneider and Bruno Eckhardt

Fachbereich Physik, Philipps-Universität Marburg, D-35032 Marburg, Germany
`tobias.schneider@physik.uni-marburg.de`

Introduction: The transition to turbulence in pipe flow is puzzling because of the absence of linear instabilities that can trigger the transition. Many experiments have hence focussed on the determination of the 'double threshold' in Reynolds number and perturbation amplitude that has to be crossed in order to obtain turbulence. Applications of dynamical systems theory and systematically tailored laboratory experiments and numerical simulations have led to new insight into the transition [1]. There is growing evidence that transient turbulent motion is generated by a strange chaotic saddle in the state space of pipe flow. Nonlinear travelling wave solutions have been detected, both in numerical simulations and in experiment. They correspond to unstable periodic orbits that are embedded in the chaotic saddle around which turbulent dynamics can form. In the system's state space there is therefore a domain that generates the turbulent dynamics. It coexists with the stable laminar profile and its basin of attraction in another domain of state space. This coexistence naturally raises the question of the 'boundary' between both domains. Since the motion on one side of this boundary is chaotic, it is visible as the *edge of chaos* in lifetime plots.

In this work we apply tools developed in [2] to analyse the *edge of chaos* that is located at the boundary between laminar and turbulent motion and we extract and characterize the dynamical objects that dominate and 'define' the boundary.

Probing the edge of chaos: Since a perturbation has to exceed a threshold in amplitude in order to trigger turbulence, an initial perturbation starting out on one side of the border will swing up to the turbulent region, whereas one on the other side will decay to the laminar profile. This can be used to detect points on the edge of chaos and to trace out the dynamics within the border.

Operationally, we detect the boundary by adding a pertubation of fixed structure but varying amplitude to the flow and numerically following its time evolution. If the amplitude is small, the pertubations smoothly decays. If the amplitude is large enough the flow will become turbulent. Inbetween both

initial conditions lies one that will not decay nor reach the turbulent state. It lives in the edge of chaos.

The edge states: Numerical experiments and theoretical arguments suggest that these edge trajectories collapse onto invariant structures that are relative attractors within the edge of chaos. In the simplest case, the relative attractors or *edge states* can be saddle points (then the stable manifold coincides with the edge of chaos). For pipe flow the invariant edge state has a simple topological structure, shown in Fig. 1. It shows no discrete rotational symmetry, does not settle down to a simple travelling wave and shows intrinsic chaotic dynamics of vortical structures in its center region (see Fig 2). Therefore, the edge state is chaotic. It is also universal in the sense that all trajectories in the boundary are attracted to the same structure. The global structure of the state also seems to vary only little with the Reynolds number.

The significance of the edge state lies in its guarding role for the transition to turbulence. If indeed there is only one state (up to the obvious rotational degree of freedom), control stragies can be applied to either encourage or prevent this state, in order to achieve or prevent relaminarization, respectively.
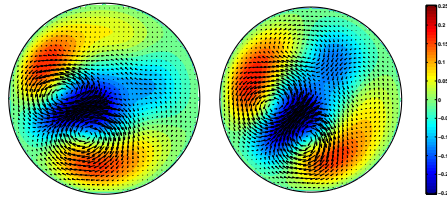
Fig. 1. Time-averaged cross sections of the edge state at Re = 2160 (left) and Re = 2875 (right). The out-of-plane components are shown in color, the in-plane components as vectors.
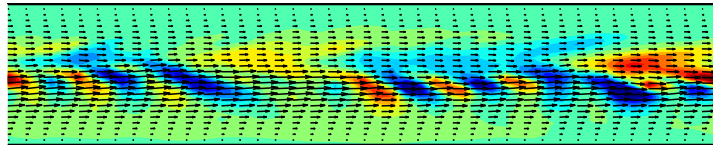
Fig. 2. Instantaneous snapshot of the edge state at Re = 2875. Cross section along the pipe axis and the symmetry axis between the vortices. The chaotic nature of the edge state shows up in the non-periodic structures along the axis.

[1] B. Eckhardt, T.M. Schneider, B. Hof and J. Westerweel, Ann. Rev. Fluid Mech., **39**, 447–468

[2] J. Skufca, J.A. Yorke, and B. Eckhardt, Phys. Rev. Lett. **96**, 174101 (2006).

Detection, Extraction and Tracking of Coherent Structures in Boundary Layers

Kudret Baysal & Ulrich Rist

Institut für Aerodynamik und Gasdynamik, Universität Stuttgart

Pfaffenwaldring 21, 70550 Stuttgart, Germany

e-mail: baysal@iag.uni-stuttgart.de

Advanced measurement techniques and numerical methods in combination with increasing computational power are allowing measurements and numerical simulations with high resolutions in space and time. The results of studies with high resolutions allow systematic investigation of the physics in a flow field. The acquisition of information out of well-resolved datasets is not evident and requires a time-consuming investigation of the flow field. The outcome of this is the necessity of an automated postprocessing step to extract and to track flow field features. In this paper we focus on vortices, also called coherent structures, which have a high importance in flow field studies.

Although their relevance in the flow field research, there is no universally accepted definition of vortices. The lack of an accepted definition leads to several vortex detection criteria. The first part of the work is a discussion about the mainly used criteria and a comparison of their results for the case of burgers vortices. The vortex detection criteria discussed in this work are local methods and give the information if a point belongs to a vortex region or not. For advanced postprocessing with the ability to study each structure or group of structures in space and time, it is necessary to have a global information. Extracting coherent structures from the flow field satisfies the demand for global information. For the extraction of coherent structures we use the knowledge that vortex centres are points of local extrema of pressure, vorticity and for the discussed vortex detection criteria. A predictor−corrector method is used to extract vortex core lines. From a starting point the predictor step is done with the eigenvector e_3 of the Hessian of the scalar. The corrector step is done on the plane spanned by e_1 and e_2 of the predicted point. The detection and extraction of coherent structures are generating three dimensional information in each time step. Investigation of a 4d field (space and time) requires an additional information in time. To achieve this the connectivity of the coherent structures in time must be defined. The temporal dependency for the connectivity is obtained by feature tracking. For feature tracking we use again a predictor−corrector method. First we predict a vortex core line in an earlier or later time step. The corrector step is a check for matching of vortex core lines from the actual time step and predicted vortex core lines.
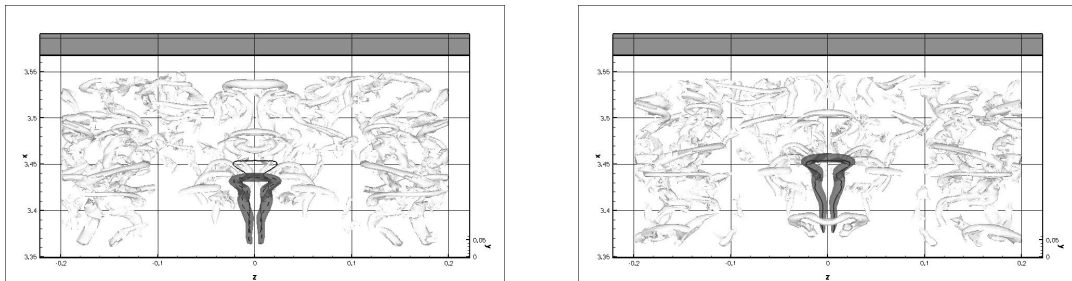

Figure 1: Visualisation of a boundary layer flow for two time steps t_n(left) and t_{n+1}(right). In t_n a vortex (highlighted) is focused. Dashed line represents the core line of the focused vortex and the solid line the predicted position of the core line in t_{n+1}. In t_{n+1} is the vortex with the best match to the predicted core line (solid line) highlighted.

Transition to Turbulence in a Mach 0.8 Swirling Mixing Layer

S. B. Müller, L. Kleiser

Institute of Fluid Dynamics, ETH Zurich, 8092 Zurich, Switzerland
sebastian.mueller@ifd.mavt.ethz.ch, Phone: +41-44-632-0918, Fax: +41-44-632-1147

We apply DNS to simulate the nonlinear evolution of a subsonic circular swirling mixing layer under the influence of viscous spatial instabilities and its transition to turbulence. Figure 1 illustrates the flow configuration under consideration.
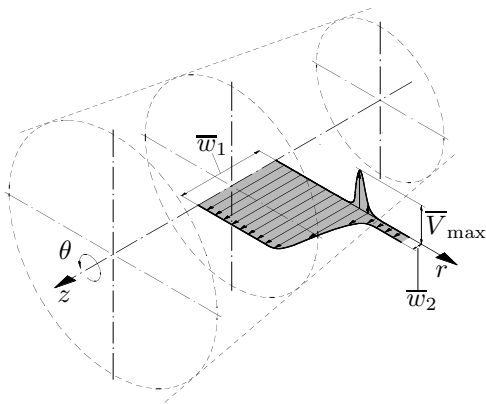

Figure 1: Swirling mixing layer configuration.

The conservative formulation of the compressible Navier-Stokes equations expressed in cylindrical coordinates and a mapping from Cartesian to cylindrical coordinates is employed. This eliminates problems related to the specific numerical treatment of additional centrifugal and Coriolis force terms that arise in other (e.g. weakly conservative) formulations. The governing equations are non-dimensionalized using the jet radius $r_j^* = D_j^*/2$, jet centerline inflow velocity W_j^*, density ρ_j^*, dynamic viscosity μ_j^* and temperature T_j^* as reference quantities. The Reynolds number is $Re = \rho_j^* W_j^* r_j^*/\mu_j^* = 5000$ and the Mach number $Ma = W_j^*/\sqrt{\gamma R^* T_j^*} = 0.8$ where $\gamma = 1.4$ is the isentropic coefficient and $R^* = 287 J/(kgK)$ is the gas constant for air. The maximum swirl velocity is set to $\overline{V}_{\max} = 0.4$.

The convective as well as diffusive terms are discretized using sixth to tenth-order (at interior points) compact central schemes and alternatively upwind-biased compact schemes by Adams & Shariff [1]. The centerline singularity of the governing equations is treated by a method proposed in [2]. This approach uses a shifted grid in the radial direction and thus avoids placing a grid point at the polar axis ($r = 0$). In the azimuthal direction a Fourier spectral method is employed. The grid is stretched in the radial and axial directions in order to adequately resolve regions with steep gradients. Time integration is done by a low-storage explicit third–order Runge-Kutta method. The size of the computational domain is $L_z \times L_r = 24 \times 10$ and the resolution of our simulations is $N_r \times N_\theta \times N_z = 255 \times 150 \times 445$ grid points.

At the inflow plane, Dirichlet conditions are applied on all conservative variables to precisely define the time-dependent inflow. In addition, a damping sponge zone is imposed to absorb any upstream-traveling acoustic disturbances. At the radial and outflow boundaries non-reflecting conditions (accounting for the curvilinear radial boundary) are employed and supplemented by sponge layers.

The inflow forcing is based on the superposition of viscous spatial linear instabilities consisting of individual wavelike solutions of the form

$$\hat{q}(r) \exp\{i \cdot (\alpha z + n\theta - \omega t)\}$$

where $\hat{q}$ is the complex eigenfunction, $\alpha = \alpha_r + i\alpha_i$ the complex streamwise wavenumber, n the azimuthal wavenumber and ω the circular frequency. For the base flow type under consideration, linear stability investigations have been performed, see Refs. [3] and [4]. Two distinct disturbance modes are obtained: a centrifugal and a shear instability, see Figure 2. Results shown in this abstract employ an axisymmetric ($n = 0$) and two helical $n = 1$ instabilities with positive and negative circular frequency as specified in Table 1 (A denotes the maximum axial-velocity disturbance amplitude).

We simulate the spatial non-parallel and nonlinear development of the instabilities in the swirling mixing layer. Figure 3 (a) displays the downstream evolution consisting of an early developing region, subsequently followed by an elongated transitional zone and the eventual breakdown into turbulence. For the
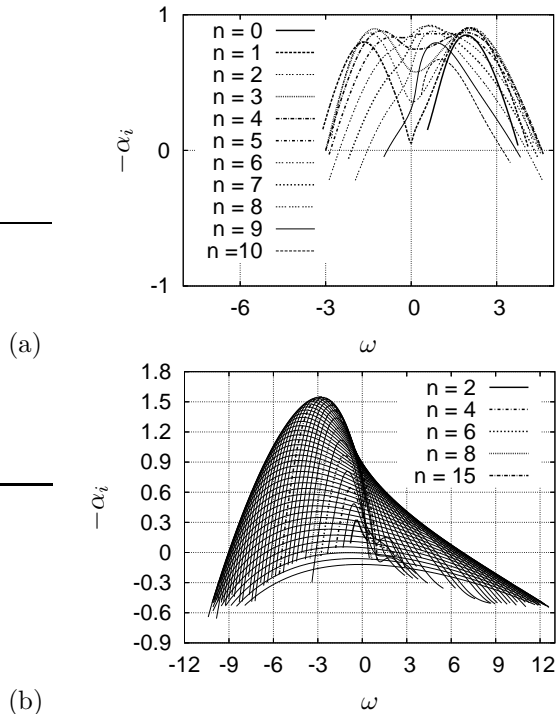
1

(a)

(b)

Figure 2: Swirling mixing layer instability growth rates $-\alpha_i$ as function of frequency ω. (a) Shear instabilities, (b) centrifugal instabilities with azimuthal wavenumbers $n = 2, \ldots, 51$.

Table 1: Inflow disturbance parameters.

n	ω	α	A
0	1.9326	$3.4065 - i0.8498$	$5 \cdot 10^{-3}$
1	2.0461	$3.5720 - i0.9030$	$5 \cdot 10^{-3}$
1	-1.6516	$-2.8659 - i0.7993$	$5 \cdot 10^{-3}$

given setup, dominant disturbances are axial shear instabilities, visualized in Figure 3 (b) by λ_2-isosurfaces. Centrifugal instabilities, which could be generated by weakly nonlinear interactions in the transitional zone, appear not to be dominant in this specific simulation. The simulation reveals a mutual competition among the disturbances imposed at the inflow.

We will present present detailed flow statistics and give a discussion of the evolution of different instability families and their nonlinear interactions. Furthermore we will also briefly comment on the influence of different numerical discretizations on the results.

References:

[1] N. A. Adams and K. Shariff. A high-resolution hybrid compact-ENO scheme for shock-

turbulence interaction problems. *J. Comput. Phys.*, 127(1):27–51, 1996.

[2] K. Mohseni and T. Colonius. Numerical treatment of polar coordinate singularities. *J. Comput. Phys.*, 157:787–795, 2000.

[3] G. Lu and S. K. Lele. Inviscid instability of compressible swirling mixing layers. *Phys. Fluids*, 11(2):450–461, 1999.

[4] S. B. Müller and L. Kleiser. Spatial linear stability analysis of compressible swirling jet flow. *Submitted*, 2006.
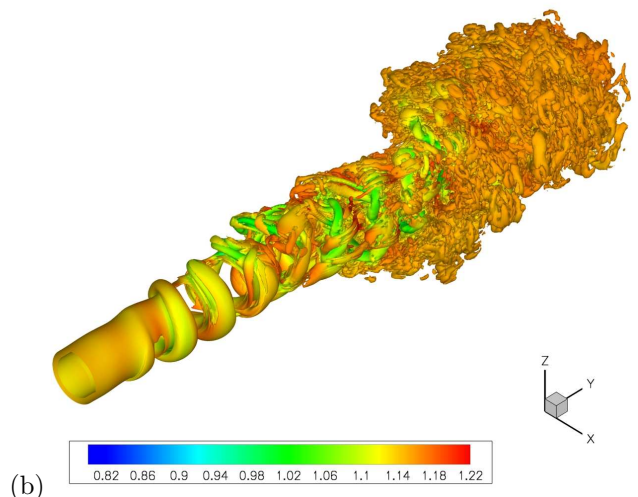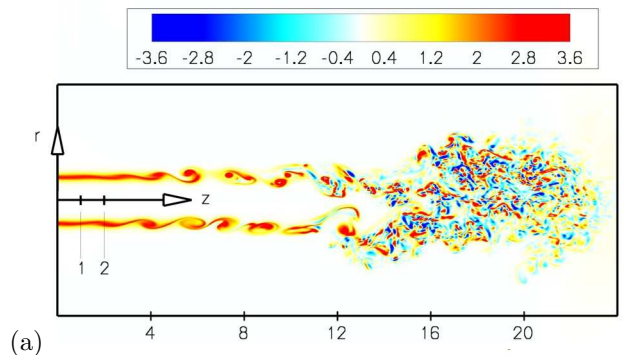
(a)

(b)

Figure 3: Swirling mixing layer. (a) Contours of instantaneous ω_θ-vorticity in the r–z–plane at $\theta = 0$. (b) Isosurface of second invariant ($\lambda_2 = -0.05$) indicating the location of vortices. The color indicates in addition the value of the instantaneous local pressure on the isosurface (note that $Y \equiv z$).

Abstract submitted for **6**[th] **ERCOFTAC SIG 33**
Workshop on Laminar-Turbulent Transition Mechanisms, Prediction and Control
June 17-20 2007, Kleinwalsertal, Austria

DNS of a Mixing Wake Behind a Finite Flat Plate

Andreas Babucke, Markus J. Kloker, Ulrich Rist

Institut für Aero- und Gasdynamik, Universität Stuttgart
Pfaffenwaldring 21, D-70550 Stuttgart
babucke@iag.uni-stuttgart.de

Abstract. The combination of wake and mixing layer appears behind a splitter plate with two different flow speeds above and below the plate. It serves as a model problem for the nozzle end of a jet and is of special interest with respect to aeroacoustics. Due to the inflection points in the velocity profile, the flow field is highly unsteady requiring Direct Numerical Simulations (DNS) for the investigation of two- and three-dimensional instability waves. Figure 1 reveals the difference between a single 2-d disturbance $(1, 0)$ and an additional 3-d mode $(1, 1)$. In both cases, the disturbances are introduced at the inflow of the upper boundary layer $(Re_{\delta 1(x0)} = 1000)$ using eigenfunctions from linear stability theory with an amplitude of $u_{max} = 0.005$. The mode $(1, 1)$ leads to an early breakdown of the Kelvin-Helmholtz vortices. Additionally, the splitter plate allows to model wall-bounded actuators to control the mixing wake instead of using artificial forcing terms as it is the case for the pure mixing layer. Directly computing the flow and acoustic field allows to evaluate passive and active devices for noise reduction, being currently investigated.
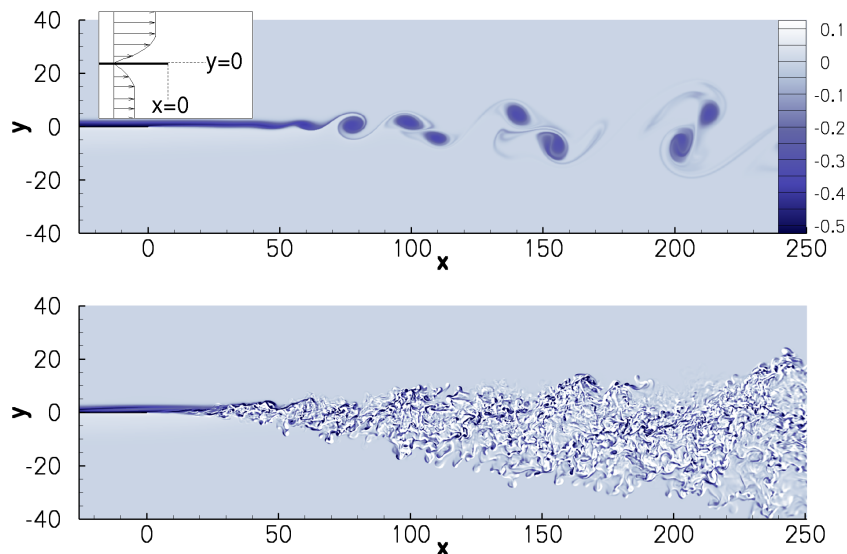
Fig. 1. Instantaneous view of the spanwise vorticity at $z = 0$. The flow is forced at the inflow with a single 2-d Tollmien-Schlichting wave (top) and an additional oblique mode $(1, 1)$ (below). Mach numbers of the upper and lower stream are $Ma_I = 0.8$ and $Ma_{II} = 0.2$ respectively, $Re = 1000$. The splitter plate ends at $x = 0$.

Effusion Cooling in Mach-6 Boundary-Layer Flow Investigated by DNS

Jens Linn & Markus J. Kloker

Institut für Aerodynamik und Gasdynamik, Universität Stuttgart

Pfaffenwaldring 21, 70550 Stuttgart, Germany

e-mail: linn@iag.uni-stuttgart.de

For aerospace or hypersonic cruise vehicles the state of the boundary layer is of great importance for the thermal loads and skin friction. Therefore, knowledge of cooling features and laminar-turbulent transition is necessary for the design and the thermal protection system (TPS). Different strategies are used to reduce the thermal loads of hypervelocity vehicles, e.g. radiation, transpiration, film cooling or ablation.

Direct numerical simulations (DNS) are carried out to investigate the effect of effusion cooling by blowing through discrete holes in an adiabatic Mach-6 boundary layer ($T_{rec}^{\star} = 629K$). The focus of the study is the generated vortices, shear-layer systems and the laminar stability properties of the boundary layer. Cold air is blown through four spanwise rows of holes aligned in downstream direction. The hole region reaches from $Re_x = 2.2054 \cdot 10^5$ to $2.7564 \cdot 10^5$. In case a the holes have a small spanwise spacing $s_z = 3d_c$ ($d_c = 0.055$ - hole diameter), in contrast to case b where the spanwise spacing is enlarged ($s_z = 12d_c = 6\delta_c$). The hole diameter d_c, the cooling gas temperature $T_{c,core}^{\star} = \frac{1}{2} T_{rec}^{\star}$ and blowing ratio $(\rho v)_c^{\star}/(\rho u)_{\infty}^{\star} = 0.15$ are for both cases equal. Thus the massflow through the holes in case b is only one quarter of case a. A crosscut of the u-velocity field downstream the rows is shown in figure 1. In case b (right), the boundary layer is deformed much stronger than in case a (left; mushroom like structures). Upstream of the holes, unsteady 2-d disturbance waves are generated by suction and blowing at the wall to check for laminar instability. Figure 2 shows the downstream development of the disturbance amplitudes for case b. The amplitude of the high frequencies, e.g. $\omega = 200$, grows up by approximately two order of magnitudes in the hole region but drops downstream. Only for $\omega = 10$ we observe a growing of the amplitude downstream of the holes for $R_x = 4 \cdot 10^5$. Lower frequencies are neutral or damped. For case a the amplification rates are even smaller as for case b. Thus the flow deformation by blowing causes a very localized disturbance growth, that does not lead to transition in the young boundary layer in the front part of the plate. Continuative studies will be made in a Mach-6.8 radiation-adiabatic cooled boundary layer at flight conditions.
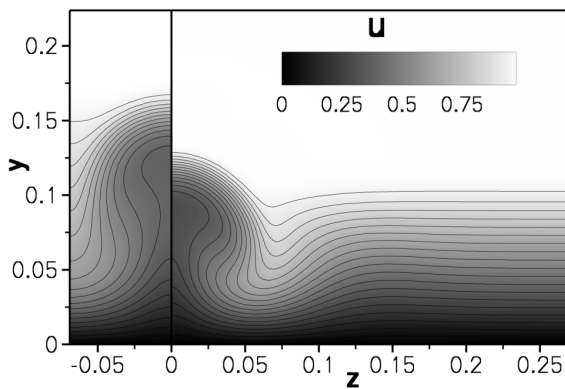

Figure 1: Visualisation of the u-velocity field in the crosscut at $Re_x = 3.128 \cdot 10^5$ for the both cases (left - case a; right - case b).
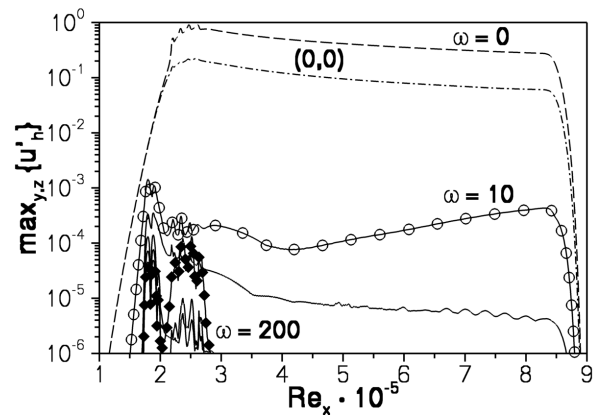
Figure 2: Downstream disturbance-amplitude development for the case b ($\omega = 10$ is $f^{\star} = \omega u_{\infty}^{\star}/(2\pi L^{\star}) = 49.78 kHz$).

Hypersonic Transition Investigations In A Flat-Plate Boundary-Layer Flow At M=20

Christian Stemmer

Lehrstuhl für Aerodynamik, Technische Universität München,
Boltzmannstr. 15, 85748 Garching b. München.

February, 15th, 2007

1 Overview

Direct numerical simulations of the complete, three-dimensional unsteady Navier-Stokes equations of hypersonic flows are conducted for ideal-gas conditions as well as chemical and thermal non-equilibrium conditions. First, comparison for the ideal gas results with Linear Stability Theory are presented to validate the proposed method. The high-speed boundary-layer flow is perturbed at the wall to introduce disturbances of two-dimensional and three-dimensional nature. The spatial evolution of these instabilities is investigated for isothermal wall conditions. Comparison with chemical and thermal non-equilibrium results for the disturbance development is presented. A five species, two-temperature model is employed to model the non-equilibrium conditions.

2 Numerical procedure

The details of the numerical procedure are described in [11, 13]. The numerical method is based on works by Adams [5, 6, 7] for supersonic ideal-gas flows. A hybrid ENO method enables the local treatment of shocks whereas the other areas are continuously dealt with compact finite differences [8]. The code was adapted to account for the treatment of dissociation. Five species continuity equations and a conservation equation for the vibrational energy have been added [11]. This encompasses the use of a second temperature, the vibrational temperature, which enables the treatment of non-equilibrium flows. The formulation of the reaction rates of the dissociation and recombination reactions was done according to Park [2, 3].

The time advancement is realized through a three-step low-storage Runge-Kutta method. The boundary conditions are no slip at the wall and periodicity in spanwise direction. At the inflow, the laminar solution to the boundary layer equations is prescribed. The free-stream boundary is treated with a characteristic boundary condition. The outflow condition is characteristic for a flow without disturbances. For the disturbances, a well-tested outflow damping zone is applied. Details on the formulation and the calculation of the thermodynamic properties can be found in Candler [4] or in Stemmer [9].

The disturbances are introduced in a wall blowing and suction slot where no net mass is introduced during a full disturbance cycle. The procedure follows the work of Eissler [10]. The disturbance modes have been chosen in comparison with Linear Stability calculations conducted earlier [12, 13].

3 Results

The presented results are for non-reactive and reactive conditions for a flight case of M=20 in a H=50km altitude atmosphere. The pressure was p=79.78 Pa and the density was ρ=1.027×10^{-3}kg/m^3. The resulting free-stream velocity was 6.596 km/s. The free-stream temperature was to be 270.65K and the wall was modelled as an isothermal wall at T_{wall}/T_∞=3. For air at this pressure, the mean free path is $l = 2.54 \cdot 10^{-4}$m and the boundary layer thickness at the inflow boundary is $\delta = 8$cm resulting in a Knudsen number of $Kn = l/\delta = 0.0032$ assuring the continuum assumption.

3.1 Comparison with Linear Stability Theory

The results from the DNS with linear disturbances introduced at the wall through blowing and suction are compared with eigenfunctions of the compressible Linear Stability Theory (LST) by Mack [1]. The
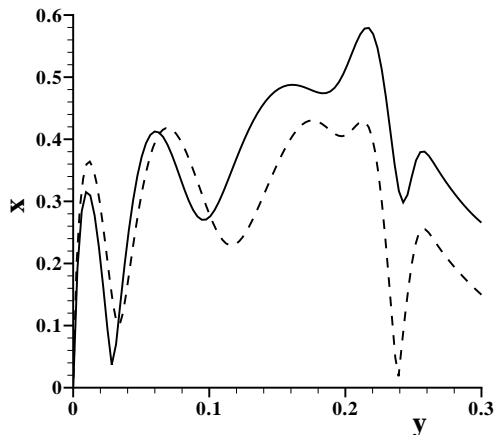

Figure 1: Comparison of wall-normal amplitudes of the down-stream velocity of a two-dimensional disturbance with the frequency F= 3.46 10^{-5} from DNS to the respective LST eigenfunction
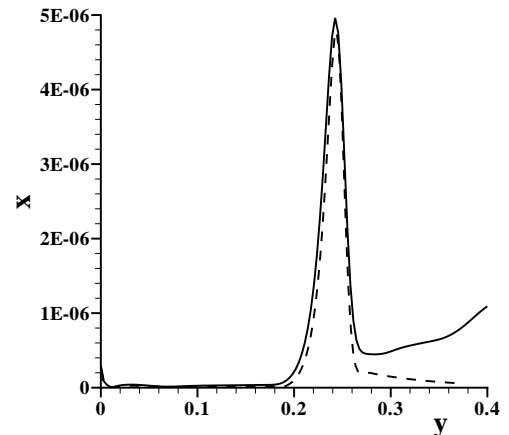
Figure 2: Comparison of wall-normal amplitudes of the density of a two-dimensional disturbance with the frequency F= 3.46 10^{-5} from DNS to the respective LST eigenfunction

eigenfunctions agree well for the downstream disturbance velocity (Fig. 1) and the disturbance density (Fig. 2). The comparisons of temperature, wall-normal velocity and pressure also agree well, but are not shown here. Small differences just outside the boundary layer (y>0.3) are due to the introduction of other disturbances at the blowing and suction strip than the compared instability mode that propagate downstream at a very flat angle due to the high Mach number.

3.2 DNS results for non-reactive and reactive conditions

3.2.1 steady base-flow calculations

Two simulations for reactive and non-reactive conditions have been carried out where the inflow has a Reynolds number of $Re = 640000$, the outflow Reynolds number is $Re = 13.2 \times 10^6$. The height of the integration domain covers more than twice the boundary layer thickness at the outflow position. At the inflow, about 50 points are inside the boundary layer. The spatial resolution was 1500×255×17 points in down-stream, wall-normal and span-wise direction respectively.

In a first step, a steady two-dimensional base flow has been calculated. Due to the limited space in this abstract, just the temperature distribution inside the boundary layer shall be presented for the two cases. In Fig. 3, the non-reactive distribution shows maximum temperatures of T∼4800K and the typical square-root like growth of the boundary layer. For the reacting flow (Fig. 5), the equilibrium boundary layer is prescribed at the inflow. The non-equilibrium flow has to adjust to this boundary conditions, which is clearly shown. The maximum temperature inside the boundary layer drops considerably to $T \sim 2300K$. The vibrational temperature (Fig. 6) also shows some adjustment and a maximum vibrational temperature of $T \sim 2300K$, but the maximum is much closer to the wall than for the translational temperature. This coincides with the location of the maximum of the dissociated species nitrogen N and oxygen O (Fig. 4)

3.2.2 disturbance calculations

For the disturbance calculations, the base flow is prescribed at all span wise positions, then the disturbances are introduced at the wall. The disturbance frequency was fixed at 14.4 kHz (F=3.46 10^{-5}). The down-stream extent of the disturbance strip was adjusted to the predicted down-stream wave-length of the disturbance through calculations with the Linear Stability Theory. A two-dimensional and a three-dimensional disturbance were introduced a the wall at a dimensionless amplitude of $u'/u_\infty = 0.01$and0.005 respectively. The obliqueness angle of the three-dimensional disturbance was $\theta = 15°$.

The amplitudes are shown in the modal frequency–span wise wave number space. In the notation (h,k), h denotes the multiples of the disturbance frequency and k denotes he multiples of the lowest span wise wave

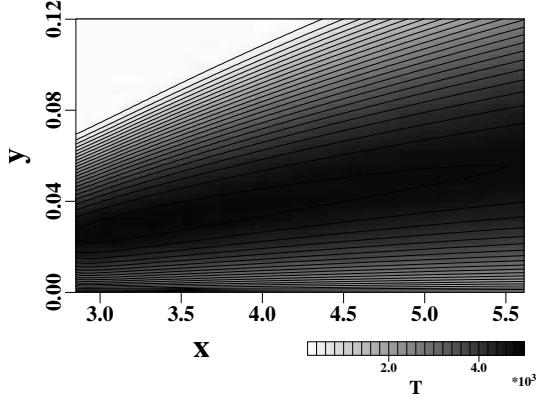Figure 3: temperature distribution inside the boundary layer for the non-reactive Ma=20 H=50km case, x and y dimensions are in [m], temperature is in [K]
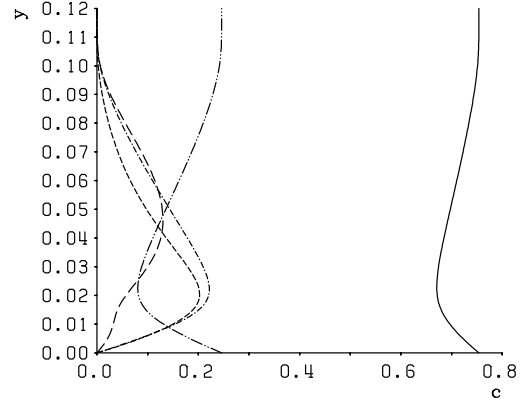

Figure 4: distribution of the concentrations of the chemical species for the reactive calculation at x=5.5m. $c_N \times 10$ ----; c_{N2} ——; c_O —·—; c_{O2} —··—; $c_{NO} \times 10$ ———.
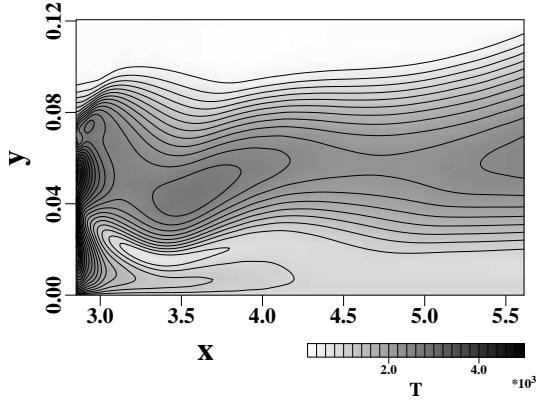

Figure 5: translational temperature distribution inside the boundary layer for the non-equilibrium Ma=20 H=50km case
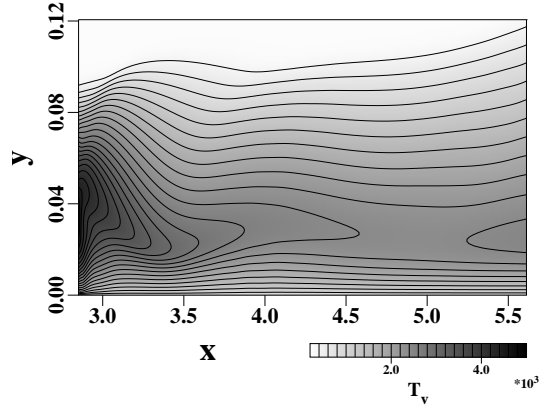

Figure 6: vibrational temperature distribution inside the boundary layer for the non-equilibrium test case

number. Fig. 7 shows the disturbance amplitudes for the non-reactive case for the two-dimensional (1,0) and the three-dimensional (1,1) disturbance. The steady two-dimensional deviation from the base flow is expressed as the amplitude of the (0,0) mode. The modes are damped right down stream of the introduction since they are limited by the resulting Mach wave which has an angle of $\alpha = 2.86°$ for the M=20 flow. Further down stream (x>9), the disturbances behave similar as to what is expected form Linear Stability Theory (see a more detailed comparison in [11]).

For the reactive case (Fig. 8), the two-dimensional disturbance is on the same amplitude level as for the non-reactive case, but the three-dimensional disturbance experiences a drop in amplitude of a factor of about 2-3. A greater difference in behaviour for these linear disturbance amplitudes would be expected since the disturbance temperatures are at a maximum of about 2-3 K.

4   Conclusion

The presented numerical method has shown its capacity to simulate the spatial development of a disturbance inside a M=20 boundary layer on an isothermal flat plate. Comparisons of DNS results with results from the Linear Stability Theory show very good agreement inside the framework of the limitations of the theory.

Disturbance calculations for reactive and non-reactive flow show little difference between the disturbance development for linear disturbances. For non-linear disturbances with higher disturbance temperature amplitudes, a considerable difference is to be expected and is part of the ongoing work in this project.
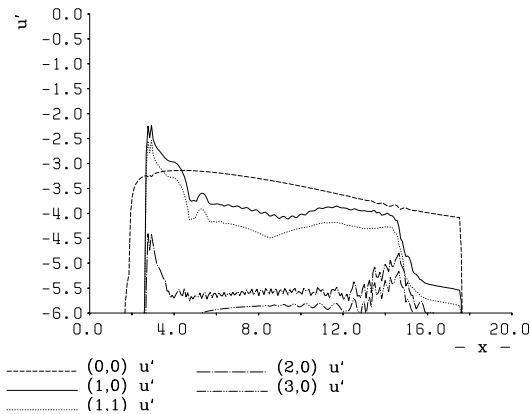
Figure 7: Comparison of maximum amplitudes of the downstream velocity u for the ideal-gas case for the disturbance with a two-dimensional and a three-dimensional wave with the frequency F= 3.46 10^{-5}
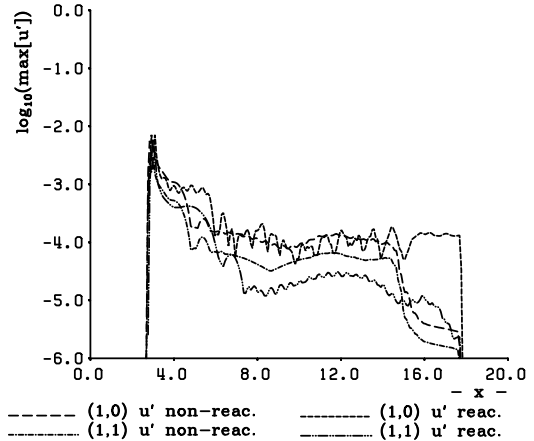
Figure 8: Comparison of maximum amplitudes of the downstream velocity u for the ideal-gas case for the disturbance with a two-dimensional and a three-dimensional wave with the frequency F= 3.46 10^{-5}

References

[1] L.M. Mack. Boundary-Layer Stability Theory, Jet Propulsion Laboratory, Pasadena, USA ,*JPL Report 900-277 Rev. A*, 1969.

[2] C. Park, A Review of Reaction Rates in High Temperature Air, *AIAA Paper 89-1740*, 1989.

[3] Park, C., *Nonequilibrium Hypersonic Aerothermodynamics.* John Wiley & Sons, New York, 1990.

[4] G. Candler. *Aerothermochemistry for Hypersonic Technology*, VKI-LS 1995-04.

[5] N.A. Adams and K. Shariff. A High-Resolution Hybrid Compact-ENO Scheme for Shock-Turbulence Interaction Problems. *J. Comp. Phys.*, **127**, 27–51, 1996.

[6] N.A. Adams. Direct Numerical Simulation of Turbulent Compression Ramp Flow. *Theor. and Comp. Fl. Dynamics*, **12**, 109–129, 1998.

[7] N.A. Adams. Direct Simulation of the Turbulent Boundary Layer along a compression ramp at M=3 and Re_θ=1685. *J. Fluid Mech.*, **420**, 47–83, 2000.

[8] S.K. Lele. Compact Finite-Difference Schemes With Spectral-Like Resolution, *J. Comp. Phys.*, **103**, 16–42, Academic Press, San Diego, 1992.

[9] C. Stemmer. Flat-Plate Boundary-Layer Hypersonic Transition. *Annual Research Briefs 2002*. Center for Turbulence Research, Stanford University, NASA Ames, 389–396, 2002.

[10] H. Bestek and W. Eißler. Direct numerical simulation of transition in Mach 4.8 boundary layers at flight conditions. In Rodi, W.; Bergeles, G. (eds.):*Engineering Turbulence Modelling and Experiments 3*, Proc. 3rd Int. Symp. Engineering Turbulence Modelling and Measurements, Heraklion-Crete, Greece, 27-29 May, 1996; Elsevier Science B.V., 1996.

[11] C. Stemmer and N.A. Adams, Investigation of hypersonic flat-plate boundary-layer transition by Direct Numerical Simulation. accepted for publication in: *High Performance Computing in Science and Engineering '04*. Transactions of the High Performance Computing Center, Stuttgart (HLRS), pp. 155-162, Springer Verlag, 2004.

[12] C. Stemmer, Hypersonic Transition Investigations In A Flat-Plate Boundary-Layer Flow At M=20., *AIAA Paper 2005-5136.*

[13] C. Stemmer and N.A. Adams, Instabilities in hypersonic boundary layers under the influence of high-temperature gas effects. *High Performance Computing in Science and Engineering '04*. Transactions of the High Performance Computing Center, Stuttgart (HLRS), pp. 119-128, Springer Verlag, 2005.

Numerical Analysis of Entropy–Layer Instability in Hypersonic Blunt Cone Flows

By S. Hein

DLR, Bunsenstraße 10, D-37073 Göttingen, Germany

Stefan.Hein@dlr.de

Abstract

The instability properties of the axisymmetric flow at Mach 8 along blunt cones of different nose radii are studied by linear local instability theory and parabolized stability equations (PSE). The cone geometry and the free–stream conditions are adapted to the experiments of Stetson *et al.* (1984). Apart from the first– and second–mode boundary–layer instabilities Stetson *et al.* (1984) also measured disturbance amplification inside the un–swallowed entropy layer i.e. above the viscous boundary layer. Here, we focus on the numerical analysis of these entropy–layer instabilities as the effect of nose bluntness on first– and second–mode instability has been discussed in detail already (see e.g. Rosenboom *et al.*, 1999, and the references therein). Our numerical results (Hein, 2005) corroborate the existence of these instability modes of the entropy layer in the frequency range reported by Stetson *et al.* (1984). These entropy–layer disturbances are most amplified as two–dimensional waves and are dominated by temperature and density fluctuations. The location of the amplitude function maxima is clearly correlated with the position of a generalised inflection point in the entropy layer, as noted by Stetson *et al.* (1984) already. Thus, these instability modes are damped downstream of the swallowing point. Due to their rather small amplification rates they probably can not trigger laminar–turbulent transition directly, however.

Dietz & Hein (1999) presented experimental and numerical results for entropy–layer instabilities of a blunted flat plate at Mach 2.5. They suggested that these modes correspond to those observed experimentally by Stetson *et al.* (1984) for hypersonic blunt cone flow, arguing that the non–dimensional frequencies match if the disturbance frequencies are made non–dimensional with a proposed entropy–layer length scale. Present results support this assumption since the properties of the blunt cone entropy–layer disturbances closely resemble those described by Dietz & Hein (1999) and thus also indicate that the proposed length scale is indeed a characteristic length scale for entropy–layer instabilities.

References

Dietz, G. & Hein, S. 1999 Entropy–layer instabilities over a blunted flat plate in supersonic flow. *Phys. Fluids* **11** (1), 7–9.

Hein, S. 2005 Nonlinear transition analysis. Research report DLR-FB 2005-10.

Rosenboom, I., Hein, S. & Dallmann, U. 1999 Influence of nose bluntness on boundary–layer instabilities in hypersonic cone flows. AIAA–Paper 99–3591.

Stetson, K., Thompson, E., Donaldson, J. & Siler, L. 1984 Laminar boundary layer stability experiments on a cone at Mach 8, part 2: blunt cone. AIAA–Paper 84–0006.

6th ERCOFTAC SIG 33 workshop

Laminar-Turbulent Transition Mechanisms, Prediction and Control

List of participants

Name	First Name	Affiliation	E-mail
ÅKERVIK	Espen	KTH Stockholm	espena@mech.kth.se
ALBRECHT	Thomas	TU Dresden	thomas.albrecht@tu-dresden.de
ARCHAMBAUD	Jean-Pierre	ONERA Toulouse	archam@onecert.fr
BABUCKE	Andreas	Universität Stuttgart	babucke@iag.uni-stuttgart.de
BAGHERI	Shervin	KTH Stockholm	shervin@mech.kth.se
BAYSAL	Kudret	Universität Stuttgart	baysal@iag.uni-stuttgart.de
BONFIGLI	Giuseppe	ETH Zürich	bonfigli@ifd.mavt.ethz.ch
BRANDT	Luca	KTH Stockholm	luca@mech.kth.se
BRAUN	Stefan	TU Wien	stefan.braun@tuwien.ac.at
CASALIS	Grégoire	ONERA Toulouse	gregoire.casalis@onera.fr
CHEDEVERGNE	François	ONERA Toulouse	francois.chedevergne@onera.fr
DE LANGE	Rick	Univ. Eindhoven	h.c.d.lange@tue.nl
FASEL	Hermann	University of Arizona	faselh@u.arizona.edu
FRIEDERICH	Tillmann	Universität Stuttgart	friederich@iag.uni-stuttgart.de
GRUNDMANN	Sven	TU Darmstadt	s.grundmann@aero.tu-darmstadt.de
HANIFI	Ardeshir	FOI Stockholm	ardeshir.hanifi@foi.se
HEIN	Stefan	DLR Göttingen	stefan.hein@dlr.de
HENNINGSON	Dan	KTH Stockholm	henning@mech.kth.se
KLOKER	Markus J.	Universität Stuttgart	kloker@iag.uni-stuttgart.de

KRIEGSEIS	Jochen	TU Darmstadt	kriegseis@sla.tu-darmstadt.de
LENZ	Birgit	Universität Stuttgart	lenz@iag.uni-stuttgart.de
LINN	Jens	Universität Stuttgart	Linn@iag.uni-stuttgart.de
MISCHENKO	Dmitry	ITAM Novosibirsk	misch2005@yandex.ru
MONOKROUSOS	Antonios	KTH Stockholm	antonios@mech.kth.se
MUELLER	Sebastian	ETH Zürich	se@ifd.mavt.ethz.ch
PELTZER	Inken	TU Berlin	Inken.Peltzer@tu-berlin.de
PIOT	Estelle	ONERA Toulouse	estelle.piot@onera.fr
PRALITS	Jan Oscar	Università di Salerno	jpralits@unisa.it
PUJALS	Gregory	École Polytechnique Paris	gregory@ladhyx.polytechnique.fr
RASHAD	Muhammad Aqeel	Universität Stuttgart	rashad@iag.uni-stuttgart.de
RIST	Ulrich	Universität Stuttgart	rist@iag.uni-stuttgart.de
RODRIGUEZ	Daniel	UPM Madrid	daniel@torroja.dmt.upm.es
SCHNEIDER	Tobias M.	Philipps-Universität Marburg	tobias.schneider@physik.uni-marburg.de
SEITZ	Arne	DLR Braunschweig	arne.seitz@dlr.de
SELENT	Björn	Universität Stuttgart	iagselen@iag.uni-stuttgart.de
STEMMER	Christian	TU München	Christian.Stemmer@tum.de
WEISMÜLLER	Michael	TU Darmstadt	m.weismueller@aero.tu-darmstadt.de
ZENGL	Marcus	Universität Stuttgart	zengl@iag.uni-stuttgart.de